The Ohio State 1991 Geopotential and Sea Surface Topography Harmonic Coefficient Models

by

Richard H. Rapp

Yan Ming Wang

Nikolaos K. Pavlis

Report No. 410

Department of Geodetic Science and Surveying
The Ohio State University
Columbus, Ohio 43210-1247

August 1991

Abstract

This report starts with the analysis of one year of Geosat altimeter data starting from the orbits computed with the GEM-T2 potential coefficient model and consistent station coordinates (Koblinsky et al., 1990). The first stage in the processing followed the general editing procedures implemented by Denker and Rapp (1990) when working with GEM-T1 orbits. Additional altimeter data, beyond that used by Denker and Rapp, was selected below -63° latitude, in the Mediterranean Sea, and in several areas of high frequency signal. The original radial orbit theory is due to Engelis. The analysis solved for corrections to the GEM-T2 potential coefficient model, coefficients in a degree 10 potential coefficient expansion, and 8 parameters for each of the 76 arcs of data analyzed. The data used included the altimeter data, the GEM-T2 potential coefficients with its error covariance matrix, and surface gravity data represented by 1° x 1° mean gravity anomalies. The root mean square orbit correction was approximately 75 cm with the corrections to the potential coefficients corresponding to geoid changes on the order of 118 cm. After applying the orbit correction terms the adjusted crossover discrepancies were ± 20 cm with a sample point residual of ± 19 cm.

The sea surface topography from this solution did not show the slope problem across the northern Pacific Ocean that was seen by Denker and Rapp with the GEM-T1 orbits. Variations of the sea surface over the one year of data were analyzed by fixing the geopotential model and orbit corrections from the one year solution and solving for a monthly sea surface topography representation to degree 15. Variations from the annual degree 15 solutions were analyzed in the time domain to find signatures at different frequencies, for example annually and seasonally. These changes were also studied to detect local variations of the sea surface.

In a third stage of analysis a combination solution with the GEM-T2 potential coefficients and the recent 30′ mean gravity anomaly data set was carried out using the same procedure as described by Rapp and Pavlis (1990). The global set of adjusted gravity anomalies was used to calculate a potential coefficient model to degree 360. The final potential coefficient model was formed by taking the coefficients from degree 2 to 50 from the first combination solution with the coefficients from degree 51 to 360 of the last solution. The standard deviations of each coefficient were computed from the adjustment process and by error propagation. The cumulative geoid undulation commission error of the 91A model to degree 10, 50, and 360 is 5 cm, 25 cm, and 49 cm, respectively.

The OSU91 model was tested through orbit predictions and data fitting; through comparisons with geoid undulations computed from Doppler and GPS located stations, and with comparisons to geoid undulations implied by Geosat altimeter data. In the latter case the root mean square difference between the Geosat undulation (after orbit and sea surface topography correction) was 34 cm for OSU91 as opposed to ± 53 cm with OSU89B.

Foreword

This report was prepared by Richard H. Rapp, Professor, Yan Ming Wang, and Nikolaos K. Pavlis, Research Associates, Department of Geodetic Science and Surveying at The Ohio State University. The research described in this report was supported, in part, under NASA'S TOPEX Altimeter Research in Ocean Circulation Mission and funded through the Jet Propulsion Laboratory under contract 958121, OSURF 720426. Additional funding was received from NASA/Goddard Space Flight Center under grant NAG 5-781, OSURF 718266.

Computer resources were provided by the Ohio State Academic Computing Services, and the Ohio Supercomputer Center through Cray Grant pas 160.

The GEM-T2 orbits needed for this study were kindly provided by C. Koblinsky and A. Brenner. The orbit analysis tests were carried out at the Naval Surface Weapons Center through the efforts of Dr. Pat Fell, and at NASA/Goddard Space Flight Center through the efforts of Steve Klosko and Frank Lerch. The GEM-T2 error covariance matrix was provided through Frank Lerch. Numerous persons and organizations provided surface gravity material that was used in the analysis.

The reproduction and distribution of this report was carried out, in part, with funds supplied by the Department of Geodetic Science and Surveying.

1. Introduction

Denker and Rapp (1990) and Denker (1990) have described the analysis of Geosat altimeter data for the recovery of an improved geopotential model, sea surface topography and, primarily, improved, in the radial direction, Geosat orbits. The research described in these two papers used Geosat data with the GEM-T1 based orbits described by Haines et al. (1989; 1990). The GEM-T1 orbits were computed with the GEM-T1 potential coefficient model and the OPNET Doppler tracking data. The tracking station positions were those transformed (not adjusted) into the reference frame consistent with that used in the development of the GEM-T1 model. The studies noted above demonstrated the validity of the orbit improvement process originally developed by Engelis (1987a) and modified for the studies noted. However a problem was identified with the degree 1 terms of the sea surface topography that were estimated from the solution. Specifically it was found that the (1, 1) terms of the spherical harmonic expansion of sea surface topography were incompatible with oceanographic information. This specifically was demonstrated by the sea surface slope across the northern Pacific Ocean. The coefficients that were found as part of the solution implied a slope different from that expected from historical oceanographic information (Levitus, 1982). When the SST (1, 1) coefficients were changed to the ones implied by the oceanographic data (Engelis, 1987b) the slope problem disappeared. These results suggested that the GEM-T1 orbits might have deficiencies that would cause degree (1, 1) problems in the determination of SST. The problems could be caused by inaccurate station coordinates (especially for the OPNET stations); inaccurate gravity model coefficients; and perhaps unmodeled effects on the satellite orbit.

Haines et al. (1989; 1990) discussed Geosat orbit determination with the GEM-T2 potential coefficient model and other improvements over the GEM-T1 orbits. One improvement was the use of Doppler tracking from several TRANET-2 tracking data and the solution of tracking station coordinates for these stations. The preliminary results reported by Haines reported the radial orbit error with the GEM-T2 analysis to be on the order of 35 cm as opposed to the 85 cm for the GEM-T1 analysis.

The GEM-T2 Geosat orbits were released in early 1990 (Koblinsky et al., 1990) and received by us in April 1990. Because of the problems identified with the GEM-T1 orbits we decided to test the GEM-T2 orbits with our software to see if improved (specifically with the (1, 1) coefficients) sea surface topography could be obtained. Several six day arcs were analyzed on a preliminary basis where we found the slope problem had been eliminated with the new GEM-T2 orbits. A decision was then made to process the full year of Geosat data starting from the GEM-T2 orbits.

Denker and Rapp (1990) did not include any surface gravity data in their solution. This was deliberately done so that results related to the orbit improvement could be emphasized. However it was clear that for any modelling effort to be complete, surface gravity, in terms of normal equations, should be incorporated into the new solution. The procedures used for doing this will be described on a subsequent section.

Rapp and Pavlis (1990) described a combination solution of the GEM-T2 potential coefficient model, surface gravity data, and gravity information derived from Geos-3/Seasat and Geosat altimeter data. The model developed there was complete to degree 360 although a rigorous adjustment of the data only to degree 50 took place.

The models (OSU89A and OSU89B) described by Rapp and Pavlis (ibid) used a terrestrial gravity data set developed in July 1989 (Kim and Rapp, 1990). Late in 1990 an update of this data base was made in which additional gravity data was incorporated. The updated file is described by Yi and Rapp (1991).

With the above as background it seemed appropriate to combine the new orbits and new data together to come up with, first a new gravity model complete to degree 50, a new sea surface topography representation, and improved Geosat orbits. This would then be followed by the development of a degree 360 potential coefficient model which would be merged with the results of the first step. In essence this report discusses an extension of the work described by Denker and Rapp (1990), Pavlis (1988) and Rapp and Pavlis (1990) to arrive at improved estimates for numerous quantities.

2. Satellite Altimeter Data Processing

2.1 Theory

We start by a brief review of the theoretical models used to relate the altimeter measurement to the parameters being sought. We closely follow (Denker and Rapp, 1990) and define a residual sea surface height Δh:

$$\Delta h = h_c - \rho - N_c - \Delta N_o - \tau - \omega \qquad (2.1)$$

where:

h_c = computed ellipsoidal height of the satellite based on the a priori ephemeris;

ρ = measured and corrected (for environmental factors) distance from satellite to the sea surface;

N_c = geoid undulation based on the same geopotential model used for the ephemeris generation;

ΔN_o = neglected (or removed) higher frequency geopotential effects;

τ = tidal effects

ω = oceanic effects (waves, etc.)

The value of Δh will depend on the corrections to the a priori potential coefficients in two parts. The first is through the undulation effects (ΔN_G) and the second is through the effect (Δh_G) on the ellipsoidal height through the a priori ephemeris. Let Δh_I be the ellipsoidal height error caused by initial state errors and other effects and let ζ be the sea surface topography. Then (ibid, eq. (5))

$$\Delta h = \Delta N_G\left(\Delta\overline{C}_{\ell m}, \Delta\overline{S}_{\ell m}\right) - \Delta h_G\left(\Delta\overline{C}_{\ell m}, \Delta\overline{S}_{\ell m}\right) - \Delta h_I + \zeta \qquad (2.2)$$

where:

$\Delta\overline{C}_{\ell m}, \Delta\overline{S}_{\ell m}$ are the corrections to the fully normalized a priori potential coefficient model of degree ℓ and order m;

The modeling of ΔN_G and Δh_G is described in Engelis (1987a). We continue with a spherical harmonic representation of the sea surface topography although problems with the representation are discussed in Denker and Rapp (ibid). We write:

$$\zeta(\bar{\phi}, \lambda) = \sum_{\ell=1}^{\ell_{MAX}^{SST}} \sum_{m=0}^{\ell} \left(\bar{C}_{\ell m}^{SST} \cos m\lambda + \bar{S}_{\ell m}^{SST} \sin m\lambda\right) \bar{P}_{\ell m}(\sin\bar{\phi}) \tag{2.3}$$

where $\bar{\phi}$ and λ are geocentric latitude and longitude. The value of Δh_I was taken the same as used by Denker and Rapp (ibid, eq. (7)):

$$\Delta h_I = a_o + a_1 \cos\dot{\psi}t + a_2 \sin\dot{\psi}t + a_3 \Delta t \cos\dot{\psi}t + a_4 \Delta t \sin\dot{\psi}t + a_5 \Delta t \sin 2\dot{\psi}t + a_6 \Delta t^2 \cos\dot{\psi}t + a_7 \Delta t^2 \sin\dot{\psi}t \tag{2.4}$$

$\dot{\psi}$ is the frequency associated with the 1cy/rev; t is the time from the beginning of the arc being processed; and Δt is the time relative to the middle of the arc.

Originally the a_6 and a_7 terms were in the Denker/Rapp procedure because such terms can represent resonance terms effects which are not modeled in the GEM-T1 model (a 43 order resonance was noted by Haines et al., 1989). Since the GEM-T2 model included a 43 order term there was a question if the a_6 and a_7 terms should be retained. Several arcs were analyzed with and without the a_6 and a_7 terms. The results indicate that the inclusion of these terms gave significant improvement (i.e. the root mean square residuals were smaller) over the case that excluded the coefficients. For all results to be described in this paper the a_6 and a_7 terms were retained in the Δh_I model.

2.2 Editing and Computational Procedures

The initial editing procedures for the Geosat analysis were the same as described in Denker and Rapp (ibid, p. 13,153) or Denker (ibid, pp. 10-17). The initial editing deleted data over land; data where the standard deviation of a linear fit to 10 per second sea height values was greater than 10 cm; data where the automatic gain control voltage exceeded 37 db; when the attitude was larger than 1°.3; when the ocean tide correction was larger than ± 1 m; etc.

After the data was selected in a 6 day arc using the criteria described above a subsequent editing was applied with the following criteria:

1. Data in shallow seas and continental shelves was deleted if the altimeter measurement fell in a 30' x 30' cell where the depth was smaller than 1000 m. This criteria is the same as used by Denker and Rapp (ibid).

2. An altimeter data point was deleted (initially) if the geoid undulation contribution from degree 51 to 360 was larger than 3 m when computed from the OSU89B potential coefficient model (Rapp and Pavlis; 1990). In the Denker/Rapp solution the 3 m tolerance was applied to the 37 to 360 contribution so that the new criteria accepts more data. In addition the OSU89B model is more accurate than the OSU86F model used by Denker/Rapp so that more appropriate editing results.

3. An altimeter data point was deleted (initially) if the along track deflection of the vertical exceeded 10" as computed from the actual sea surface height data. This criteria is the same as used by Denker/Rapp.

4. No data below -64° latitude was deleted because of latitude considerations. Such data was deleted by Denker and Rapp (ibid) because of suspected inaccuracies of the OSU86F reference

3. Normal Equations for the Geopotential Coefficients Obtained from Surface Gravity Data

In the present study the formation of normal equations for the complete set of geopotential coefficients up to harmonic degree 50, from the analysis of terrestrial gravity measurements, closely followed the modeling and estimation procedures discussed in detail by Pavlis (1988). Therefore, in the following paragraphs only a brief outline of these procedures will be given, and the emphasis will be placed on the description of the improved gravity anomaly data which were used in this analysis, on certain aspects of the modeling which were re-examined and modified, and on the presentation of the results obtained.

3.1 The OSU October 1990 Gravity Database

The fundamental terrestrial 1° x 1° mean gravity anomaly dataset used in this study is designated "OSU October 1990" (Yi and Rapp, 1991), and represents the latest update of the global gravity anomaly database maintained at the Ohio State University. With respect to its predecessor (OSU July 1989—Kim and Rapp, 1990), it is improved by the incorporation of improved 944 1° x 1° mean gravity anomalies. Of the 944 newly accepted values, 9 anomalies had no previous estimates and 935 anomalies replaced previous values which were primarily geophysically predicted. The OSU July 1989 dataset, on the other hand, is substantially better than the June 1986 file (Despotakis, 1986) which was originally used for the normal equations formed by Pavlis (1988). For example, improved gravity anomaly data for Africa, included in the July 1989 dataset, have replaced corresponding values in the June 1986 file, which were identified to be contaminated by significant systematic errors (Pavlis, 1988, section 5.3.2).

The October 1990 database contains in total 50802 1° x 1° mean free-air gravity anomalies. Of these, 45932 values originate from actual gravity measurements, while 4870 values are estimates obtained from geophysical prediction techniques. In Table 1, statistics related to the mean anomalies of the October 1990 dataset are given, while in Figure 1 the geographic distribution of the available data is displayed.

Table 1. Statistics of the 1° x 1° Mean Free-air Anomalies in the OSU October 1990 Database

	Gravity Measurements	Geophysical Prediction	Combined
Number of values	45932	4870	50802
Percentage of area	79.2	6.6	85.7
Minimum value	-270	-123	-270
Maximum value	303	127	303
Mean value	-0.5	-1.0	-0.5
RMS value	27.6	25.3	27.4
RMS standard deviation	12.0	17.3	12.5

(Gravity anomaly units are mgals; mean and RMS values given above are weighted by the area of each 1° x 1° block.)

3.2 Creation of Mean Anomaly Files Input to the Adjustment

The analysis made by Pavlis (1988) has demonstrated that the geophysically predicted anomalies are in many cases systematically biased with respect to the anomalies that are implied by global geopotential models derived from the analysis of satellite perturbations only (ibid, section 5.3.2). Pavlis and Rapp (1990) have shown that a preferable alternative to the use of geophysically

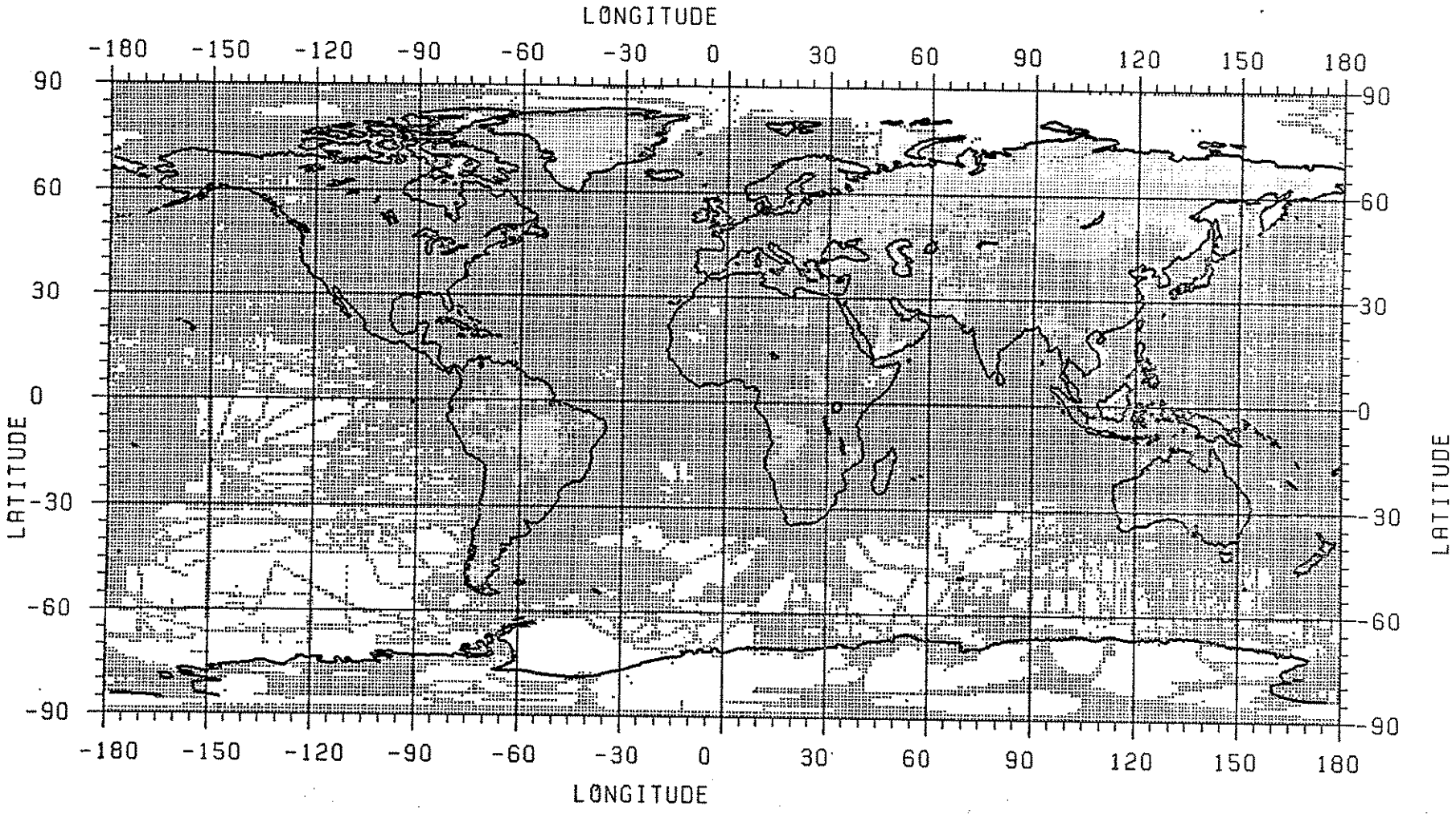

Figure 1. Geographic Distribution of the 50802 1° x 1° Mean Free-air Anomalies in the October 1990 Database. "x" Identifies Values Originating From Gravity Measurements (45932) and "." Geophysically Predicted Values (4870).

(iv) Gravity formula transformation δg_r

The specific formulation used to evaluate 1° x 1° area-mean values of the above correction terms is given in detail in (ibid, section 2.3). It needs to be mentioned here that the OSU89B geopotential model, complete to degree 180, was used to evaluate 1° x 1° area-mean values of the ellipsoidal corrections (denoted IE_h, IE_γ, and IE_P). Also, throughout this analysis the following parameters were used to define the geometry and the gravity potential of the reference ellipsoid (ibid, p. 60):

$a = 6378137.$ m
$1/f = 298.257$
$GM = 3986004.36 \times 10^8$ m^3/s^2
$\omega = 7.292115 \times 10^{-5}$ rad/s

and the transformation of the October 1990 anomalies, which refer to the GRS 1967 gravity formula, to the gravity formula implied by the above constants was performed as explained in (ibid, pp. 60-61). Denoting by $\bar{\Delta}g'$ the corrected anomaly, one has:

$$\bar{\Delta}g'_{ij} = \bar{\Delta}g_{ij}^{OCT90} + (\delta g_s)_{ij} \qquad (3.2)$$

where the total systematic correction δg_s (ibid, equation 4.12):

$$(\delta g_s)_{ij} = [\delta g_A - (IE_h + IE_\gamma + IE_P) + \delta g_{h^2} + \delta g_r]_{ij} \quad . \qquad (3.3)$$

The $\bar{\Delta}g'$ values in SET A represent surface mean free-air anomalies in the Molodensky sense. Their frequency content is not uniform worldwide but depends on factors such as the distribution of gravity measurements inside each 1° x 1° block and the averaging process used to estimate each mean value. In contrast, the $\bar{\Delta}g^{TI}$ values in SET A are formally interpreted as mean free-air anomalies continued to the surface of the reference ellipsoid, and their spectral content extends (by definition) only up to harmonic degree 50. Extensive analysis discussed by Pavlis (1988, section 5.2.5) has shown that the leakage of power from the higher-frequency component of $\bar{\Delta}g_{ij}$, to the lower-frequency coefficients being solved for from the incomplete set of discrete area-mean values $\bar{\Delta}g'_{ij}$, can be minimized by removing the higher-frequency content of $\bar{\Delta}g'_{ij}$ (above degree 50) prior to the formation of normal equations. The higher-frequency component, $\bar{\delta}g^{HF}$, can be evaluated in terms of 1° x 1° area-mean values, using an existing high-degree geopotential model such as OSU89B, by:

$$\bar{\delta}g_{ij}^{HF} = \frac{1}{\Delta\sigma_i}\frac{GM}{(r_i^E)^2}\sum_{n=51}^{360}(n-1)\left(\frac{a}{r_i^E}\right)^n \sum_{m=-n}^{n} \bar{C}_{nm}^{89B}\bar{IY}_{nm}^{ij} \quad . \qquad (3.4)$$

In the implementation of this procedure the following two aspects need to be considered carefully:

1. The harmonic coefficients used to evaluate $\bar{\delta}g^{HF}$ must represent as precisely as possible the higher-frequency component of the data which will be used in the adjustment.

2. $\bar{\delta}g^{HF}$ must be evaluated at the same level at which the mean values $\bar{\Delta}g'_{ij}$ refer (the topographic surface of the Earth).

To comply with the first of the above requirements (since no high-degree expansion was available at the time, that included the gravity data from our new source), the following steps were taken:

(a) Each of the 944 1° x 1° blocks, containing a value from the new data source, was divided into the four corresponding 30' x 30' blocks that it covers. To each of them a 30' mean anomaly estimate was assigned, which is identical with the corresponding 1° x 1° mean value. A total of 3776 $\bar{\Delta}g_{30'}$ were thus produced. After application of the atmospheric, ellipsoidal, second-order gradient and gravity formula corrections and analytical downward continuation to the reference ellipsoid (Rapp and Pavlis, 1990), these "split-up" values were merged with the adjusted global 30' mean anomaly file that produced the OSU89B geopotential model (ibid). In this merging, a "split-up" value from China replaced a previous 30' value only if the previous estimate was a "fill-in" anomaly or a "split-up" from previously available 1° x 1° estimate. In this manner, 3669 (out of the 3776) China 30' mean values were accepted in the merged file. Of these, 3144 values replaced "fill-in" data and 525 values replaced previous "split-up" data.

(b) The resulting global 30' mean anomaly file from the above merging was harmonically analyzed as explained by Rapp and Pavlis (ibid, equation 20) to yield a "modified OSU89B" set of coefficients complete to degree and order 360. This set, denoted $\bar{C}_{nm}^{89B'}$, was then used in equation (3.4) to evaluate 1° x 1° mean values of $\bar{\delta}_g^{HF}$. As it can be seen from (3.4), the high-frequency contribution to the data is evaluated on the surface of the reference ellipsoid, while the data $\bar{\Delta}g_{ij}$, refer to the topographic surface of the Earth. To account for this incompatibility, the analytical continuation term g_1 (Wang, 1988) was used in two different ways, which led to two alternative files to be used as input for the formation of normal equations:

Method 1: Input anomalies referring to the topographic surface of the Earth.

The global 30' x 30' set of g_1 values computed by Wang (ibid) on the basis of the TUG87 mean elevations (Wieser, 1987), was harmonically analyzed (according to a quadrature formula similar to equation (20) in Rapp and Pavlis (1990)), to yield a set of (spherical) harmonic coefficients $\bar{G}_{nm}$, complete to degree 360. Using the coefficients $\bar{G}_{nm}$, two correction terms were evaluated, both in terms of 1° x 1° mean values:

$$\left(\bar{g}_1^L\right)_{ij} = \frac{1}{\Delta\sigma_i}\,\frac{GM}{\left(r_i^E\right)^2}\sum_{n=2}^{50}(n-1)\left(\frac{a}{r_i^E}\right)^n\sum_{m=-n}^{n}\bar{G}_{nm}\bar{I}\bar{Y}_{nm}^{ij} \tag{3.5}$$

$$\left(\bar{g}_1^H\right)_{ij} = \frac{1}{\Delta\sigma_i}\,\frac{GM}{\left(r_i^E\right)^2}\sum_{n=51}^{360}(n-1)\left(\frac{a}{r_i^E}\right)^n\sum_{m=-n}^{n}\bar{G}_{nm}\bar{I}\bar{Y}_{nm}^{ij} \tag{3.6}$$

The anomalies to be input to the adjustment, denoted $\bar{\Delta}g^{(1)}$, were then defined by:

$$\bar{\Delta}g_{ij}^{(1)} = \begin{cases} \bar{\Delta}g_{ij}^{OCT90} + \left(\delta g_s\right)_{ij} - \left(\bar{\delta}g^{HF} - \bar{g}_1^H\right)_{ij} \\ \bar{\Delta}g_{ij}^{TI} - \left(\bar{g}_1^L\right)_{ij} \end{cases} \tag{3.7}$$

depending on their origin (actual measurements or topographic/isostatic values). From the definition of the analytical continuation term g_1 (Wang, 1988), it can be seen that $\bar{\Delta}g^{(1)}$ refer to the topographic surface of the Earth. The anomalies $\bar{\Delta}g^{(1)}$ constitute the file designated SET 1, which was one of the two files considered as input to the least-squares adjustment.

Method 2: Input anomalies reduced to the reference ellipsoid.

Here, the 1° x 1° mean values of the term g_1 (denoted $\bar{g}_1$) as computed by Wang (1988) are used, and the anomalies to be input to the adjustment are defined by:

$$\bar{\Delta}g_{ij}^{(2)} = \begin{cases} \bar{\Delta}g_{ij}^{OCT90} + (\delta g_s)_{ij} + (\bar{g}_1)_{ij} - (\bar{\delta}g^{HF})_{ij} \\ \bar{\Delta}g_{ij}^{TI} \end{cases} \tag{3.8}$$

The anomalies $\bar{\Delta}g^{(2)}$ constitute the file designated SET 2, and represent values reduced to the surface of the reference ellipsoid.

In theory, the two alternative treatments of the input anomaly data should yield the same result, provided that the observation equations appropriately consider the surface to which the data refer. In practice however, the approximations involved in the evaluation of the g_1 terms (Wang, 1988), and the errors introduced in the computation of $\bar{g}_1^L$ and $\bar{g}_1^H$ result in small but systematic differences as it will be seen later. It should be mentioned here that the harmonic decomposition of g_1, which is necessary to evaluate $\bar{g}_1^L$ and $\bar{g}_1^H$, is not a trivial step since g_1 has a discontinuity at the continental boundary ($g_1 \equiv 0$ over the ocean).

In Table 2 statistics related to the anomalies of SET 1 and SET 2, as well as their differences, are given. When forming these files, all Δg^{TI} anomalies were assigned identical standard deviation of 20 mgal, based on the accuracy assessment for these values discussed by Pavlis and Rapp (1990). Also, the minimum standard deviation for any anomaly regardless of source was set to 2 mgal to avoid over optimistic accuracy estimates. The distribution of data in both SET 1 and SET 2 is obviously identical to that of SET A given in Figure 2.

Table 2. Statistics of the 1° x 1° Mean Anomalies Used in the Normal Equations Formed.

	SET 1 $\bar{\Delta}g^{(1)}$	SET 2 $\bar{\Delta}g^{(2)}$	$\bar{\Delta}g^{(1)} - \bar{\Delta}g^{(2)}$
Number of values	54048	54048	54048
Percentage of area	87.3	87.3	87.3
Minimum value	-199.4	-199.4	-10.4
Maximum value	141.3	141.2	9.2
Mean value	-0.3	-0.1	-0.2
RMS value	19.0	19.2	0.7
RMS standard deviation	13.0	13.0	—

3.3 Estimation of Geopotential Coefficients from Surface Gravity Data

The anomalies $\bar{\Delta}g^{(1)}$ and $\bar{\Delta}g^{(2)}$ previously defined lead to the following observation equations respectively:

$$v_{ij}^{(1)} = \frac{1}{\Delta\sigma_i} \frac{GM}{\bar{r}_{ij}^2} \sum_{n=0}^{50}{}' (n-1) \left(\frac{a}{\bar{r}_{ij}}\right)^n \sum_{m=-n}^{n} \bar{C}_{nm}^T \bar{I} \bar{Y}_{nm}^{ij} - \bar{\Delta}g_{ij}^{(1)} \tag{3.9}$$

$$v_{ij}^{(2)} = \frac{1}{\Delta\sigma_i}\frac{GM}{(r_i^E)^2}\sum_{n=0}^{50}{}' (n-1)\left(\frac{a}{r_i^E}\right)^n \sum_{m=-n}^{n} \bar{C}_{nm}^T \bar{Y}_{nm}^{ij} - \bar{\Delta}g_{ij}^{(2)} \qquad (3.10)$$

where $v_{ij}^{(k)}$ is the residual associated with the $\bar{\Delta}g_{ij}^{(k)}$ observation (k = 1, 2) and $\bar{C}_{nm}^T$ represent the adjusted geopotential coefficients obtained on the basis of surface gravity data alone (even zonal harmonic coefficients are remainders after subtraction of the coefficients of the normal potential). The geocentric distance $\bar{r}_{ij}$ in (3.9) was evaluated as explained in (Pavlis, 1988, section 2.3.4) using the TUG87 (Wieser, 1987) 1° x 1° mean elevations to realize the topographic surface of the Earth. r_i^E on the other hand is the distance from the geocenter to the point on the ellipsoid at the mid latitude of the $(i, j)^{th}$ block and thus possesses equatorial symmetry. The primes of the summations in (3.9) and (3.10) indicate absence of the first-degree terms. The inclusion of the zeroeth-degree term is necessitated by the fact that the incomplete set of discrete mean values used gives rise to covariances between $\bar{C}_{oo}^T$ and the rest of the coefficients, which must be taken into account (Pavlis, 1988).

Both observation equations (3.9) and (3.10) are of the form:

$$V = A\hat{X} - L_b \quad . \qquad (3.11)$$

Minimization of the weighted norm of the residuals (V^TPV) under the condition (3.11) yields the normal equation system:

$$(A^TPA)\hat{X} = A^TPL_b \qquad (3.12)$$

and the least-squares estimate $\hat{X}$ is:

$$\hat{X} = (A^TPA)^{-1}A^TPL_b \quad . \qquad (3.13)$$

In the above A is the design matrix, $\hat{X}$ is the vector containing $\bar{C}_{nm}^T$, L_b is the vector of observations $\bar{\Delta}g_{ij}^{(k)}$ (k = 1, 2) and the weight matrix P is defined by:

$$P = \sigma_o^2 \sum_{L_b}^{-1} \qquad (3.14)$$

with σ_o^2 being the a-priori variance of the unit weight (taken to be 1) and Σ_{L_b} the variance-covariance matrix of the observations. The a-posteriori variance of unit weight is given by:

$$\hat{\sigma}_o^2 = \frac{V^TPV}{d.f.} \qquad (3.15)$$

where d.f. are the degrees of freedom, and the variance-covariance matrix of the estimates is:

$$\sum_x = \sigma_o^2 (A^TPA)^{-1} \qquad (3.16)$$

For the purpose of combining the normal equations obtained here with corresponding normals obtained from the analysis of satellite perturbations, as well as with normals from altimeter

measurements, it is critical that Σ_{Lb} properly reflects the accuracy of surface gravity data. However, the inhomogeneity of the data sources based on which global mean anomaly databases are compiled (Kim and Rapp, 1990) makes it difficult to provide realistic estimates of the anomaly error variances, let alone error covariances between the mean values. In addition, consideration even of simplistic models for the error covariances would make the formation of normal equations practically impossible (for degrees of expansion equal to 50 or higher), due to computational limitations. Accordingly, following previous experiences (Rapp and Pavlis, 1990), it was decided to consider a diagonal Σ_{Lb} matrix, but modify the original error estimates for the anomalies in an attempt to compensate for the neglected error covariances. Denoting by σ_{ij}^{O} the standard deviations of the anomalies in SET 1 (which are identical to those in SET 2) and by σ_{ij}^{M} the modified values used to form Σ_{Lb}, the following relationship was imposed:

$$\max(8, 2 \times \sigma_{ij}^{O}) \le \sigma_{ij}^{M} \le \min(16, 2 \times \sigma_{ij}^{O}) \quad . \qquad (3.17)$$

This modification yields a ratio 4 : 1 between maximum and minimum weights used in the adjustment, and approximately corresponds to the weighting scheme used by Rapp and Pavlis (ibid) for 30' x 30' mean anomalies. According to the modification (3.17), the RMS standard deviation of the anomalies input to the adjustment is 13.7 mgal, so that the overall accuracy of either SET 1 or SET 2 remains practically unchanged (see Table 2). With Σ_{Lb} (and thus P) being diagonal, the formation of A^TPA and A^TPL_b can be done efficiently using analytical expressions that avoid the use of matrix algebra, as explained by Pavlis (1988, section 4.2.1).

According to the above, two sets of normal equations were formed using SET 1 and SET 2 as input data respectively. Both normal equation sets correspond to an expansion complete to degree and order 50. From each normal system the corresponding coefficient estimates were computed. These are designated V1 (from SET 1) and V2 (from SET 2). In both cases 2598 unknown coefficients are estimated on the basis of 54048 1° x 1° mean anomalies, so that the degree of freedom (d.f.) is 51450. In Table 3, statistical information related to the solutions V1 and V2 is given.

Table 3. Statistical Information Related to the Gravity Solutions V1, V2 and C1, C2.

		V1	V2	C1	C2
$\hat{\sigma}_o^2$		0.302	0.303	0.354	0.353
Min v_{ij}	(mgal)	-117.8	-117.7	-119.5	-119.3
Max v_{ij}	(mgal)	187.5	187.5	195.2	195.3
Mean v_{ij}	(mgal)	0.0	0.0	0.4	0.2
RMS v_{ij}	(mgal)	7.3	7.3	8.2	8.1
Number of $\lvert v_{ij} \rvert > 7$ mgal		11116	11118	14200	14207
$\bar{k}$		—	—	1.078	1.089

As it can be seen from Table 3, the solutions V1 and V2 are only marginally different (as expected). The average percentage difference between them is 4.4%, while the RMS undulation and anomaly differences are 1.14 m and 0.73 mgal respectively. In Figure 3 the locations of the 11118 residuals from V2 which exceed in magnitude 7 mgal are shown. It is clear from this figure that V2 fits well the input data over well surveyed (gravimetrically) continental areas (North America, Australia, Europe and Africa), while most of the large residuals occur in ocean areas. This is primarily due to the incompatibility between the high-frequency component of the surface

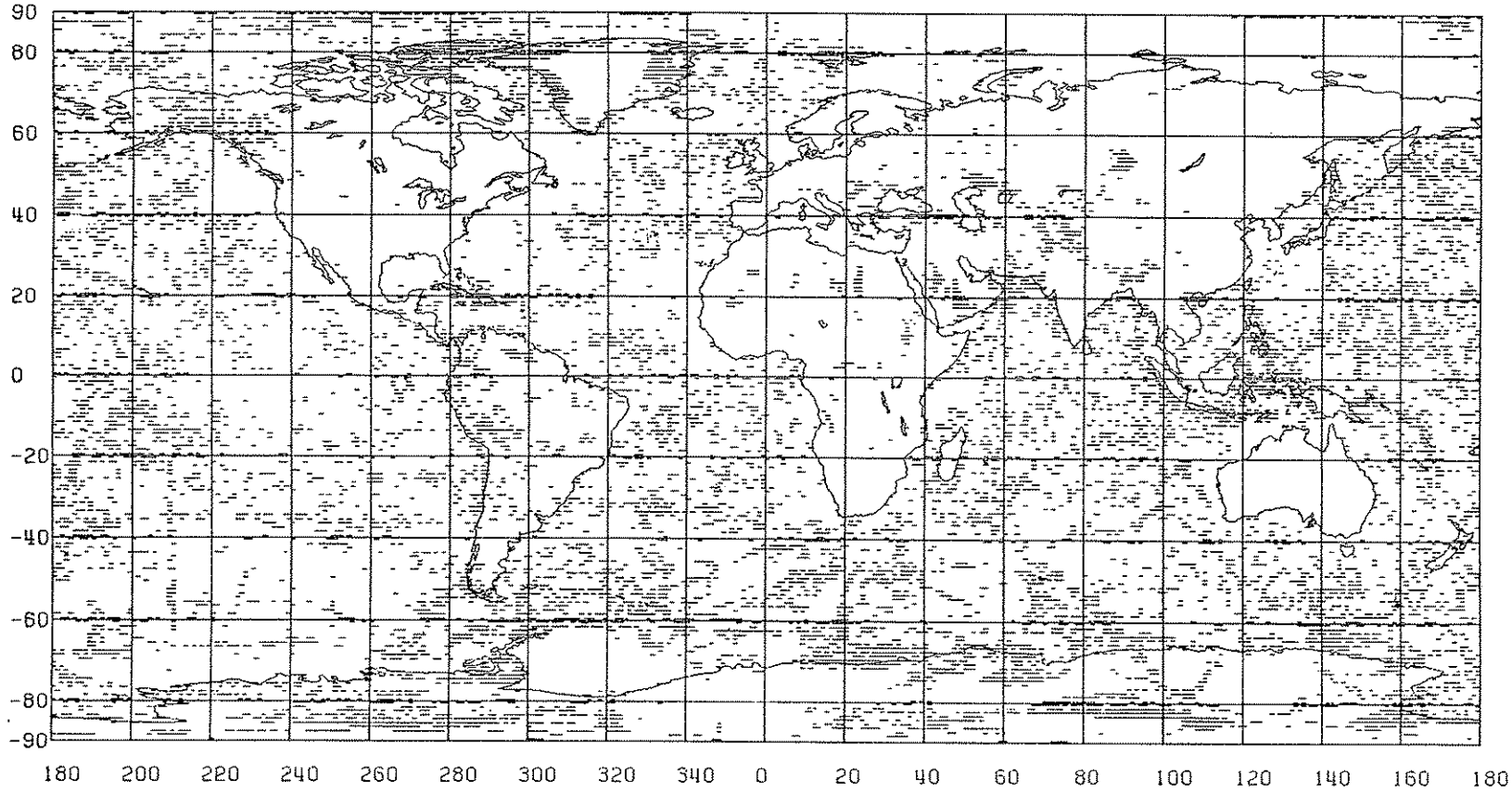

Figure 3. Location of 11118 Residuals From the Solution V2 Whose Magnitude Exceeds 7 mgal.

anomalies over the ocean, with the corresponding component of the altimetry-derived anomalies that are used in the evaluation of the "modified OSU89B" coefficients (see also (Pavlis, 1988)). It should be emphasized here that the residuals from the solutions employing only surface gravity data, represent dominantly a "goodness-of-fit" of the estimated coefficients to the input data. Long-wavelength errors that may be present in the surface anomalies cannot be detected without the incorporation of superior independent information from satellite-derived normals.

The statistical information given in Table 3 does not provide any evidence that may be used to decide which of the two alternative treatments of the input data (surface values or values reduced to the ellipsoid) yields better results. Accordingly, it was decided to compare the results from the two methods in greater detail over areas where:

— High-quality surface gravity data are available
— Significant variation in elevation is present
— Independent information, such as undulations obtained from GPS and leveling are available for comparisons.

However, any comparisons between GPS-derived geoidal undulations and undulations computed from the solutions V1 or V2 may be masked by long-wavelength errors that are present in the surface gravity data. For this reason, as well as for the purpose of testing the compatibility of the solutions V1 and V2 with a satellite-derived model, two preliminary combined solutions were performed whereby the coefficients from V1 and V2 were combined (in a least-squares sense) with the GEM-T2 coefficients (Marsh et al., 1990). The error variance-covariance matrix accompanying each solution was used as weight in order to estimate the "combined" model as a weighted average of the two contributing coefficients sets. The resulting "combined" models are designated C1 (V1 + GEM-T2) and C2 (V2 + GEM - T2). Statistics pertaining to the adjustments that produced C1 and C2 are given in Table 3. As it can be seen the RMS residuals from these adjustments are only by about 10% higher than the corresponding values obtained when fitting the surface gravity data alone. This provides an overall measure of the compatibility between the terrestrial and the satellite implied solutions. In Figure 4, the locations of 14207 residuals from C2, exceeding in magnitude 7 mgal are shown. In this figure extended areas in Asia and South America are identified, where the terrestrial and satellite-implied anomalies are in disagreement. Note that many of these areas cannot be identified in Figure 3, since the residuals from the terrestrial-only solution represent primarily a goodness-of-fit to the data as explained before. As part of the combination adjustments, calibration factors (see Section 4) were also computed, considering the "combined" models versus GEM-T2 as a subset solution. These are given in Table 3 and their values indicate that the weighting scheme used for the surface anomalies, yields satisfactory results. The average percentage difference between the solutions C1 and C2 is 2.7%, while the RMS undulation and anomaly differences are 0.08 m and 0.36 mgal respectively.

Using the harmonic coefficients of the solutions C1 and C2, geoidal undulations were computed next according to:

$$N = \frac{GM}{r\gamma} \sum_{n=2}^{50} \left(\frac{a}{r}\right)^n \sum_{m=-n}^{n} \overline{C}_{nm} \overline{Y}_{nm}(\theta, \lambda) \qquad (3.18)$$

where the notation definitions are given in (Rapp and Pavlis, 1990, pp. 21899-21900). The differences $\Delta N_{12} = N(C1) - N(C2)$ over the areas of Europe and North America are shown in Figures 5 and 6 respectively. From these figures it can be seen that ΔN_{12} are highly correlated with elevation. The signatures of the Alps in Europe and of the Rocky Mountains and Sierra Nevada in North America are clearly identifiable.

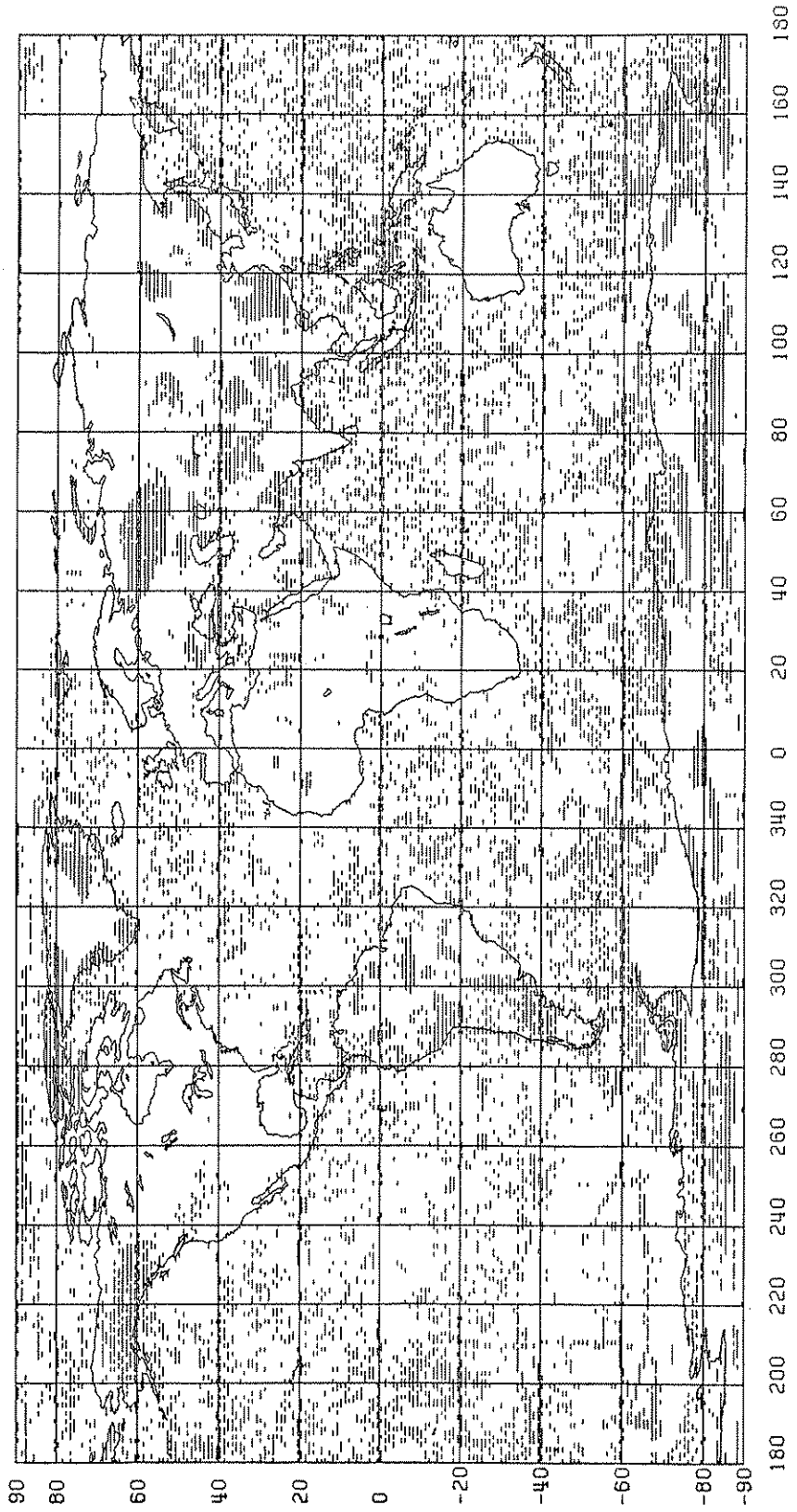

Figure 4. Location of 14207 Residuals From the Solution C2 Whose Magnitude Exceeds 7 mgal.

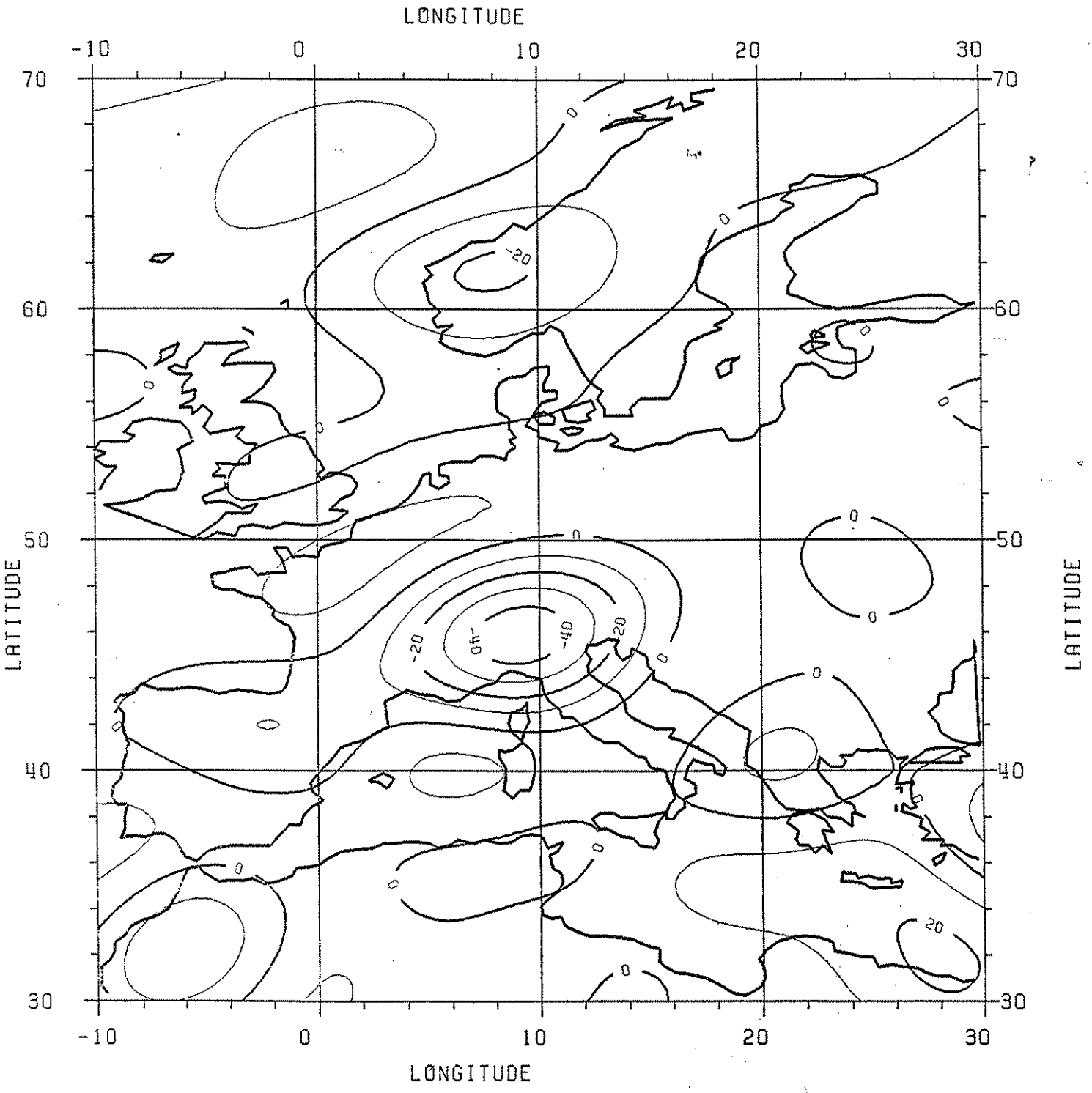

Figure 5. Undulation Differences N(C1) - N(C2) in Europe. Point Values Computed on 1° x 1° Grid and Plotted with Contour Interval CI = 10 cm.

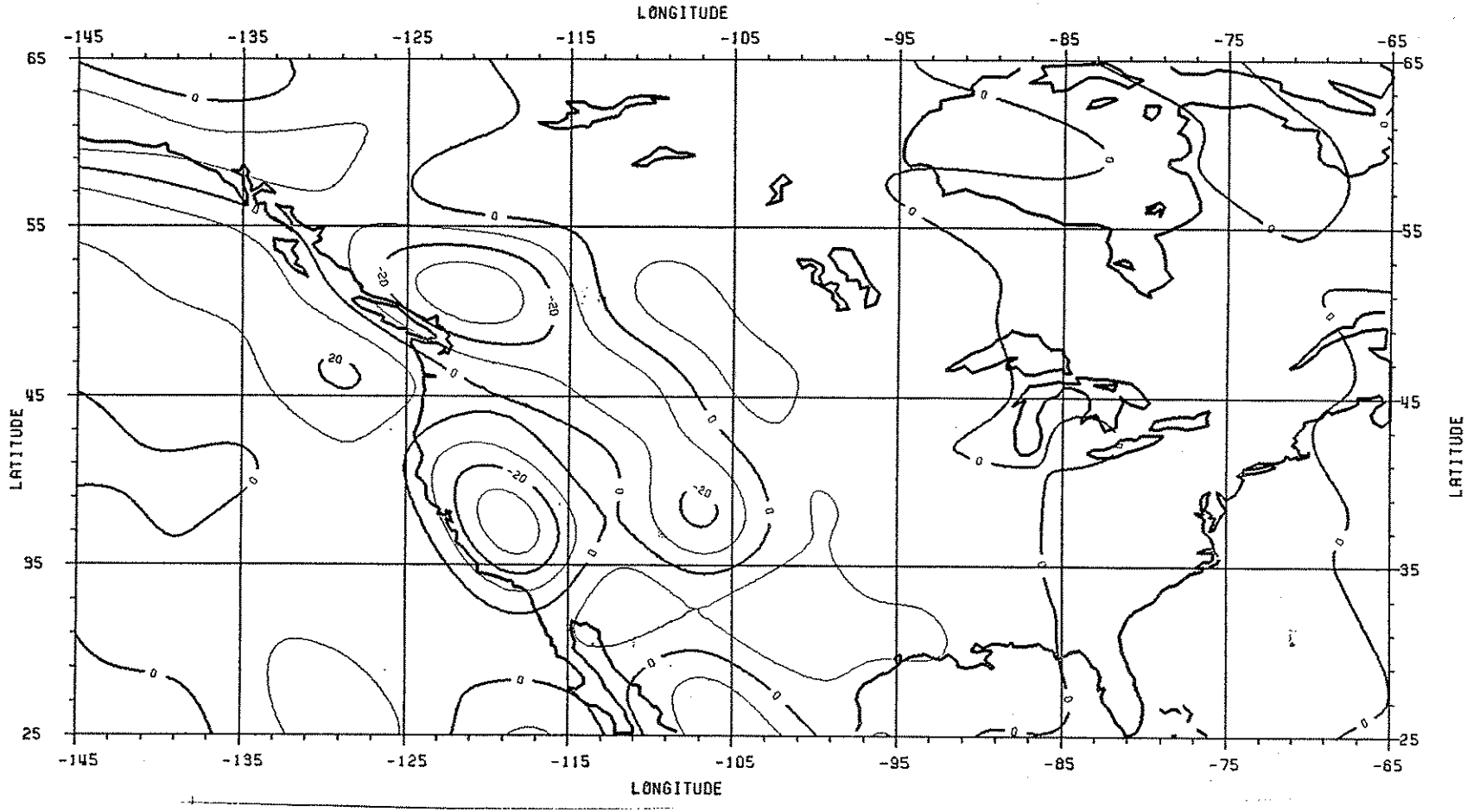

Figure 6. Undulation Differences N(C1) - N(C2) in North America. Point Values Computed on 1° x 1° Grid and Plotted with Contour Interval CI = 10 cm.

In the area of Europe 12 GPS stations forming part of the European GPS traverse (Torge et al., 1989) were selected in the area of interest, in order to compare the geoidal undulations derived from GPS positioning and leveling to the corresponding values obtained from the solutions C1 and C2. For this purpose the contribution to the gravimetric undulation from degree 51 to 360 was computed using the coefficients of the model described in Section 6. The results from these comparisons are summarized in Table 4.

Table 4. Undulation Comparisons at Selected GPS Stations in Europe. $\Delta N_1 = N_{GPS} - N(C1)$, $\Delta N_2 = N_{GPS} - N(C2)$.

Station Number	$\varphi(^\circ)$	$\lambda(^\circ)$	(m) h_{ell}	(m) N_{GPS}	(m) ΔN_1	(m) ΔN_2
1	50.9227	9.7604	250.190	47.64	0.16	0.23
2	50.5089	9.6814	336.324	48.25	0.28	0.31
3	50.2988	10.4542	336.478	47.55	0.28	0.28
4	50.0894	10.9823	318.680	47.04	-0.01	-0.03
5	49.7782	11.0287	299.920	47.09	0.19	0.14
6	49.3477	11.0215	392.799	47.07	0.33	0.23
7	49.0361	11.1316	604.813	47.21	0.72	0.58
8	48.6780	11.5877	439.395	46.56	0.63	0.45
9	48.3248	11.5709	540.154	46.23	0.69	0.47
10	48.0417	11.6324	613.217	46.22	0.85	0.60
11	47.7803	11.7235	804.996	46.94	0.91	0.63
12	47.4901	11.2521	954.553	49.13	1.33	1.00
				Mean Difference	0.53	0.41
				Standard Deviation Diff.	0.37	0.26

From Table 4 it is evident that N(C2) is in better overall agreement with N_{GPS} than N(C1). It is recognized here that the sample of the 12 GPS stations used for the comparisons is too small to support a definitive argument as to wether the surface values or the values continued to the ellipsoid provide a better modeling of the terrestrial anomaly data. The undulation differences between the two alternative solutions, being on the order of 20 to 40 cm over mountainous areas, require very accurate independently derived undulations so that meaningful comparisons can be made. Nevertheless, based on the limited evidence presented here, it was decided that the normal equations formed considering the anomalies continued to the ellipsoid (solution V2) are to be preferred. These normal equations were subsequently used in combination with GEM-T2 and the normals obtained from satellite altimetry, to provide the solutions discussed in section 4.

The combination of two normal equation sets obtained from different data is straight forward in case the two sets were formed using the same approximate values for the unknown parameters (Pavlis, 1988, p. 68). If this is not the case, one of the two sets needs to be "translated" to the approximate values of the second. To illustrate the principle let:

$$N\hat{X} = U \tag{3.19}$$

be the normals obtained here from surface gravity, where:

$$N = A^T P A \quad ; \quad U = A^T P L_b \tag{3.20}$$

These refer to the ellipsoidal even zonal coefficients as approximate values, so that (3.19) can be written as:

$$N\left(\hat{X}_{TOT} - X_{ELL}\right) = U \tag{3.21}$$

where $\hat{X}_{TOT}$ are the adjusted gravitational harmonic coefficients and X_{ELL} the vector containing the values of the even zonal coefficients of the ellipsoidal gravitational potential (and zeroes for the rest of the coefficients present in $\hat{X}_{TOT}$). If X_{T2} contains the values of the coefficients in GEM-T2, equation (3.21) can be written as:

$$N\left[\left(\hat{X}_{TOT} - X_{T2}\right) + \left(X_{T2} - X_{ELL}\right)\right] = U \tag{3.22}$$

or:

$$N\left(\hat{X}_{TOT} - X_{T2}\right) = U - N\left(X_{T2} - X_{ELL}\right) \tag{3.23}$$

so that, to refer the normals (3.21) to the GEM-T2 approximate values the vector U needs to be "translated" by - $N(X_{T2} - X_{ELL})$. The principle (obviously) applies to any change of approximate values.

4.0 The Initial Combination Solutions to Obtain a Potential Coefficient Model to Degree 50

The general least squares adjustment procedure, with a priori parameter weights, was used in the estimation of the unknowns. The equations are described in Rapp and Pavlis (1990, p. 21, 889). For this discussion we define the normal equation form as follows:

$$N = A^T P A \tag{4.1}$$

where A is the design matrix and P is the weight matrix assumed here to be a diagonal matrix. We have two types of normal equations: one from the altimeter data, N_A; the other from surface gravity data, N_G. The solution vector (actually the correction vector to the a priori parameter values) is:

$$V_X = - (N_A + N_G + P_{T2} + P_X)^{-1}(U_A + U_G) \tag{4.2}$$

where P_{T2} is the inverse of the error covariance of the GEM-T2 potential coefficient model, P_X are the a priori weights on the selected parameters of the adjustment. U_A and U_G are the misclosure vectors.

In our adjustment the a priori weights were used in two cases: 1) sea surface topography coefficients and 2) potential coefficients not included in GEM-T2. In the sea surface topography coefficients we need to fix (see discussion in Denker and Rapp, 1990, p. 13,158) the degree 1, 0 term. This term can not be separated from the 1-cy/rev orbit correction term and therefore we fix the value at an oceanographic estimate. This values is 0.1297 m based on the harmonic analysis of the Levitus sea surface topography by Engelis (1987b, Table 1, p. 28, Ocean Solution to Degree 10). The initial value of the other coefficients were taken as zero with standard deviations (to degree 10) based on the root mean square coefficient implied by the ocean solution. For SST solutions to degree 15 the standard deviation for coefficients from degree 11 to 15 was taken to be the same as that at degree 10. The standard deviations used are given in Table 5. Also included in this table are the standard deviations implied by the SST signal model given by Nerem et al (1990a, eq. 20). With the exception of degree 1, the standard deviations used in this paper are roughly 50% larger than used by Nerem et al. This simply implies that we put less of a constraint on our SST estimates than was described in the Nerem et al study.

Table 5. A Priori Standard Deviations for Each SST Harmonic Coefficient (Unit = cm)

Degree	This Paper	Nerem
1	12.8	19.0
2	22.4*	7.88
3	10.5	4.71
4	6.41	3.27
5	6.22	2.46
6	6.36	1.95
7	4.35	1.61
8	2.66	1.35
9	2.29	1.17
10	1.31	1.02
11	1.31	
12	1.31	
13	1.31	
14	1.31	
15	1.31	

* based on a degree variance of 2500 cm^2.

A priori estimates for the C_{21} and S_{21} potential coefficients were also included. These coefficients were not incorporated in the altimeter observation equations but they were in the gravity anomaly observation equations. Consequently the gravity normal equations have such coefficients and correlations do exist between these coefficients and others in the solution. To force the final $C_{2,1}$ and $S_{2,1}$ coefficients to be zero a high weight was assigned to force the zero a priori value.

This analysis used one year of Geosat data represented by 22 ERMs. Since each ERM represents the same geographic region, the use of 22 ERMs would cause a disproportionate fit of the model to the altimeter data. Consequently a down weighting of the altimeter data is needed to assume a balanced solution. The down weighting problem was discussed by Denker and Rapp (1990, p. 13,156).

Initial combination solutions were made with down weighting factors of 1/24 and 1/96 using the initial V1 surface gravity normal equation set as described in Section 3. Solutions were made with sea surface topography expansions to degree 10 and 15. Using the improved V2 gravity normal equations sea surface topography solutions to degree 10 and 15 were also made with the 1/24 and 1/96 down weighting of the altimeter normal equations. Table 6 defines the various solutions made for this study.

Table 6. Designation of One Year Solutions

Solution	SST(max)	Alt. Weights	Surface Normals
FYS10.W24GV	10	1/24	V1
FYS10.W96GV	10	1/96	V1
FYS15.W24GV	15	1/24	V1
FYS10.W24GW	10	1/24	V2
FYS10.W96GW	10	1/96	V2
FYS15.W96GW	15	1/96	V2

As noted in Section 3 the solutions corresponding to the V1 normal equation set were found slightly poorer in several tests than the V2 solution. Therefore, in subsequent analysis our results will primarily refer to the V2 solution.

We first compare the effect of the altimeter down weighting factor on the corrections to residual sea surface heights, geoid undulation corrections, crossover discrepancies, etc. Results for six arcs out of the 76 used are shown in Table 7. All values are given for the solution of sea surface topography to degree 10. In this table ζ is the root mean square sea surface height implied by the harmonic coefficients and Δh (residual) is the root mean square residual of the altimeter measurement observation equation, eq. 2.2.

Table 7 can be compared to Table 4 in Denker and Rapp (1990). The comparison will show that the value of $\Delta h_G + \Delta h_I$ has been reduced in this new solution by about 30% and ΔN_G has been reduced by 51%. The sea surface topography, rms residuals, and rms crossover discrepancies are all comparable in both solutions. We also see from Table 7 that the results are insensitive to the 1/24 or 1/96 weighting scheme. We do see a small (1 cm) increase in the Δh (residual) and crossover discrepancy when going from the 1/24 to 1/96 weighting. The increase is expected; the small rms is welcome.

Table 7. Root Mean Square Value of Corrections to the Various Terms in the Error Model, and Crossover Discrepancies Based on the Adjusted Orbits and the One Year Solution. Units are cm.

Arc	Solution	$\Delta h_G + \Delta h_I$	ΔN_G	ζ	Δh Model	ΔhResidual	AdjCrossover Diff.
1	S10.W24GW	71	119	64	143	18	19
	S10.W96GW	71	118	63	142	19	20
2	S10.W24GW	82	115	66	149	19	21
	S10.W96GW	81	114	65	149	19	22
3	S10.W24GW	80	117	66	152	18	21
	S10.W96GW	80	117	65	151	19	23
22	S10.W24GW	70	119	81	162	19	21
	S10.W96GW	70	118	81	162	20	22
23	S10.W24GW	73	117	82	161	20	21
	S10.W96GW	72	116	81	161	21	22
24	S10.W24GW	77	117	83	169	18	20
	S10.W96GW	76	116	82	169	19	21

The next comparison was to compare the heights at the one day overlaps in the six day arcs. The results are shown in Table 8 for the degree 10 SST case.

Table 8. Mean and RMS Value of Satellite Height Differences at One Day Overlapping Arc Segments. Units are cm.

		Difference	
Overlap Arcs	Solution	Mean	RMS
1/2	S10.W24GW	2	5
	S10.W96GW	2	5
2/3	S10.W24GW	-4	5
	S10.W96GW	-4	5
22/23	S10.W24GW	-3	4
	S10.W96GW	-3	4
23/24	S10.W24GW	4	6
	S10.W96GW	4	6

This table gives results that indicate there is no sensitivity to the altimeter weighting scheme in the orbit overlap comparisons.

Next we calculated the calibration factors for several solutions with respect to the GEM-T2 model and the standard deviations of the coefficients implied by the error covariance matrix. The calibration factor was introduced by Lerch et al. (1988) and used by various investigators (e.g. Rapp and Pavlis, 1990, p. 21, 898) to calibrate various models. Let ΔF_n be the root mean square (rms) coefficient difference, at degree n, between two potential coefficient models. Specifically:

$$\Delta F_n = \left[\sum_{m=0}^{n} \frac{\Delta C_{nm}^2 + \Delta S_{nm}^2}{N_n} \right]^{1/2} \qquad (4.3)$$

where N_n is the number of coefficients at degree n. The rms coefficient error at degree n, for the solution case would be:

$$\sigma_n = \left[\sum_{m=0}^{n} \frac{\sigma^2_{(C_{nm})} + \sigma^2_{(S_{nm})}}{N_n} \right]^{1/2} \tag{4.4}$$

with a similar expression, σ_n^*, for the GEM-T2 model. We define a term ℓ_n^* as follows:

$$\ell_n^2 = \sigma_n^{*2} - \sigma_n^2 \tag{4.5}$$

For a given degree the calibration factor is:

$$k_n = \Delta F_n / \ell_n \tag{4.6}$$

The average calibration factor is:

$$\bar{k} = \frac{1}{N^*} \sum_{n=2}^{50} N_n k_n \tag{4.7}$$

Values of $\bar{k}$ are given in Table 9.

Table 9. Calibration Factors ($\bar{k}$)

Solution	Value
FYS10.W24GW	1.16
FYS15.W24GW	1.15
FYS10.W96GW	1.14

The values in Table 9 indicate the low sensitivity of the calibration factor to the altimeter weighting factor. Assuming the weighting procedures used in the solution are appropriate, the value of $\bar{k}$ = 1.14 indicates the standard deviations implied by the GEM-T2 error covariance matrix may be slightly optimistic. (Recall that the ideal value of $\bar{k}$ would be one.)

In order to further investigate the impact of the different altimeter weighting procedures the standard errors of the geoid undulations and sea surface topography were computed. This was done by calculating the propagated error in the parameters of the solution to the undulation error and the sea surface topography error on a 3°6 grid. The root mean square error was calculated for land and ocean areas. An ocean area was defined to be where $-70° \leq \phi \leq 70°$ and $h < -200$ m, using a 30' x 30' elevation file. The results are given in Table 10 for geoid undulation and Table 16 in Section 5 for sea surface topography. Also shown are global averages computed from the gridded values and the error degree variances. These two values will be similar but not identical since the use of the error degree variance approach neglects the error correlation of the coefficients.

Table 10. Standard Error of Geoid Undulation Based on Selected Degree 50 Combination Solutions. Units are cm.

Solution	Ocean	Land	Global	Through Degree Variances
FYS10.W24GW	9.6	36.5	23.2	21.9
FYS10.W96GW	14.2	39.4	26.2	24.8

From Table 10 we see that the undulation error in the ocean areas is 26% of the undulation error in the land areas. The use of the 1/96 weighting procedure increases the undulation error from 9.6 cm (1/24 case) to 14.2 cm. A smaller percentage change is seen for the undulation error

on land. Also note that the error computed through the degree variances is slightly (6%) smaller than when the more rigorous approach is used.

A comparison was made of the geoid undulations implied by the 1/24 and 1/96 weighting solutions. The differences are shown in Table 11.

Table 11. Comparison of Geoid Undulations Implied by the FYS10.W96GW and FYS10.W24GW Solution to Degree 50. Units are in cm.

	Ocean	Land	Global
RMS Dif.	6.4	22.3	14
Minimum Dif.	-61.4	-92.6	-92.6
Maximum Dif.	43.0	94.7	94.7

The RMS differences seen in this table are quite consistent with the standard errors of the solutions seen from Table 10. Of interest is how the weight changes on the altimeter data effect the undulations on land.

At this point several external evaluations were carried out to help in the selection of the preferred altimeter weighting scheme. A complete discussion of external comparisons will be made in Section 8 but two pertinent comparisons will be addressed here. In these comparisons, the degree 50 potential coefficient model (W96GW or W24GW) was augmented by the coefficients of the OSU89B model from degree 51 to 360.

The first comparison was with geoid undulations computed at the GPS stations described in Rapp and Pavlis (ibid, p. 21,900-21,901). Table 12 shows the standard deviation of the undulation difference (GPS derived minus model) for the two different weighting procedures.

Table 12. Standard Deviation of GPS/Leveling Implied Geoid Undulation Minus Model Geoid Undulation for Two Altimeter Weighting Procedures. Units are cm.

	Model	
Traverse	FYS10.W24GW	FYS10.W96GW
Europe	37	34
Canada	37	37
Australia	39	35
Scandinavia	35	32
Tennessee	24	21

The values given in Table 12 imply the 1/96 weighting gives slightly better comparisons at the GPS sites. Examination of geoid undulation difference maps showed differences that could reach 95 cm although the rms undulation difference between the two solutions was 14 cm.

The next test involved the comparison of the geoid undulation implied by a Geosat ERM with the undulation implied by the geopotential model. The comparison is generally described by Rapp and Pavlis (ibid, Section 4.4). In the comparison to be described here the satellite orbits and sea surface topography to degree 10 were implied by a preliminary solution with a 1/24 weight. Table 13 shows these comparisons for 768286 points on approximately ERM 7.

Table 13. Comparison of Potential Model and Altimeter Implied Geoid Undulations

	Model	
	FYS10.W24GW	FYS10.W96GW
Std. Dev.	33.2 cm	34.0 cm
No. ≥ 1.5 m	4149	4386
No. ≥ 2.0 m	1326	1437

The numerical results indicate a slightly poorer fit when the 1/96 weighting was used. This is clearly expected but the only very slight deterioration indicates the 1/96 can be used without any significant deterioration of the altimeter fits.

Taking into account the information given in the past several tables the 1/96 weighting procedure was selected to be that used for the OSU91A solution. The main reason for the selection was related to the increased undulation discrepancies at the GPS stations when using the 1/24 procedure. This, coupled with the only slight altimeter fit deterioration when the 1/96 weights were used, led to the 1/96 weighting procedure for the final solution.

Figure 7 shows the geoid undulation commission error implied by the FYS10.W96GW solution. This map can be compared to Figure 8 in Denker and Rapp (ibid) or Figure 11 of Rapp and Pavlis (ibid). However it should be noted that the Figure 7 map reflects the errors in the complete degree 50 model while the other figures were based on coefficients to degree 36 that were in the GEM-T1 model. We see from this figure the significantly improved accuracy in the ocean areas as compared to the land. This, of course, was also apparent, from Table 10. The geoid accuracy in the well surveyed (gravimetrically) areas (U.S., Europe, Australia) is on the order of 30 cm while the accuracy is 50 to 60 cm in the poorer areas. Of obvious note is the smaller errors in the polar regions despite the fact that data coverage is sparse. A reasonable explanation for why this error is lower is needed. The accuracy by degree, and cumulatively, will be discussed in Section 6. We can repeat, from Table 10, that the global undulation accuracy of the model (1/96) is 26 cm which may be contrasted with 33 cm for the OSU89B model to degree 50 (Rapp and Pavlis, ibid, Table 11).

The bias (or a_0) term in equation (2.4) was examined for all 76 arcs. For the (1/24) weighting the bias was 62.0 ± 2.1 cm while for the (1/96) weighting it was 62.3 ± 2.1 cm indicating no essential bias difference in the weighting schemes. Adopting the (1/96) bias value would imply an equatorial radius of 6378137.00 m minus 0.623 m or 6378136.38 m. The bias values were individually examined and plotted in Figure 8 starting with the first arc. The bias value is plotted at a time associated with the middle of the arc. A cyclic variation with an amplitude of about 2 cm is seen. The data was spectrally analyzed with the spectrum shown in Figure 9. There are two clear lines; one at 2 cycle/year and the other at 22 cycles/year. The first line is associated with a semi-annual variation while the second line is associated with the length (17.05 days) of a Geosat ERM. The key point is to understand why there should be a semi-annual variation in the bias term. Is the variation connected with seasonal pressure changes on the oceans; is it associated with changes in the tropospheric corrections; do seasonal winds play a role; are there tide errors with a semi-annual signal; etc. Additional study is needed to explain the bias variation.

This Section has examined the first stage in our development of a geopotential model to degree 50, a sea surface topography model to degree 10, and orbit correction parameters for 76 Geosat arcs covering the first year of the ERM. Different weighting procedures were tested, evaluated, and selected for further use. The root mean square rms residual for the altimeter observation was typically ± 19 cm with the rms crossover discrepancy being on the order of ± 22

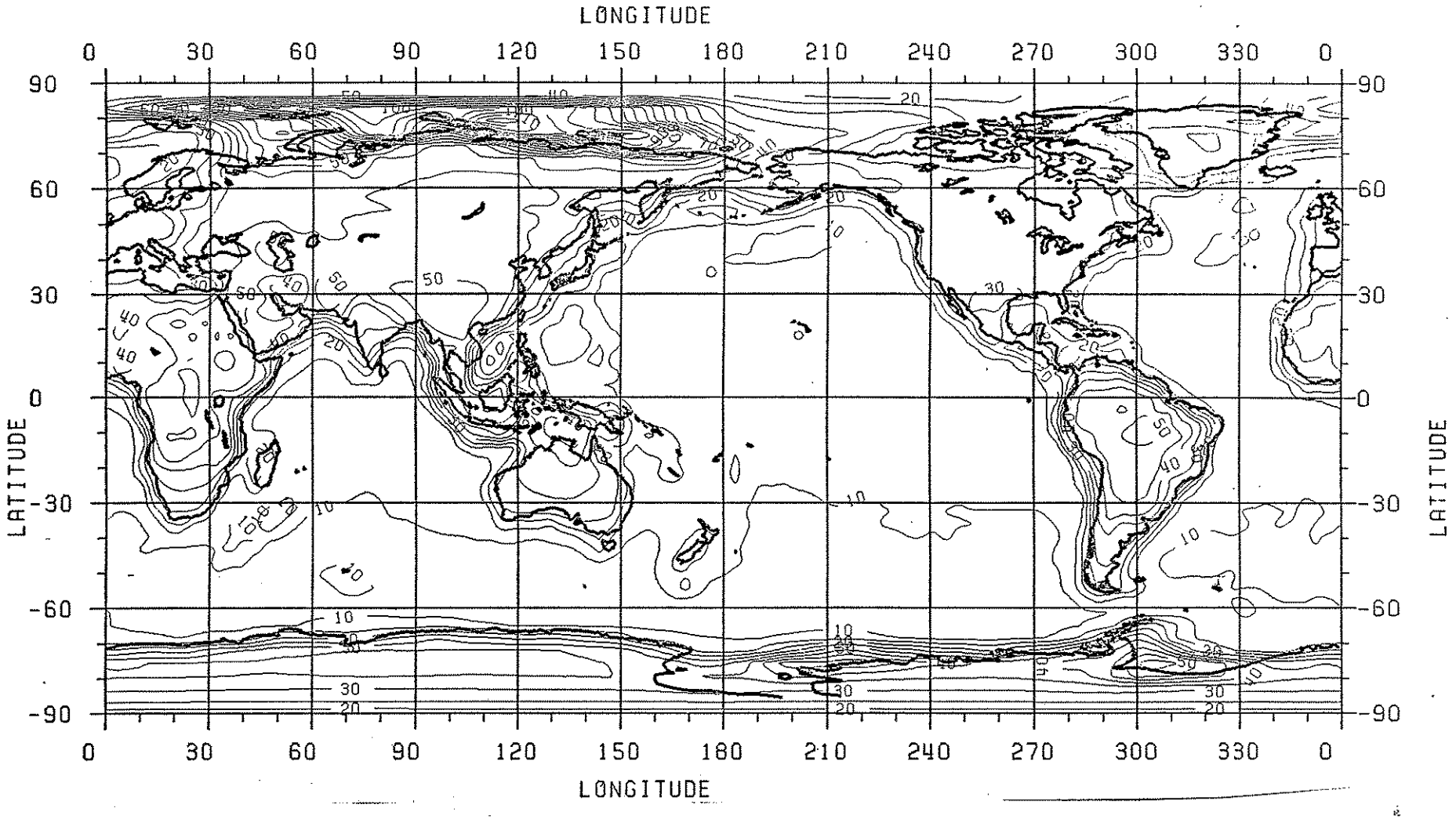

Figure 7. Geoid Undulation Standard Deviation Implied by the FYS10.W96GW Solution. Contour Interval is 5 cm with Data Given on a 3°.6 Grid.

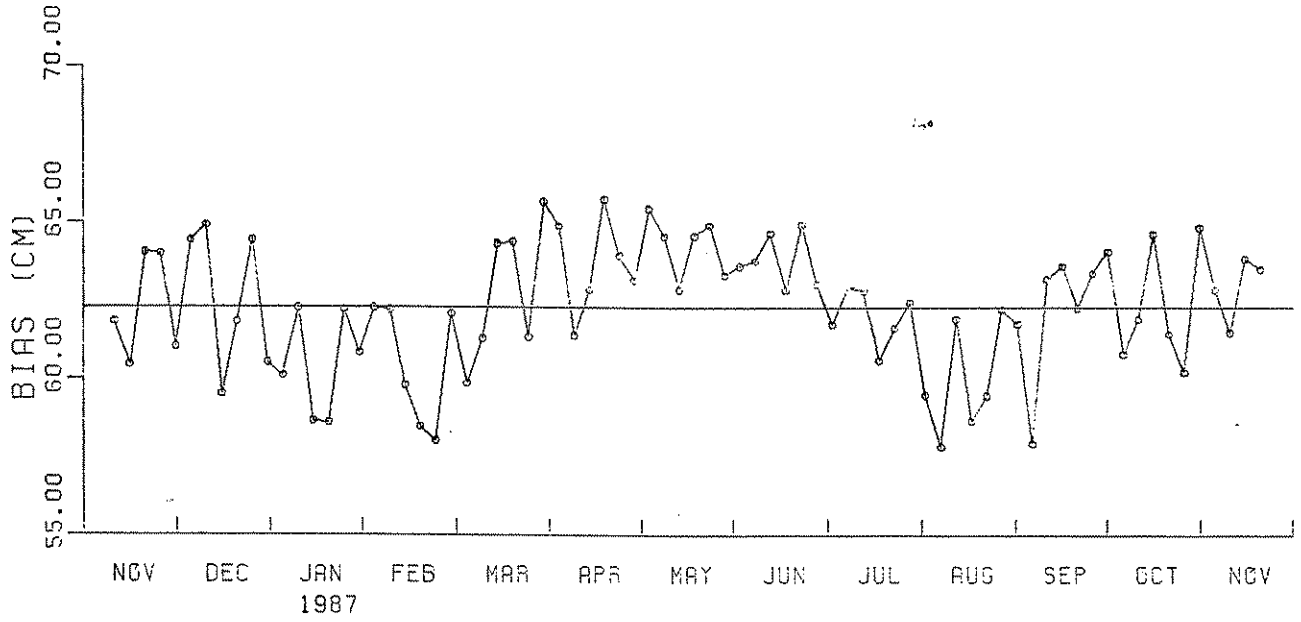

Figure 8. Geosat Bias Term (a_0) for 76 Arcs Based on the FYS10.W96GW Solution.

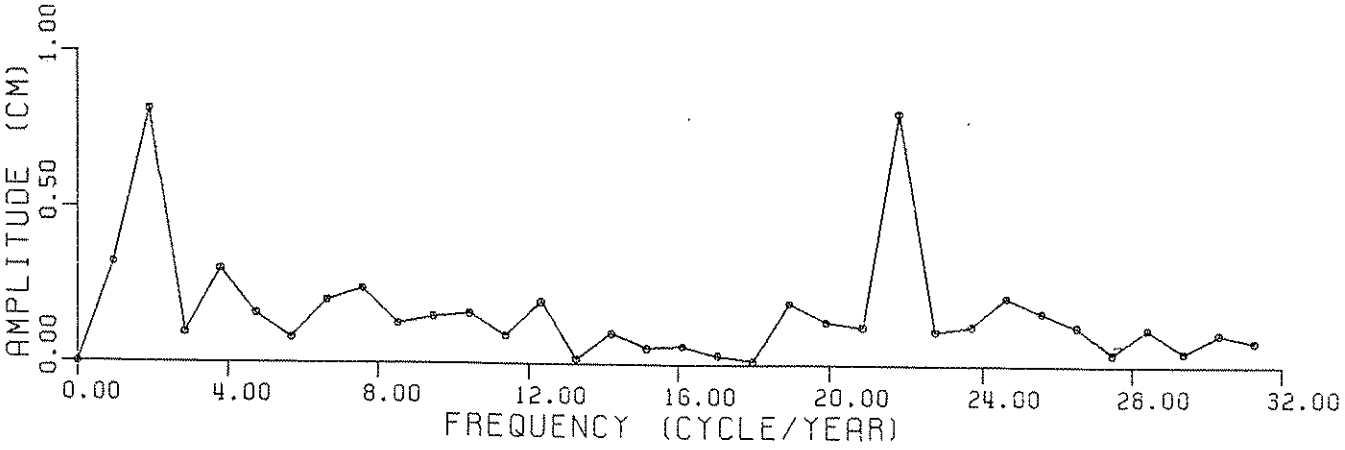

Figure 9. Spectrum of Geosat Bias Terms for the 76 Arcs Used in the FYS10.W96GW Solution.

cm. This is a considerable improvement from the 49 cm crossover discrepancies associated with the original GEM-T2 orbits (Haines et al, 1990, p. 2884). In the next section we consider details of the sea surface topography solutions.

5.0 The Sea Surface Topography Representations

5.1 The One Year Average

As noted in the previous section a number of solutions for sea surface topography were made. Expansions to degree 10 and degree 15 were made with our final altimeter weighting scheme of 1/96. For each solution the degree (1, 0) term was fixed at the value implied by the Engelis harmonic analysis of the Levitus SST information. The harmonic coefficients and their standard deviation are given in Table 14 for the degree 10 and Table 15 for the degree 15 solution.

In Figures 10 and 11 the sea surface topography for the degree 10 and degree 15 solution are given. Figure 10 can be compared to Figure 6 Denker and Rapp (1990). The essential difference between the two is that the solution of this report shows a reasonable slope across the northern Pacific Ocean, while the Denker/Rapp initial solution did not. In order to achieve a reasonable slope, Denker/Rapp were forced to fix the degree (1, 1) harmonics at oceanographically implied values. In the current solution no such fixing is required. This does imply that the GEM-T2 orbits, with a consistent gravity model and geocentric station set, yields better long wavelength oceanographic information than the GEM-T1 orbits.

Another difference between the 10, 10 solution of this paper and the Denker/Rapp solution is the high near 0° latitude, and 210° longitude. This high was not apparent in Denker/Rapp but it has been seen in the solutions (PGS3853) of Nerem et al. (1990).

The geostrophic currents implied by the degree 10 solution are shown in Figure 12. This map can be compared to Plate 1 of Denker and Rapp (ibid) where similarities exist but numerous differences can be seen. For example, the California current is more reasonably represented on the newer map than the earlier version. There is a complex circulation pattern around latitude 0° and longitude 210°. The solution is finding it difficult to separate the North Equatorial Current from the Equatorial Counter Current. This is not unreasonable since a degree 10 solution corresponds to a linear resolution of 1998 km. Other major currents (e.q. Kuroshio Current, Mozambique Current, Gulf Stream (in a broad sense), South Equatorial Current, Brazil Current, Antarctic Circumpolar Current, etc.) are evident from the flow map. However there is no sign of the Agulhas Current off the south tip of Africa. The degree 15 flow vector map shows more detail than seen in Figure 12. However these details are fragmented and not quite believable. For the record it is shown as Figure 13.

We have examined in greater detail sea surface topography implied by the degree 10 solution in the Mediterranean Sea. Figure 14 shows the SST with a 10 cm contour interval. This figure shows a decrease of the SST in a northeast direction. The maximum change in SST in the Mediterranean Sea, from Africa ($\phi = 31°$, $\lambda = 18°$) to the north end of the Agean Sea is 98 cm. From the entrance to the Mediterranean to the north end of the Agean Sea, the SST difference is 94 cm.

Figure 14 may be compared to Figure 31 of Lisitzin (1974) which displays the mean sea level in the Mediterranean Sea. The slope pattern follows quite well that shown in Figure 14. For example, the mean sea level change from the entrance to the Mediterranean to the Agean Sea is 80 cm (Agean is lower). This compares well with the 94 cm found in this study.

We have evaluated sea surface topography estimates from several other harmonic models in the Mediterranean Sea. None show patterns resembling the Lisitzin result. This is because there SST solutions did not incorporate any data form the Mediterranean region in their solution.

Table 14. Sea Surface Topography Harmonic Coefficients and Their Standard Deviation Implied by the First Year of the ERM. Degree 10 Model. Units are meters.

n	m	c	s	σ(c)	σ(s)
1	0	0.1297		0.0010	
2	0	-0.4933		0.0341	
3	0	0.1667		0.0292	
4	0	-0.0582		0.0277	
5	0	0.1045		0.0257	
6	0	0.1818		0.0229	
7	0	-0.0312		0.0189	
8	0	0.0466		0.0150	
9	0	-0.0374		0.0119	
10	0	0.0101		0.0090	
1	1	-0.1550	-0.0978	0.0268	0.0333
2	1	-0.0628	0.0366	0.0173	0.0409
3	1	-0.0415	-0.0308	0.0179	0.0392
4	1	0.0231	0.0015	0.0185	0.0305
5	1	-0.0056	0.0149	0.0160	0.0273
6	1	0.0294	0.0119	0.0164	0.0241
7	1	0.0912	0.0290	0.0142	0.0205
8	1	-0.0559	-0.0389	0.0119	0.0160
9	1	0.0217	0.0429	0.0117	0.0140
10	1	0.0372	-0.0224	0.0084	0.0095
2	2	0.0106	0.0324	0.0200	0.0181
3	2	0.0329	-0.0511	0.0281	0.0209
4	2	-0.0104	-0.0400	0.0293	0.0216
5	2	0.0107	-0.0024	0.0255	0.0206
6	2	-0.0008	0.0188	0.0208	0.0181
7	2	0.0285	0.0302	0.0172	0.0158
8	2	-0.0028	0.0145	0.0144	0.0134
9	2	0.0000	-0.0267	0.0123	0.0118
10	2	-0.0207	0.0017	0.0095	0.0093
3	3	-0.0174	-0.0269	0.0165	0.0177
4	3	0.0282	-0.0107	0.0191	0.0203
5	3	0.0077	-0.0266	0.0204	0.0221
6	3	0.0156	-0.0718	0.0189	0.0207
7	3	0.0255	-0.0356	0.0153	0.0163
8	3	0.0201	0.0064	0.0127	0.0132
9	3	-0.0343	0.0282	0.0116	0.0117
10	3	0.0074	0.0150	0.0084	0.0082
4	4	-0.0048	-0.0265	0.0134	0.0157
5	4	-0.0337	0.0180	0.0170	0.0162
6	4	-0.0014	-0.0094	0.0166	0.0170
7	4	0.0179	-0.0229	0.0151	0.0159
8	4	0.0319	-0.0162	0.0124	0.0127
9	4	0.0079	-0.0032	0.0106	0.0106
10	4	0.0108	-0.0168	0.0078	0.0077
5	5	0.0039	0.0050	0.0129	0.0135
6	5	0.0173	0.0029	0.0139	0.0141
7	5	0.0282	0.0024	0.0135	0.0135
8	5	0.0012	0.0054	0.0117	0.0120
9	5	0.0221	-0.0172	0.0101	0.0102
10	5	-0.0117	0.0070	0.0074	0.0075
6	6	0.0109	-0.0179	0.0124	0.0100
7	6	0.0244	0.0161	0.0111	0.0114
8	6	0.0081	-0.0050	0.0101	0.0103
9	6	-0.0049	-0.0056	0.0092	0.0090
10	6	-0.0092	0.0121	0.0068	0.0066
7	7	0.0205	0.0056	0.0099	0.0086
8	7	-0.0060	0.0053	0.0097	0.0090
9	7	0.0018	0.0098	0.0083	0.0081
10	7	-0.0013	0.0065	0.0065	0.0062

8	8	-0.0030	0.0151	0.0085	0.0081
9	8	0.0024	0.0075	0.0079	0.0082
10	8	-0.0180	0.0103	0.0060	0.0060
9	9	0.0098	0.0108	0.0074	0.0074
10	9	-0.0094	0.0165	0.0063	0.0060
10	10	0.0135	-0.0012	0.0064	0.0069

The standard error of the sea surface topography is shown for the degree 10 solution in Figure 15. This map is comparable to Figure 9 of Denker/Rapp. From this figure we see that the standard deviation is fairly uniform over the oceans, increasing as one approaches land areas. The standard error of the SST has been computed in the ocean areas ($-70° \le \phi \le 70°$); $h < -200$ m) for three solutions developed for this report. There values are shown in Table 16.

Table 16. Standard Error of Sea Surface Topography in the Ocean Areas. Units are cm.

Solution	Standard Deviation	Through Deg Variances
FYS10.W24GW	±7.0	14.9
FYS10.W96GW	8.4	16.6
FYS15.W96GW	11.6	20.6

From Table 16 we see that the standard deviation of the sea surface topography in the ocean areas increases from 7.0 cm with the 1/24 weighting to 8.4 cm with the 1/96 weighting (for the degree 10 case). These values are approximately 50% of that found through the error degree varianced. Recall that the error degree variances reflect the higher standard deviations in the land areas. The error for the 15, 15 solution is higher because twice as many coefficients are included in the degree 15 model.

It is usual to plot the power spectrum of the sea surface topography and compare it to corresponding error (SST and geoid) spectra. Denker and Rapp (1990) have pointed out serious limitations of this process since the SST is defined only over the oceans. Nevertheless, for continuity purposes we show in Figure 16, the square root of the power spectra of the two sea surface topography solutions, as well as the errors, by degree, of these models and the geoid undulation errors that are part of solution leading to the degree 10 SST model.

From Figure 16 we see that up to degree 6, the spectrum from the degree 15 solution is less than that of the degree 10 solution. For example, at degree 10, the signal from the degree 10 solution is 6.9 cm while it is (at the same degree) 5.0 cm from the degree 15 solution. This suggests some spectral leakage from the higher harmonics into the lower harmonics. After degree 10, the signal from the degree 15 solution is nearly flat.

The degree errors of the degree 15 solution are always greater than the degree 10 solution. At degree 10, it is 30% higher. The geoid undulation error is always smaller than the signal suggesting that SST determination out to degree 15 could be made. However the discussion in Denker and Rapp (1990, p. 13,157) notes the high negative correlation between the SST coefficients and the potential coefficients (geoid information) between degree 10 and 15. This case would still exist for the solutions described in this report.

We next examine the second degree zonal harmonic of sea surface topography. In principle this harmonic is independent of the tidal (non-tidal, zero, mean) reference system, if the sea surface and geoid are consistently treated. Some papers, however, have published $c_{2,0}$ values in non-consistent systems. However, knowing the system, one can convert to a common system. Some of the conversion procedures are described in Rapp (1989). Other solutions are described in Nerem et al (1990, p. 3167) and Marsh et al. (1990, p. 13,143). The SST coefficients given in

Table 15. Sea Surface Topography Harmonic Coefficients and Their Standard Deviation Implied by the First Year of the ERM. Degree 15 Model. Units are meters.

n	m	c	s	σ(c)	σ(s)
1	0	0.1297		0.0010	
2	0	-0.5173		0.0375	
3	0	0.1899		0.0328	
4	0	-0.0761		0.0300	
5	0	0.1070		0.0288	
6	0	0.1659		0.0252	
7	0	-0.0188		0.0222	
8	0	0.0186		0.0175	
9	0	-0.0351		0.0154	
10	0	0.0099		0.0108	
11	0	0.0029		0.0101	
12	0	-0.0125		0.0090	
13	0	-0.0009		0.0084	
14	0	-0.0008		0.0082	
15	0	0.0007		0.0077	
1	1	-0.1540	-0.0913	0.0286	0.0350
2	1	-0.0585	0.0207	0.0190	0.0428
3	1	-0.0455	-0.0410	0.0199	0.0411
4	1	0.0320	0.0148	0.0203	0.0319
5	1	-0.0108	0.0055	0.0178	0.0288
6	1	0.0243	0.0265	0.0179	0.0258
7	1	0.0685	0.0251	0.0176	0.0232
8	1	-0.0380	-0.0356	0.0146	0.0180
9	1	0.0206	0.0151	0.0143	0.0166
10	1	0.0259	-0.0020	0.0103	0.0111
11	1	-0.0108	-0.0022	0.0101	0.0108
12	1	0.0121	0.0044	0.0092	0.0099
13	1	-0.0034	-0.0186	0.0093	0.0096
14	1	-0.0060	0.0218	0.0084	0.0090
15	1	0.0113	0.0000	0.0079	0.0084
2	2	0.0160	0.0296	0.0223	0.0213
3	2	0.0335	-0.0540	0.0296	0.0227
4	2	0.0036	-0.0381	0.0306	0.0232
5	2	0.0060	0.0009	0.0267	0.0222
6	2	-0.0066	0.0160	0.0221	0.0196
7	2	0.0335	0.0184	0.0193	0.0180
8	2	0.0110	0.0012	0.0163	0.0156
9	2	-0.0207	-0.0170	0.0149	0.0147
10	2	-0.0016	-0.0006	0.0106	0.0105
11	2	0.0182	-0.0072	0.0104	0.0104
12	2	0.0002	-0.0079	0.0092	0.0093
13	2	-0.0105	0.0033	0.0093	0.0093
14	2	0.0218	-0.0080	0.0090	0.0091
15	2	-0.0152	0.0086	0.0091	0.0091
3	3	-0.0143	-0.0185	0.0190	0.0203
4	3	0.0169	-0.0248	0.0209	0.0217
5	3	0.0129	-0.0247	0.0220	0.0234
6	3	0.0096	-0.0575	0.0204	0.0221
7	3	0.0088	-0.0419	0.0173	0.0180
8	3	0.0206	-0.0050	0.0148	0.0150
9	3	-0.0221	0.0240	0.0136	0.0134
10	3	-0.0027	0.0084	0.0104	0.0103
11	3	-0.0025	-0.0084	0.0099	0.0098
12	3	0.0020	0.0021	0.0094	0.0092
13	3	0.0022	0.0056	0.0094	0.0093
14	3	-0.0016	-0.0070	0.0089	0.0087
15	3	0.0119	-0.0046	0.0086	0.0085
4	4	-0.0118	-0.0250	0.0153	0.0186
5	4	-0.0270	0.0105	0.0186	0.0179

6	4	0.0045	-0.0078	0.0178	0.0189
7	4	0.0165	-0.0090	0.0167	0.0175
8	4	0.0272	-0.0126	0.0142	0.0144
9	4	-0.0012	0.0030	0.0126	0.0126
10	4	0.0091	-0.0117	0.0099	0.0099
11	4	0.0035	0.0074	0.0096	0.0095
12	4	0.0041	0.0006	0.0092	0.0093
13	4	-0.0006	0.0099	0.0088	0.0088
14	4	0.0018	-0.0107	0.0086	0.0086
15	4	0.0006	-0.0003	0.0087	0.0087
5	5	0.0076	0.0049	0.0155	0.0159
6	5	0.0163	0.0062	0.0160	0.0160
7	5	0.0323	0.0013	0.0154	0.0152
8	5	0.0065	0.0167	0.0134	0.0137
9	5	0.0216	-0.0171	0.0122	0.0122
10	5	-0.0118	-0.0097	0.0095	0.0095
11	5	-0.0021	-0.0123	0.0092	0.0093
12	5	-0.0080	0.0091	0.0088	0.0087
13	5	0.0015	-0.0017	0.0090	0.0090
14	5	0.0042	0.0035	0.0087	0.0088
15	5	0.0075	0.0008	0.0081	0.0081
6	6	0.0054	-0.0117	0.0154	0.0127
7	6	0.0303	0.0054	0.0136	0.0136
8	6	0.0032	-0.0027	0.0123	0.0121
9	6	-0.0056	0.0016	0.0113	0.0107
10	6	-0.0073	0.0034	0.0091	0.0090
11	6	-0.0059	-0.0063	0.0088	0.0087
12	6	0.0142	-0.0036	0.0084	0.0083
13	6	-0.0018	-0.0034	0.0084	0.0084
14	6	0.0082	-0.0123	0.0079	0.0079
15	6	0.0064	0.0117	0.0080	0.0080
7	7	0.0128	-0.0024	0.0135	0.0120
8	7	0.0106	0.0062	0.0123	0.0112
9	7	0.0011	0.0004	0.0108	0.0106
10	7	-0.0076	0.0009	0.0087	0.0084
11	7	0.0011	0.0010	0.0085	0.0084
12	7	-0.0046	0.0036	0.0079	0.0079
13	7	-0.0012	-0.0066	0.0081	0.0080
14	7	-0.0150	0.0049	0.0080	0.0079
15	7	-0.0120	-0.0098	0.0076	0.0075
8	8	-0.0028	0.0139	0.0120	0.0110
9	8	0.0096	0.0111	0.0102	0.0103
10	8	-0.0190	0.0179	0.0084	0.0081
11	8	-0.0019	0.0031	0.0078	0.0076
12	8	0.0063	0.0054	0.0076	0.0074
13	8	0.0016	0.0034	0.0076	0.0075
14	8	-0.0093	-0.0027	0.0073	0.0072
15	8	0.0017	0.0110	0.0071	0.0070
9	9	0.0116	0.0081	0.0104	0.0104
10	9	-0.0045	0.0181	0.0086	0.0082
11	9	0.0015	0.0031	0.0080	0.0079
12	9	-0.0058	0.0123	0.0071	0.0070
13	9	0.0072	-0.0061	0.0071	0.0071
14	9	-0.0083	0.0012	0.0067	0.0066
15	9	0.0022	-0.0121	0.0069	0.0069
10	10	0.0126	-0.0069	0.0084	0.0089
11	10	-0.0029	0.0069	0.0074	0.0078
12	10	0.0104	-0.0039	0.0069	0.0070
13	10	-0.0052	0.0063	0.0064	0.0063
14	10	0.0033	0.0131	0.0062	0.0062

15	10	0.0015	0.0086	0.0060	0.0060
11	11	0.0019	-0.0092	0.0081	0.0081
12	11	-0.0072	0.0105	0.0070	0.0072
13	11	0.0043	-0.0085	0.0069	0.0069
14	11	0.0029	0.0027	0.0059	0.0059
15	11	-0.0071	-0.0072	0.0057	0.0057
12	12	0.0047	-0.0035	0.0071	0.0071
13	12	-0.0013	0.0095	0.0064	0.0063
14	12	0.0010	-0.0013	0.0059	0.0059
15	12	-0.0032	0.0100	0.0051	0.0051
13	13	0.0074	-0.0022	0.0064	0.0066
14	13	0.0015	0.0020	0.0060	0.0062
15	13	0.0059	-0.0061	0.0051	0.0052
14	14	0.0034	0.0001	0.0061	0.0062
15	14	0.0006	-0.0048	0.0054	0.0053
15	15	0.0140	0.0004	0.0060	0.0061

Table 14 have been derived from a consistent tidal system and no correction term is needed. Table 17 summarizes some determinations of $c_{2,0}$ for SST.

Table 17. The Second Degree Fully Normalized Harmonic Coefficient of Sea Surface Topography. Units are cm.

Solution	Data	Value
Mather (1978)	Geos-3	-43
Mather(1978)	Oceanographic	-46
Engelis (1987)	Oceanographic	-28
Ohio State (1988)	Seasat (17 days)	-47
Marsh et al (1990)	Seasat	-44
Nerem et al (1990)	Geosat (3/17 days)	-33
Denker/Rapp(1990)	Geosat (one year)	-39
Putney et al (1991)	Geosat (3 months)	-34
TEG-2 (1991)	Geosat	-40
This paper	Geosat (one year)	-49

From Table 17 we see there is a wide range of values for this coefficient. The value obtained in this paper is consistent with the ocean results of Mather (1978) and the Ohio State 1988 Seasat (17day) solution carried out by Knudsen (1988, private communication). The value is smaller for the Geosat solution that has used less data than the new Ohio State solution.

5.2 Temporal Variations of the Ocean Surface

The sea surface heights developed from the GEM-T2 improved orbits enables us to study the time variations in the ocean surface. For this paper we will examine the variations in two ways that are described in the next two sections. The study of large scale time variations has been described by Denker (1990, Section 4.4) and Nerem et al. (1990b).

5.2.1 Temporal Variations Through Data Related to the Harmonic Analysis of Sea Surface Topography

The sea surface topography defined so far represents the average over the first year of the ERM mission, November 1986 through October 1987. It is possible to study time variations in this year by creating SST expansions for specific time periods using the altimeter data from the time period. This expansion can be referred to the one year surface by removing the coefficients defined by the one year mean. Then sea surface height differences can be calculated. This

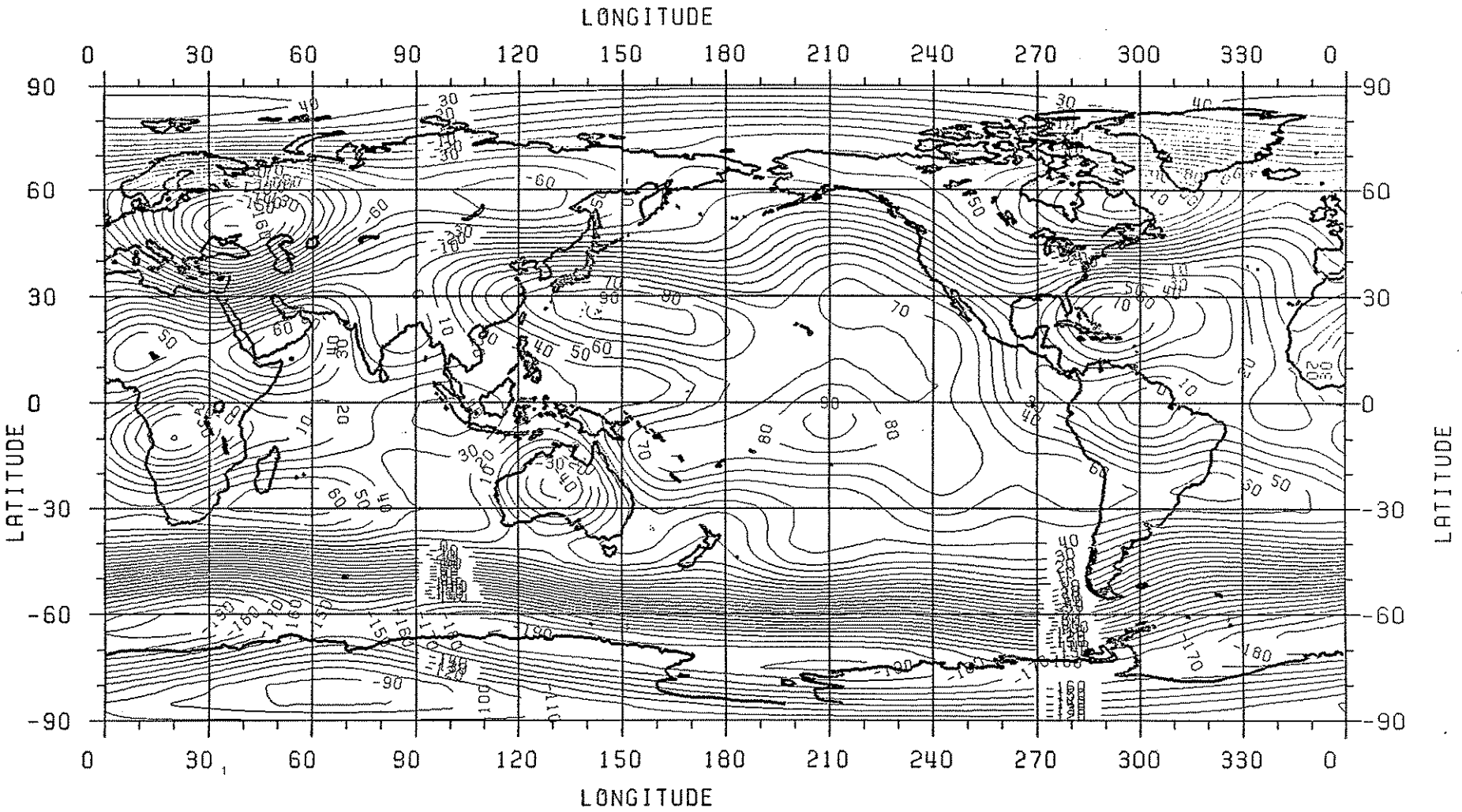

Figure 10. Sea Surface Topography Implied by Degree 10 Solution From One Year (1986/87) of Geosat Data. Contour interval is 10.

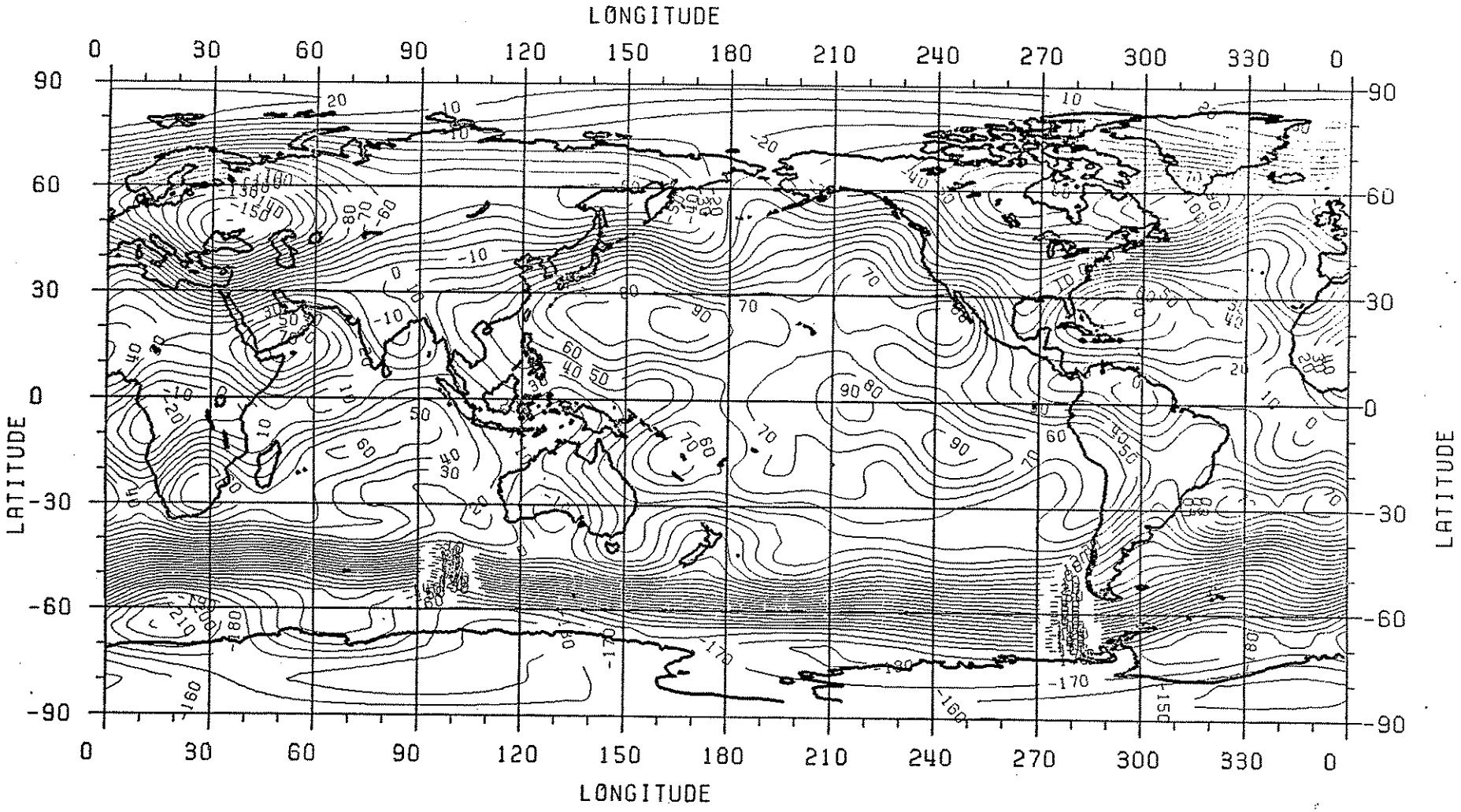

Figure 11. Sea Surface Topography Implied by Degree 15 Solution From One Year (1986/87) of Geosat Data. Contour Interval is 10 cm.

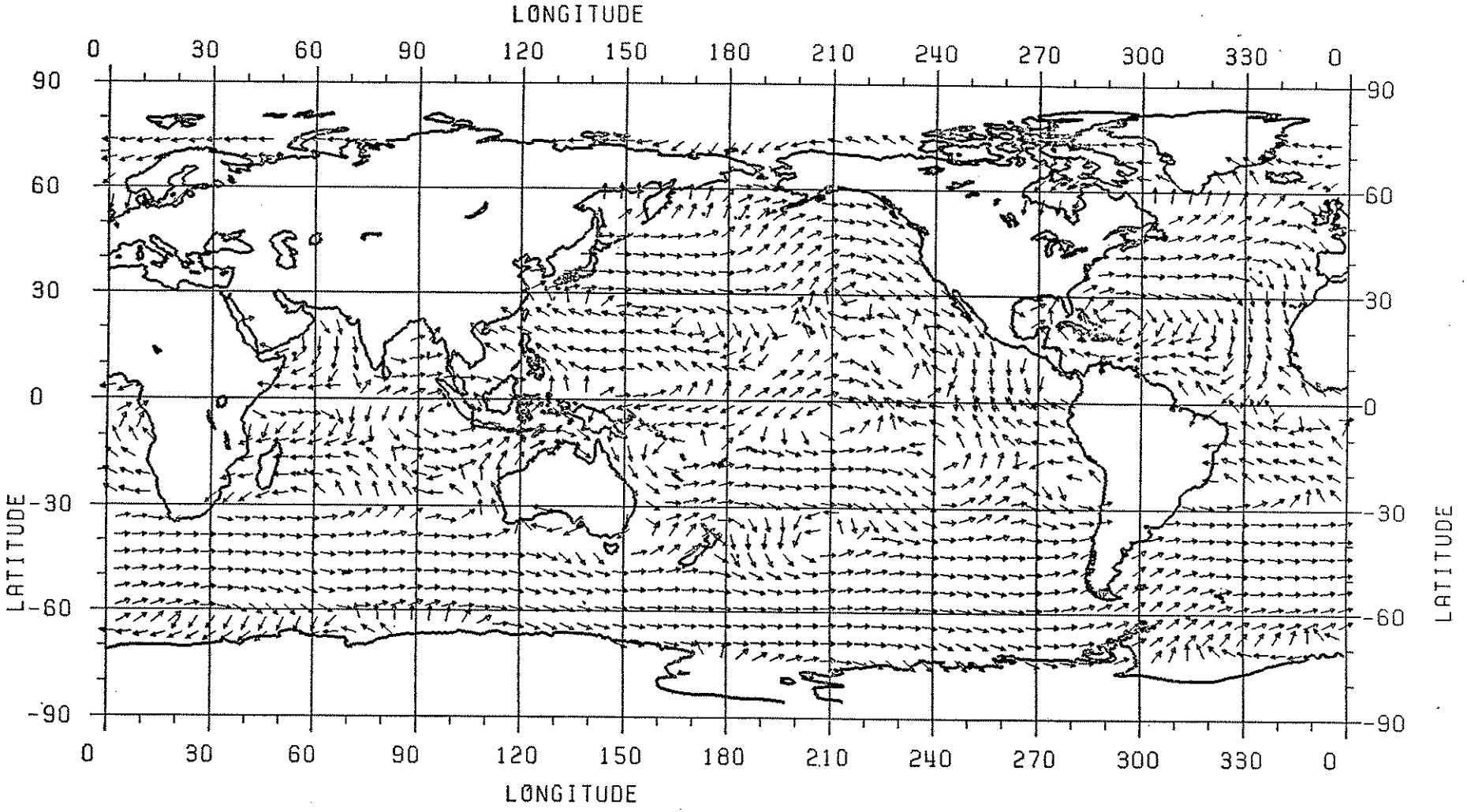

Figure 12. Geostrophic Flow Patterns Implied by the Degree 10 Sea Surface Topography Model. Data Calculated On A 5° Grid.

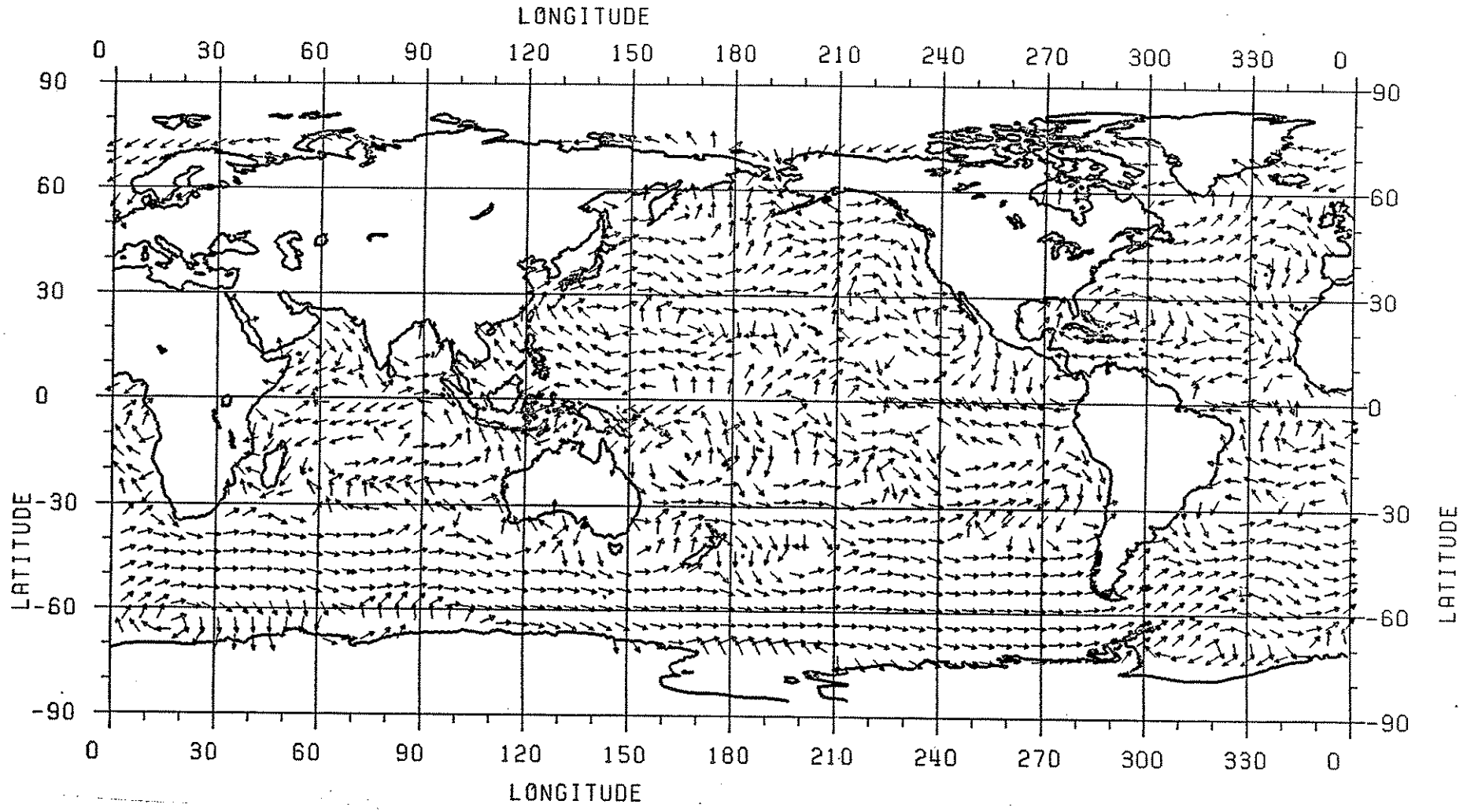

Figure 13. Geostrophic Flow Patterns Implied by the Degree 15 Sea Surface Topography Model. Data Calculated On A 5° Grid.

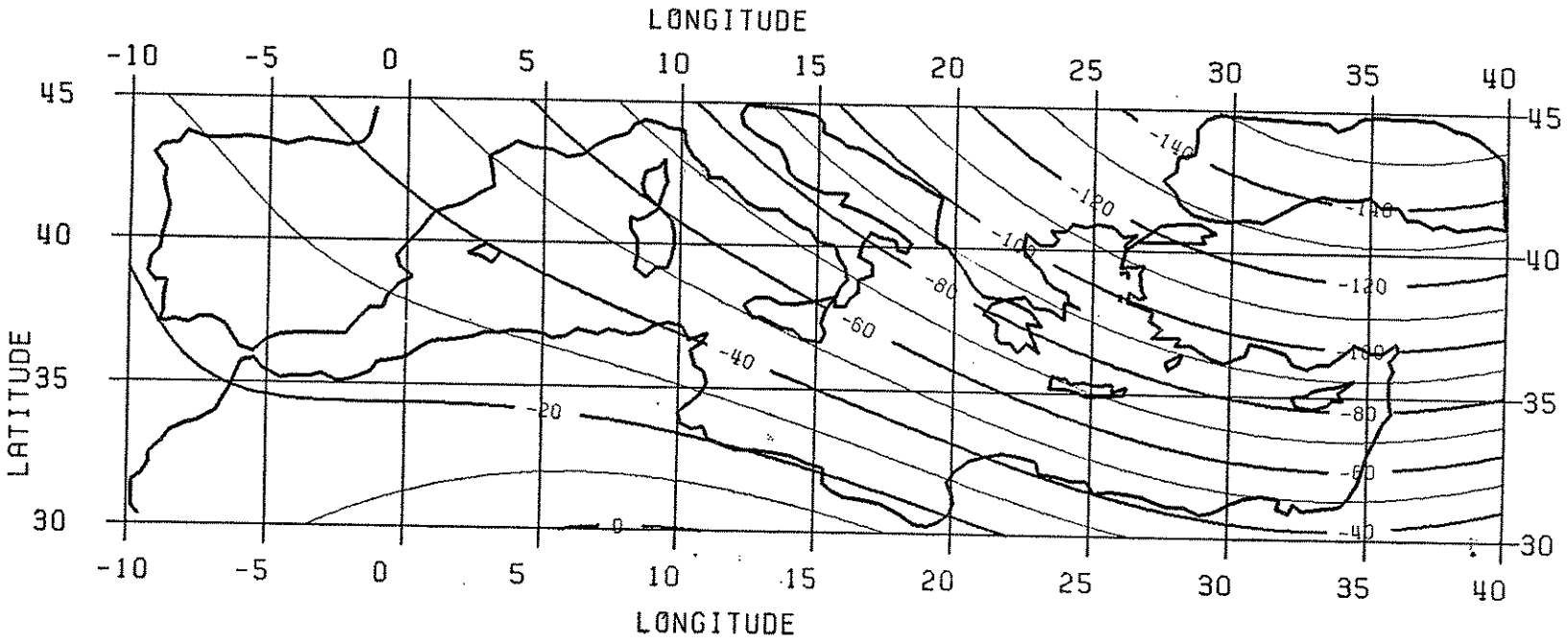

Figure 14. Sea Surface Topography in the Mediterranean Sea from the Degree 10 Ohio State Model. Contour Interval is 10 cm.

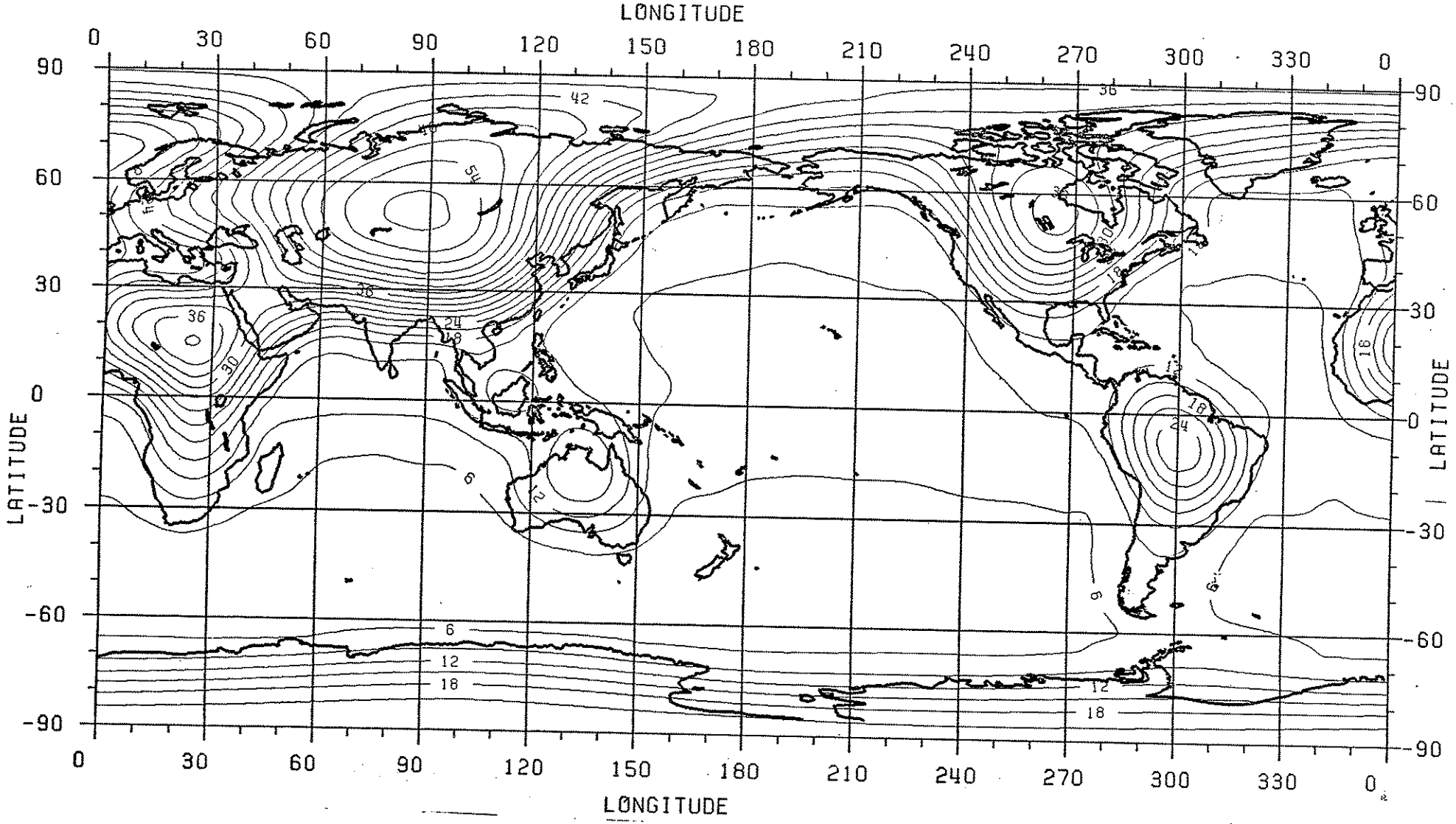

Figure 15. Standard Error of the Sea Surface Topography Degree 10 Solution. Contour Interval is 3 cm.

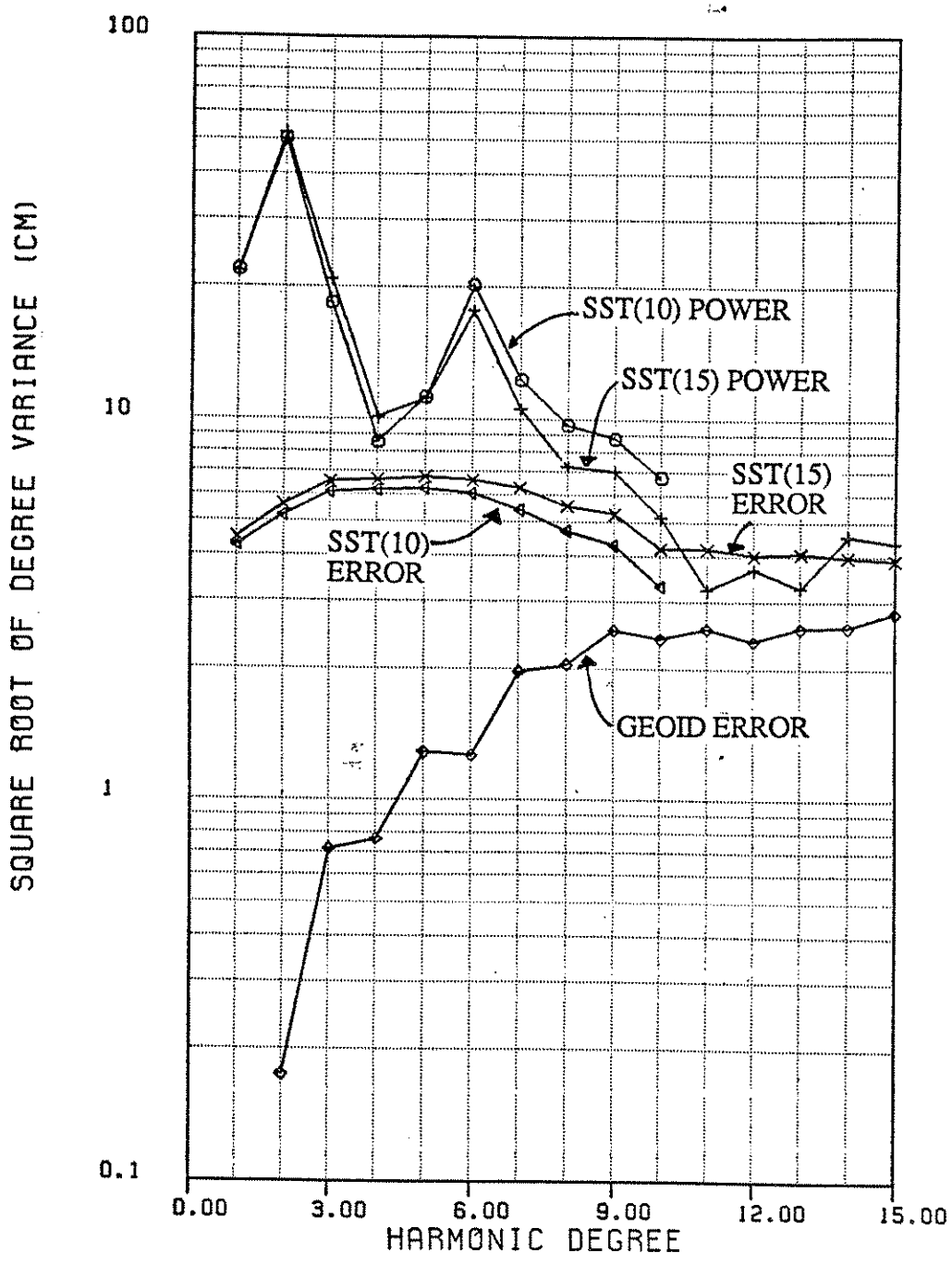

Figure 16. Square Root of Signal and Error Degree Variances for Degree 10 and Degree 15 SST Models, and Geoid Error.

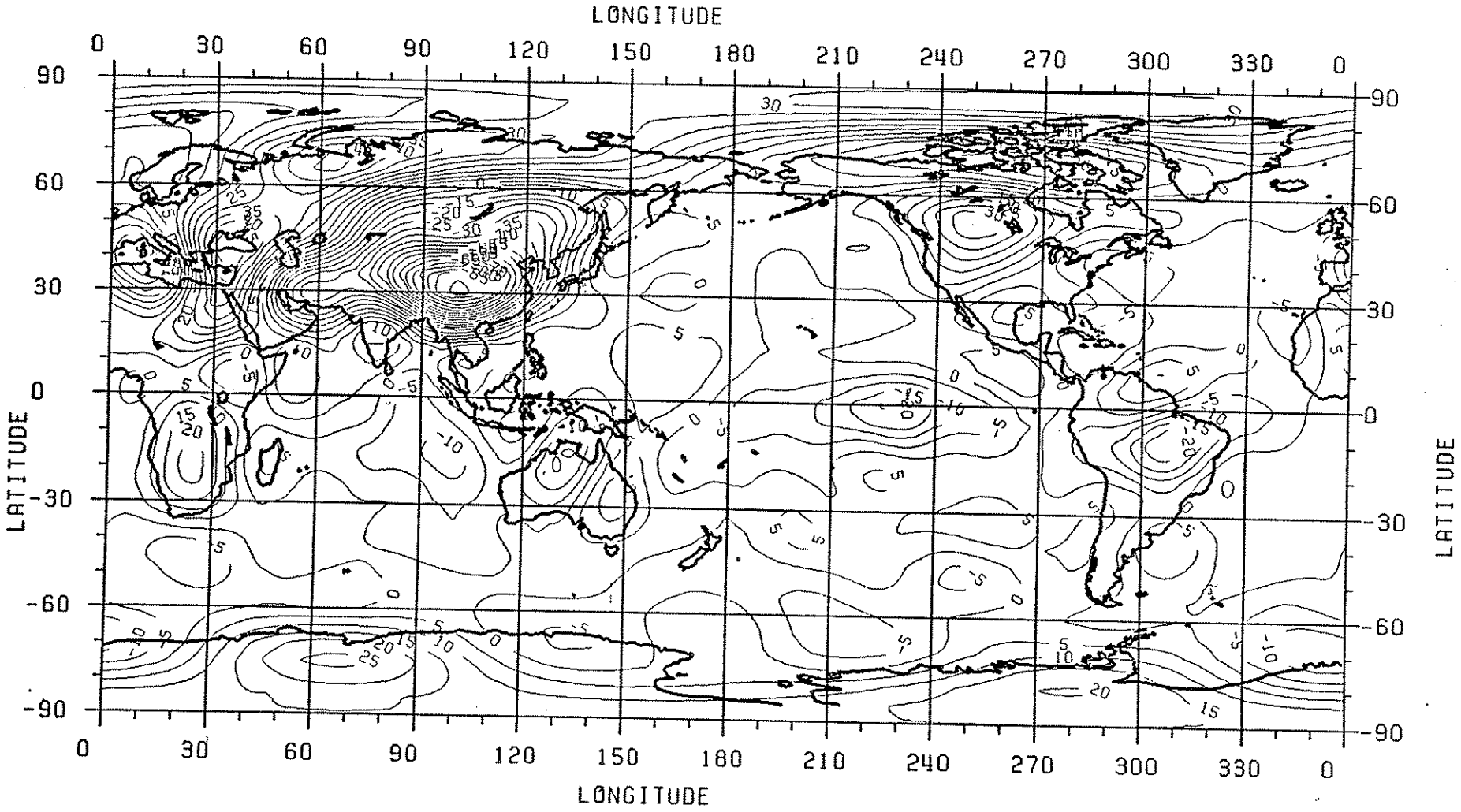

Figure 17. Sea Surface Residual, April 1987 Minus One Year (November 1986-October 1987) Mean. Degree 15 Field. Contour Interval is 5 cm.

procedure was used by Denker (1990, Section 4.4) who examined differences with 2 month averages. He found the differences to be small, approximately 4 cm over the oceans.

In this study a modification of the procedure developed by Denker was made. First, the orbit correction parameters and the adjusted gravity field to degree 50 was held fixed using the (10, 10) SST model. Then a SST model to degree 15 was computed on a monthly basis starting from November 6, 1986. The degree 15 field was chosen to see if time-changes at the higher resolution (vs degree 10) could be seen. It was recognized that the coefficients between degree 1 and 15 could be contaminated by constant (in time) geoid error but the time variations would be meaningful. In doing this the mean sea surface topography was defined by averaging 12 monthly solutions to degree 15. The residual fields were then generated by removing the mean field from the monthly field in the spectral domain. The actual values of the residual sea surface topography were then calculated on a monthly basis. In Figure 17 the residual SST is shown for the month (starting on the 7th) of April 1987. The most significant feature is the -20 cm depression near the

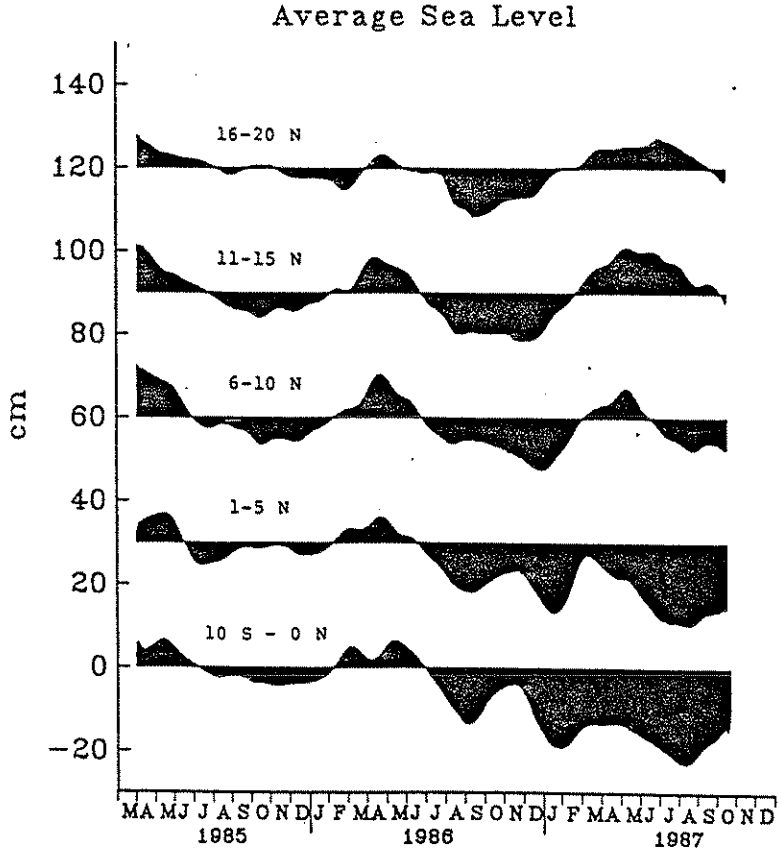

Figure 18. Geosat-derived Sea Level, Averaged in Zonal Bands Between 130° and 165°E. Each Band Contains Approximately 80 Independent Time Series Expressed as Anomalies Relative to the Annual Mean, April 1985-1986. Curves are Offset by 20 cm Relative to Each Other. (From Cheney and Miller (1990, p. 2982)).

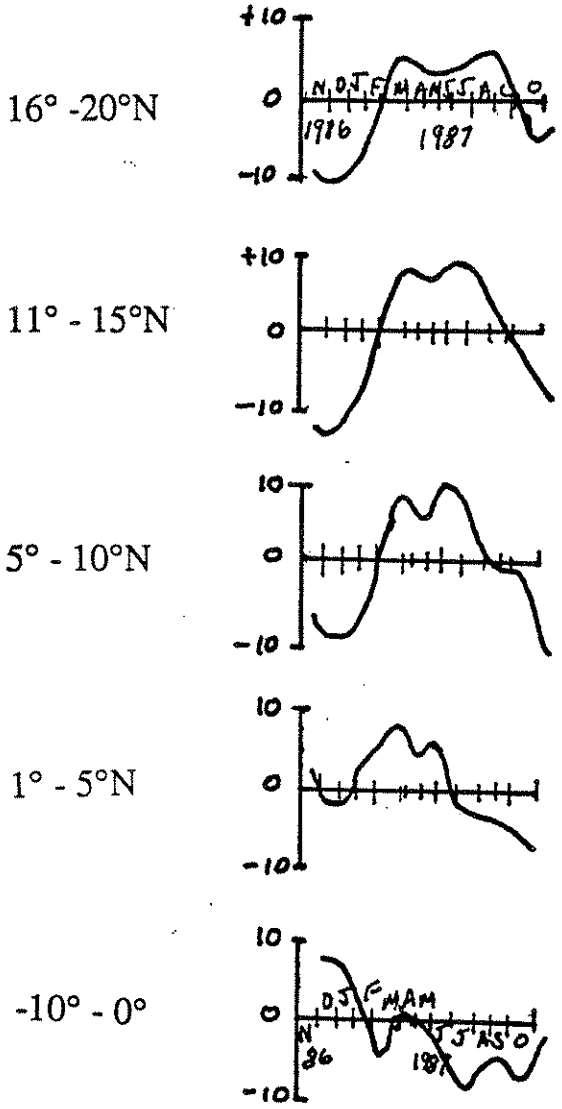

Figure 19. Sea Surface Topography Residuals in the Pacific Ocean, November 86-October 87. Monthly Averages in 130°E to 163°E Using a Degree 15 Expansion for Five Latitude Bands. Units are cm.

equator at longitude 240°. This residual is weaker (-10 cm) in February March, and stronger April. Starting in June 1987 there is no significant deviation from the annual mean in this area. This deviation is probably related to the El Ninõ current in this time period as will be discussed shortly. Variations in other geographic regions are on the order of 5 cm, as found by Denker (ibid). Since the expansion of SST is only to degree 15 (corresponding to a resolution of 1332 km) mesoscale variations can not be seen with this procedure. However large scale variations can be quantified as will be discussed in the next section.

We next examine the sea level changes implied by the degree 15 analysis to see if one can detect the 1986-1987 El Nino event. In this study we first considered the results of Cheney and Miller (1990) and Miller and Cheney (1990). Figure 6 in Cheney and Miller, shown in this report as Figure 18, shows sea surface height residuals with respect to the annual mean of April 1985-April 1986. This figure is based on "approximately 80 independent, time series...". The data was averaged in zonal bands between 130° and 165°E.

In order to see if our results showed similar signals the relative degree 15 SST was evaluated on a 1° x 1° grid. The data was then averaged in the same bands as used by Cheney and Miller. In our case this meant an average of 160 points except for the lowest latitude band in which 234 points were averaged. The results shown in Figure 19 are plotted on a scale similar to that shown in Figure 18. Comparison of Figures 18 and 19 indicates a good, but not perfect agreement. The positive residual at the two northern latitude bands during May-July 1987 is quite consistent in the two figures. The negative anomaly during June-August 1987 for the southern most latitude band agrees well in both figures. But our results show a positive anomaly in November 1986, a feature not seen in Cheney and Miller (ibid). The change in the residual from November 1986 to August 1987 is 20 cm from Figure 18 and is 14 cm from Figure 19.

One should be cautious in interpreting the positive and negative residuals because the absolute zero in the Cheney and Miller analysis is arbitrary. The point here is that temporal changes of the ocean surface can be detected through a degree 15 SST representation. The changes show a significant agreement with other analysis carried out in a significantly different way.

Another test carried out was suggested by the results plotted in Fig. 4a of Cheney and Miller (1990). This plot shows the variation of sea level in a 8° x 1° cell in the Pacific near Ponape. To compute our results the 12 sea surface topography degree 15 representations were evaluated in the 8° x 1° cell whose northwest corner was 7° in latitude and 154° in longitude. The 1° x 1° grid values were averaged. The average was then removed from the 12 values. The residual plot is shown in Figure 20.

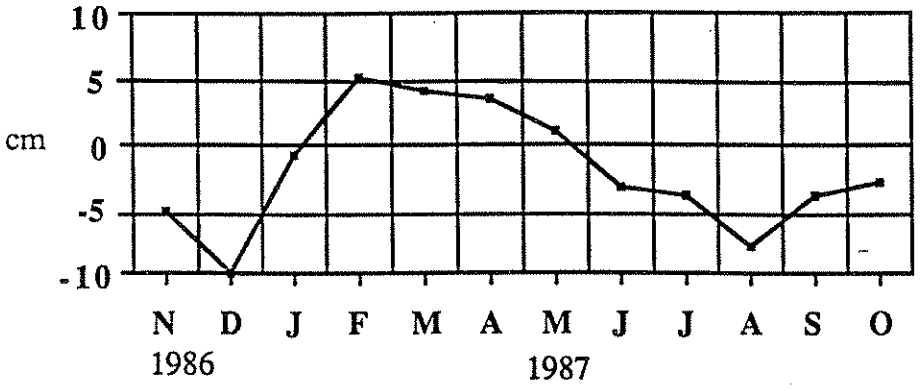

Figure 20. Sea level Variation Over One Year Based on A Degree 15 Representation of SST. Cell's northwest corner is 7° (ϕ), 154° (λ).

The diagram shows a low in December (86) with a change of 15 cm to a peak in February (87). The Cheney/Miller result shows the low in January with the peak in March. The change is 20 cm. Our solution shows a near linear decrease of 13 cm from February to August while the Cheney/Miller change is 20 cm from March (87) to September (87). The times appear to be offset by a month and the amplitude of the changes somewhat less in our analyses. However the general agreement is quite encouraging.

5.2.2 Temporal Variations Through Spectral Analysis

As described in previous sections a solution was obtained in which the sea surface topography, the geopotential and the orbit error were simultaneously determined by processing the one year Geosat altimeter data. Based on this solution the time variation of the sea surface topography will be studied.

The geoid is assumed to have no time variation in some time period. The assumption may not be exactly correct, but it is believed that it is a very good approximation for studying the time variation of the sea surface topography and the current geoid determination accuracy. Let sea surface topography ζ be represented in a series involving time:

$$\zeta(\varphi, \lambda, t) = \sum_{\ell,m} \left[\bar{c}_{\ell m}(t)\cos m\lambda + \bar{s}_{\ell m}(t) \cdot \sin m\lambda\right] \bar{P}_{\ell m}(\sin\varphi) \tag{5.1}$$

The coefficients of the spherical harmonics $\bar{c}_{\ell m}$ and $\bar{s}_{\ell m}$ are functions of the time. The non time dependent version of (5.1) is eq. (2.3). SST may change continuously in time. The frequencies of the SST time variation range from zero to infinity. In practice, the SST can only be sampled at a time interval for a limited time period. Therefore only the frequencies of a limited band can be detected.

By fixing the geopotential and orbits correction from the one year solution, the SST can be expanded into a series for every month. Approximately 6 six days arcs of Geosat data were used to form a monthly SST solution: The 12 monthly solutions can be written as

$$\zeta(\varphi, \lambda, t_k) = \sum_{\ell,m} \left[\bar{c}_{\ell m}(t_k)\cos m\lambda + \bar{s}_{\ell m}(t_k)\sin m\lambda\right] \bar{P}_{\ell m}(\sin\varphi)$$
$$k = 0, 1, \ldots, 11 \tag{5.2}$$

where k is the number of the month starting from November 8, 1986.

Basically, the information of the sea level change during the time period November 1986 to October 1987 is included in the 12 monthly SST solutions. Assume that we can fit the SST to the following model:

$$\zeta(\varphi, \lambda, \tau) = \zeta_o(\varphi, \lambda) + \dot{\zeta}(\varphi, \lambda)\, t \tag{5.3}$$

where $\dot{\zeta}$ denotes the sea level change rate. The ζ and $\dot{\zeta}$ are in the form:

$$\zeta_o(\varphi, \lambda) = \sum_{\ell,m} \left(\bar{c}^{\circ}_{\ell m}\cos m\lambda + \bar{s}^{\circ}_{\ell m}\sin m\lambda\right) \bar{P}_{\ell m}(\sin\varphi) \tag{5.4}$$

$$\dot{\zeta}(\varphi, \lambda) = \sum_{\ell,m} \left(\dot{\bar{c}}_{\ell m}\cos m\lambda + \dot{\bar{s}}_{\ell m}\sin m\lambda\right) \bar{P}_{\ell m}(\sin\varphi)$$

and the coefficients $\bar{c}^{\circ}_{\ell m}$, $\dot{\bar{c}}_{\ell m}$ and $\bar{s}^{\circ}_{\ell m}$, $\dot{\bar{s}}_{\ell m}$ are determined by fitting a straight line to the 12 sets of coefficients $\bar{c}_{\ell m}(t_k)$ and $\bar{s}_{\ell m}(t_k)$ in the least squares sense. That is:

$$\begin{aligned} \bar{c}_{\ell m}(t_k) &= \bar{c}^{\circ}_{\ell m} + \dot{\bar{c}}_{\ell m} t_k + R_{ck} \\ & \qquad\qquad k = 0, \ldots, 11 \\ s_{\ell m}(t_k) &= \bar{s}^{\circ}_{\ell m} + \dot{\bar{s}}_{\ell m} t_k + R_{sk} \end{aligned} \tag{5.5}$$

where R_{ck}, R_{sk} are the residuals of the misfit. The $\bar{c}^{\circ}_{\ell m}$, $\dot{\bar{c}}_{\ell m}$ and $\bar{s}^{\circ}_{\ell m}$, $\dot{\bar{s}}_{\ell m}$ will be determined by

$$\begin{aligned} &\sum_{k=0}^{11} R_{ck}^2 = \text{Minimum} \\ &\sum_{k=0}^{11} R_{sk}^2 = \text{Minimum} \end{aligned} \tag{5.6}$$

If the standard errors of the coefficients $\bar{c}_{\ell m}(t_k)$ and $\bar{s}_{\ell m}(t_k)$ are available, condition (5.6) becomes

$$\begin{aligned} &\sum_{k=0}^{11} \frac{R_{ck}^2}{\sigma^2_{c\ell mk}} = \text{Minimum} \\ &\sum_{k=0}^{11} \frac{R_{ck}^2}{\sigma^2_{s\ell mk}} = \text{Minimum} \end{aligned} \tag{5.7}$$

The condition (5.6) is a special case of (5.7). It was assumed that the standard error of the coefficients are equal to one. The solution with condition (5.7) can be found in many books, e.g., Press et al., (1986, p. 504).

In order to study the energy distribution of the time variation of the sea surface topography corresponding to frequencies, eq. (5.2) is written in a discrete Fourier-series:

$$\zeta(\varphi, \lambda, k) = \frac{1}{N} \sum_{n=0}^{N-1} \sum_{\ell,m} \left(A_{n\ell m}\cos m\lambda + B_{n\ell m}\sin m\lambda\right) \bar{P}_{\ell m}(\sin\varphi)\, e^{2\pi i k n/N}$$
$$k = 0, \ldots, 11 \tag{5.8}$$

where $i = \sqrt{-1}$. N is the number of the monthly SST solutions and it is assumed to be even. The coefficients $A_{n\ell m}$ and $B_{n\ell m}$ are time independent and defined by:

$$A_{n\ell m} = \sum_{k=0}^{N-1} \bar{c}_{\ell m}(t_k)\, e^{-2\pi i k n/N}$$

$$B_{n\ell m} = \sum_{k=0}^{N-1} \bar{s}_{\ell m}(t_k)\, e^{-2\pi i k n/N} \qquad (5.9)$$

The discrete Fourier transformation and its inverse can be found in many books, e.g., Brigham (1988, Chapter 6). The frequency f_k is defined by:

$$f_k = \frac{k}{N \cdot \Delta} \qquad k = 0, \ldots, 11 \qquad (5.10)$$

where Δ is the time interval and for our case that is 1 month.

Based on the sampling theorem, the Nyquist frequency is given by

$$f_N = \frac{1}{2 \cdot \Delta} \qquad (5.11)$$

which is 1 cycle/2 month. Therefore the frequency band ranges from 0 to 1 cycle/2 month for our SST time variation studies. The physical meaning of the frequencies is:

k = 0 annual average of SST
k = 1 annual SST variation
k = 2 semi-annual SST variation
k = 3 4 month SST variation
k = 4 seasonal SST variation
k = 5 2.4 month SST variation
k = 6 2 month SST variation

Eq. (5.8) can also be written in a cosine series. By setting

$$A_{n\ell m} = a_{n\ell m} + i b_{n\ell m}$$
$$B_{n\ell m} = \hat{a}_{n\ell m} + i \hat{b}_{n\ell m} \quad , \qquad (5.12)$$

we then have:

$$\left(A_{n\ell m}\cos m\lambda + B_{n\ell m}\sin m\lambda\right)$$
$$= \left(a_{n\ell m}\cos m\lambda + \hat{a}_{n\ell m}\sin m\lambda\right) + i\left(b_{n\ell m}\cos m\lambda + \hat{b}_{n\ell m}\sin m\lambda\right) \qquad (5.13)$$

Inserting (5.13) into (5.8), we get

$$\zeta(\varphi, \lambda, k) = \frac{1}{N} \sum_{n=0}^{N-1} \sum_{\ell,m} \left(\alpha_{n\ell m} + i\beta_{n\ell m}\right) e^{2\pi i n k/N} \qquad (5.14)$$

with

$$\alpha_{n\ell m} = \left(a_{n\ell m}\cos m\lambda + \hat{a}_{n\ell m}\sin m\lambda\right)\overline{P}_{\ell m}(\sin\varphi)$$
$$\beta_{n\ell m} = \left(b_{n\ell m}\cos m\lambda + \hat{b}_{n\ell m}\sin m\lambda\right)\overline{P}_{\ell m}(\sin\varphi) \qquad (5.15)$$

If we write $e^{2\pi ink/N} = \cos 2\pi nk/N + i\sin 2\pi nK/N$, and note that the ζ is a real function, so that eq. (5.14) becomes:

$$\zeta(\varphi, \lambda, k) = \frac{1}{N}\sum_{n=0}^{N-1}\sum_{\ell,m}\left(\alpha_{n\ell m}\cos\frac{2\pi kn}{N} + \beta_{n\ell m}\sin\frac{2\pi kn}{N}\right) \qquad (5.16)$$

The Fourier coefficients of a real function satisfies the following relationship (ibid, p. 397):

$$F_{N-n} = (F_n)^* \qquad (5.17)$$

where F_n is the Fourier coefficient of a real function, and the asterisk denotes the complex conjugate. If we write

$$F_n = \alpha_{n\ell m} + i\beta_{n\ell m} \quad , \qquad (5.18)$$

then we have from eq. (5.17)

$$\alpha_{n\ell m} = \alpha_{(N-n)\ell m}$$
$$\beta_{n\ell m} = -\beta_{(N-n)\ell m} \qquad (5.19)$$

In addition we have

$$\cos\frac{2\pi kn}{N} = \cos\frac{2\pi k(N-n)}{N}$$
$$\sin\frac{2\pi kn}{N} = -\sin\frac{2\pi k(N-n)}{N} \qquad (5.20)$$

By using eqs. (5.19) and (5.20), (5.16) becomes

$$\zeta(\varphi, \lambda, k) = \frac{1}{N}\sum_{\ell,m}\alpha_{o\ell m} + \frac{2}{N}\sum_{n=1}^{N/2}\sum_{\ell,m}\delta_n\cdot\left(\alpha_{n\ell m}\cos\frac{2\pi nk}{N} - \beta_{n\ell m}\sin\frac{2\pi nk}{N}\right) \qquad (5.21)$$

with

$$\delta_n = \begin{cases} 0.5 & \text{if } n = N/2 \\ 1 & \text{if } n = 1, \ldots, N/2 - 1 \end{cases} \qquad (5.22)$$

If we set

$$\alpha_{n\ell m} = \Omega_{n\ell m}\cos\omega_n$$
$$\beta_{n\ell m} = \Omega_{n\ell m}\sin\omega_n \qquad (5.23)$$

with

$$\Omega_{n\ell m} = \sqrt{\alpha^2_{n\ell m} + \beta^2_{n\ell m}}$$

$$\omega_n = \tan^{-1}\frac{\beta_{n\ell m}}{\alpha_{n\ell m}} \quad , \tag{5.24}$$

eq. (5.21) then can be written as a cosine series:

$$\zeta(\varphi, \lambda, k) = \frac{1}{N}\sum_{\ell,m} \alpha_{o\ell m} + \frac{2}{N}\sum_{n=1}^{N/2}\sum_{\ell,m} \delta_n \Omega_{n\ell m}\cos\left(\frac{2\pi nk}{N} + \omega_n\right) \tag{5.25}$$

The frequencies contained in (5.25) are positive and range from 0 to the Nyquist frequency f_N. Eq. (5.25) gives the SST at the time t = k month, k = 0, ... 11. If SST needs to be computed at the arbitrary time between Nov. 1986 and Oct. 1987, eq. (5.25) can be easily written as (c.f. Cizek, 1986, eq. (5.36b)):

$$\zeta(\varphi, \lambda, t) = \frac{1}{N}\sum_{\ell,m} \alpha_{o\ell m} + \frac{2}{N}\sum_{n=1}^{N/2}\sum_{\ell,m} \delta_n \Omega_{n\ell m} \cdot \cos\left(\frac{2\pi n}{N} t + \omega_n\right) \quad , \tag{5.26}$$

and SST can be evaluated at the time t by summing the above series. If N is a large number, a more efficient computation procedure using FFT is described in (ibid, p. 94).

The power spectrum of the SST is defined as

$$\begin{cases} P(\varphi, \lambda, f_n) = \dfrac{4}{N^2}\displaystyle\sum_{k=1}^{N/2}\sum_{\ell,m} \delta_n^2 \Omega^2_{n\ell m}\cos\left(\dfrac{2\pi kn}{N} + \omega_n\right) \quad , \\ \qquad\qquad = \dfrac{2\delta_n^2}{N^2}\displaystyle\sum_{\ell,m} \Omega^2_{n\ell m} \qquad n = 1, \ldots, N/2 \\ P(\varphi, \lambda, f_o) = \dfrac{1}{N^2}\displaystyle\sum_{\ell,m} \Omega^2_{o\ell m} \qquad n = 0 \end{cases} \tag{5.27}$$

Based on Parseval's theorem, the sum of the power spectrum of the SST is the square mean of the SST:

$$\sum_{n=0}^{N/2} P(\varphi, \lambda, f_n) = \frac{1}{N}\sum_{k=0}^{N-1} \zeta^2(\varphi, \lambda, t_k) \tag{5.28}$$

From eq. (5.28) the mean square of the SST time variation is given by:

$$\frac{1}{N}\sum_{k=0}^{N-1} \left[\zeta(\varphi, \lambda, t_k) - \bar{\zeta}(\varphi, \lambda)\right]^2$$

$$= \sum_{n=1}^{N/2} P(\varphi, \lambda, f_n) = \sum_{n=1}^{N/2} \frac{2\delta_n^2}{N^2} \sum_{\ell,m} \Omega_{n\ell m}^2 \qquad (5.29)$$

where $\bar{\zeta}$ denote the mean value of the SST and it is given by

$$\bar{\zeta}(\varphi, \lambda) = \frac{1}{N} \sum_{k=0}^{N-1} \zeta(\varphi, \lambda, t_k)$$

$$= \frac{1}{N} \sum_{\ell,m} \alpha_{o\ell m} \qquad (5.30)$$

The estimation of the power spectrum of the SST is based on the means of the periodogram (Brigham, 1988 p. 367). The statistical meaning of the power spectrum is discussed in (ibid) and Elliott et al. (1982). A brief and comprehensive discussion can also be found in Press et al. (1986, p. 422). These discussions are interesting and important for interpretation the power spectrum defined by eqs. (5.27) and (5.29) correctly but it exceeds the scope of this report, and we simply interprete the quantities defined by eq. (5.27) as the power of the SST corresponding to different frequencies.

It is worthwhile to mention that Nerem et al. (1990b) modeled the coefficients of the sea surface topography by:

$$\bar{c}_{\ell m}(t) = \bar{c}^{\circ}_{\ell m} + \dot{\bar{c}}_{\ell m} t + \sum_{i=1}^{5} \left(A^i_{n\ell m} \cos\omega_i t + B^i_{n\ell m} \sin\omega_i t \right) \qquad (5.31)$$

$$\bar{s}_{\ell m}(t) = \bar{s}^{\circ}_{\ell m} + \dot{\bar{s}}_{\ell m} t + \sum_{i=1}^{5} \left(a^i_{n\ell m} \cos\omega_i t + b^i_{n\ell m} \sin\omega_i t \right) \qquad (5.32)$$

where $\bar{c}^{\circ}_{\ell m}$ and $\bar{s}^{\circ}_{\ell m}$ are the coefficients of the mean sea surface topography topography. The $\dot{\bar{c}}_{\ell m}$ and $\dot{\bar{s}}_{\ell m}$ are the coefficients of the sea level change rate. The series are the periodic time variation of the SST.

If the coefficients are determined by using the least-squares technique, the model can fit the actual SST well in the meaning of best fit. But the interpretation of the amplitude or power spectrum must be carefully made.

Two years of Geosat ERMs data were used for the SST time variation studies (ibid). The frequencies in the ERMs data range from zero to 1 cycle/34.10 days. Only selected frequencies (eqs. (5.31), (5.32)) were included in the model. The frequencies which were not modeled in (5.31) and (5.32) would be aliased into the model and mixed with the selected frequencies. The amplitude of the selected frequencies would be falsified by unmodeled frequencies. Because of the aliasing problem it is not meaningful to talk about the annual or semi-annual SST variation and so on.

Another consideration is the separation of the coefficients of the secular SST change $\dot{\bar{c}}_{\ell m}$ and $\dot{\bar{s}}_{\ell m}$ from the coefficients of the Fourier-series in (5.31) and (5.32). The secular SST changes $\dot{\bar{c}}_{\ell m} t$ and $\dot{\bar{s}}_{\ell m} t$ are not orthogonal to the base function of the Fourier-series, the cosine and sine. It will be of interest to look at the correlation between them in the least-squares solutions.

In this section the secular SST changes were solved by using eq. (5.5). The periodic SST variation was contained in the terms R_{ck} and R_{sk} which were considered as misfit. One can argue that we have the similar situation as described in the last paragraph. The difference is that only the secular SST changes were solved by using eq. (5.5). We feel a little safer for the reason that the periodic SST variation may effect the straight line fit very little.

In the following we will give the results of the secular SST change during the period Nov. 1986 to Oct. 1987 and the temporal variations of the SST through spectral analysis. Figure 21 shows the yearly sea surface topography change rate computed from eq. (5.7). The SST changed considerably in some regions. For example, in the west Pacific ocean a -15 cm/yr rate of the SST is found between the longitude 140° to 180° around the equator. This decrease may be due to the El Ninõ phenomenon (Cheney and Miller, 1990). The SST rate was about -15 cm in the Atlantic Ocean between latitude 0° to 20°. A small SST change is found in the region of the Brazil and Falkland currents. Globally the RMS values of the SST change during the period Nov. 1986 to Oct. 1987 is 8.6 cm. The global mean, based on a 1° x 1° grid, of the SST change (this is equivalent to the global sea level change) was found to be -0.2 mm in the ocean which is defined as

$$\text{ocean} = \begin{cases} -70° \le \varphi \le 70° \\ h \le -200 \text{ m} \end{cases},$$

where h is depth of the ocean. The very small mean value means that almost no change in the oceanwide mean sea level has been detected by our solutions.

The spectral analyses of the SST time variation enable us to study the SST variation in the frequency domain. The variation is decomposed into the components of the annual, semi-annual and seasonal variation and so on (cf. eq. (5.25)). The power spectrum of the components of the SST variation is half of the square of the amplitude of the Fourier-series in (5.25). It is more convenient in the geometric sence to use the amplitude rather than the power spectrum defined by eq. (5.27). Table 18 gives the RMS value of the amplitude of the SST time variation corresponding to different time periods:

Table 18. RMS Values of the Amplitude Corresponding to Frequency f_k.

k	RMS Value
1	5.8 cm
2	4.2
3	2.5
4	2.0
5	1.7
6	0.8

Table 18 shows clearly that the amplitude becomes smaller, when the frequency gets higher. No strong seasonal variation (k = 4) was found.

Figure 22 and 23 show the amplitude of the annual (k = 1) and seasonal (k = 4) SST variation. A relative strong (9 cm) annual variation appears in the west Pacific ocean and around the equator. Another relatively strong variation occurs in the Atlantic ocean above the equator. The seasonal variation is small. In the western Pacific 2 to 4 cm SST variation can be found.

The time variation of the SST was studied on a global basis. We consider the SST as a function of the geographic location (ϕ, λ) and the time (t) and sampled it at the monthly time interval. The sampling interval can be smaller, but it is limited by the repeat time of Geosat which is 17.05 days. The SST was expanded up to degree and order 15 so that the resolution (~ 1300 km) is somewhat too broad to identify the detailed SST variation, e.g., the variations due to narrow currents. Such variations can be examined by working directly with the altimeter data and with the improved orbits. The use of the harmonic analysis will be limited, for now, to broad feature changes. These results are preliminary and could be expanded if additional (in time) Geosat data were analyzed.

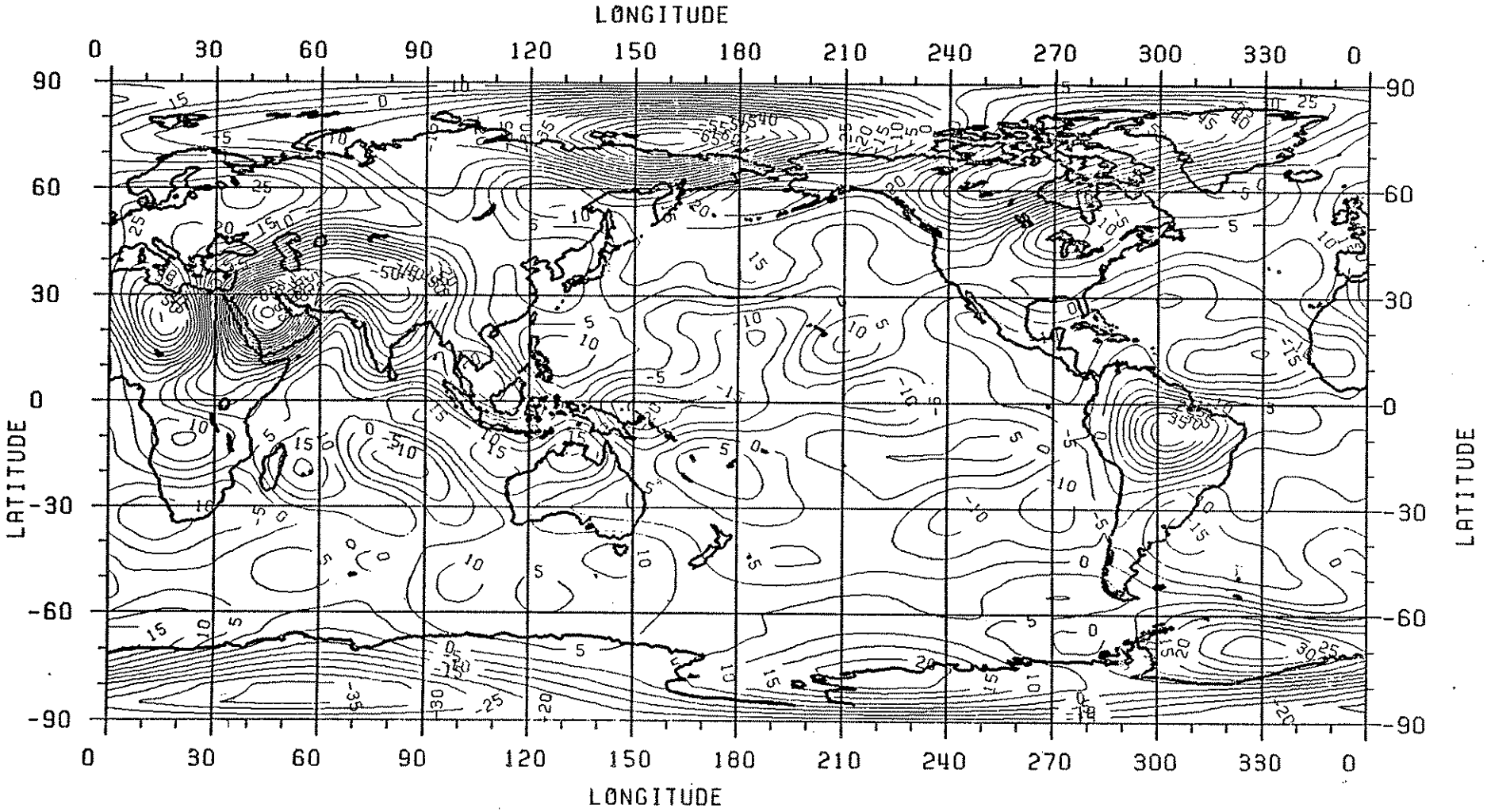

Figure 21. Rate of Change of the Sea Surface Implied By One Year of Geosat Data Using A Spherical Harmonic Expansion to Degree 15. Units are cm/year. Contour interval = 5 cm.

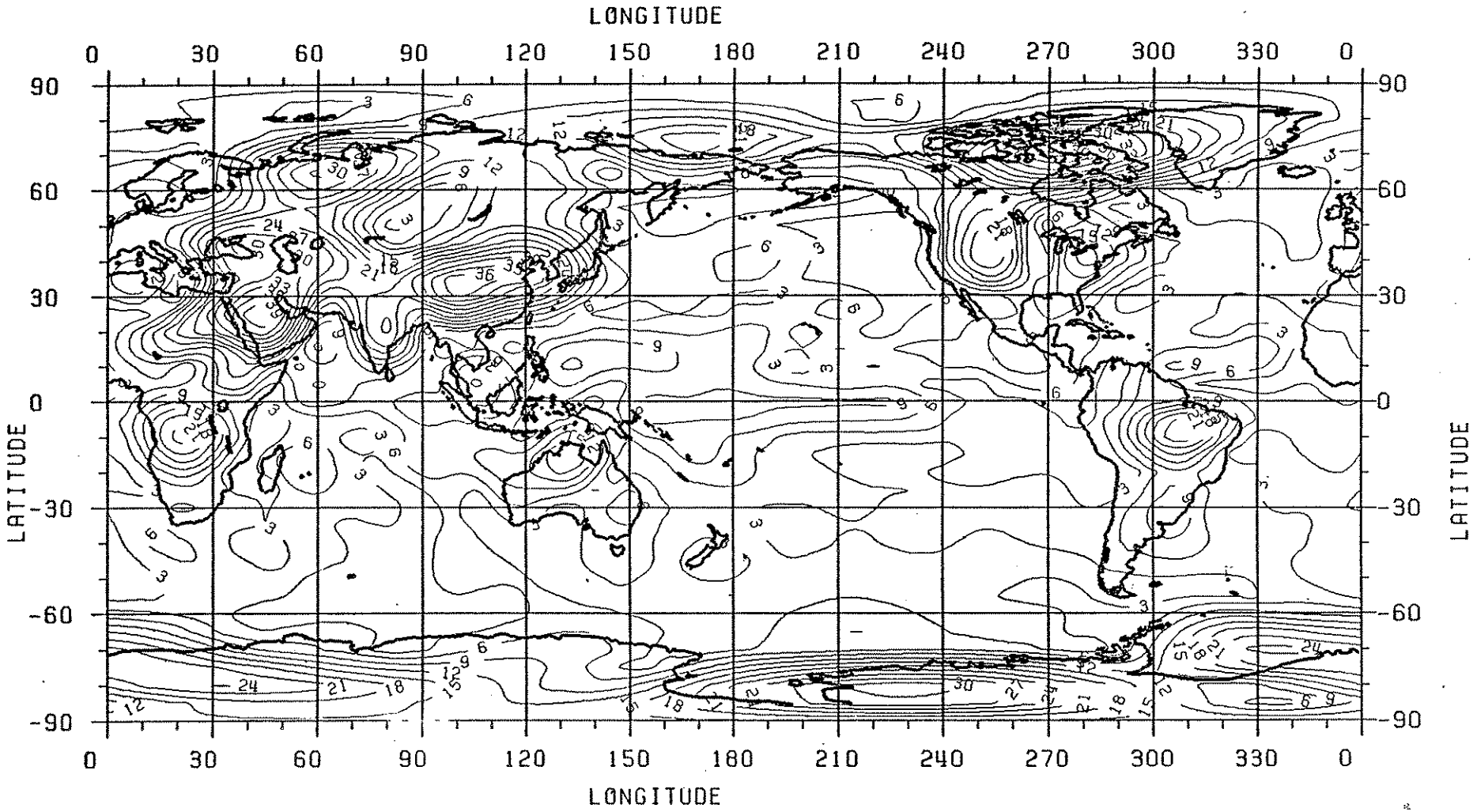

Figure 22. Amplitude of the Annual Variation (k = 1) of SST Derived from One Year of Geosat Data Based on a Spherical Harmonic Expansion To Degree 15. Contour interval = 3 cm.

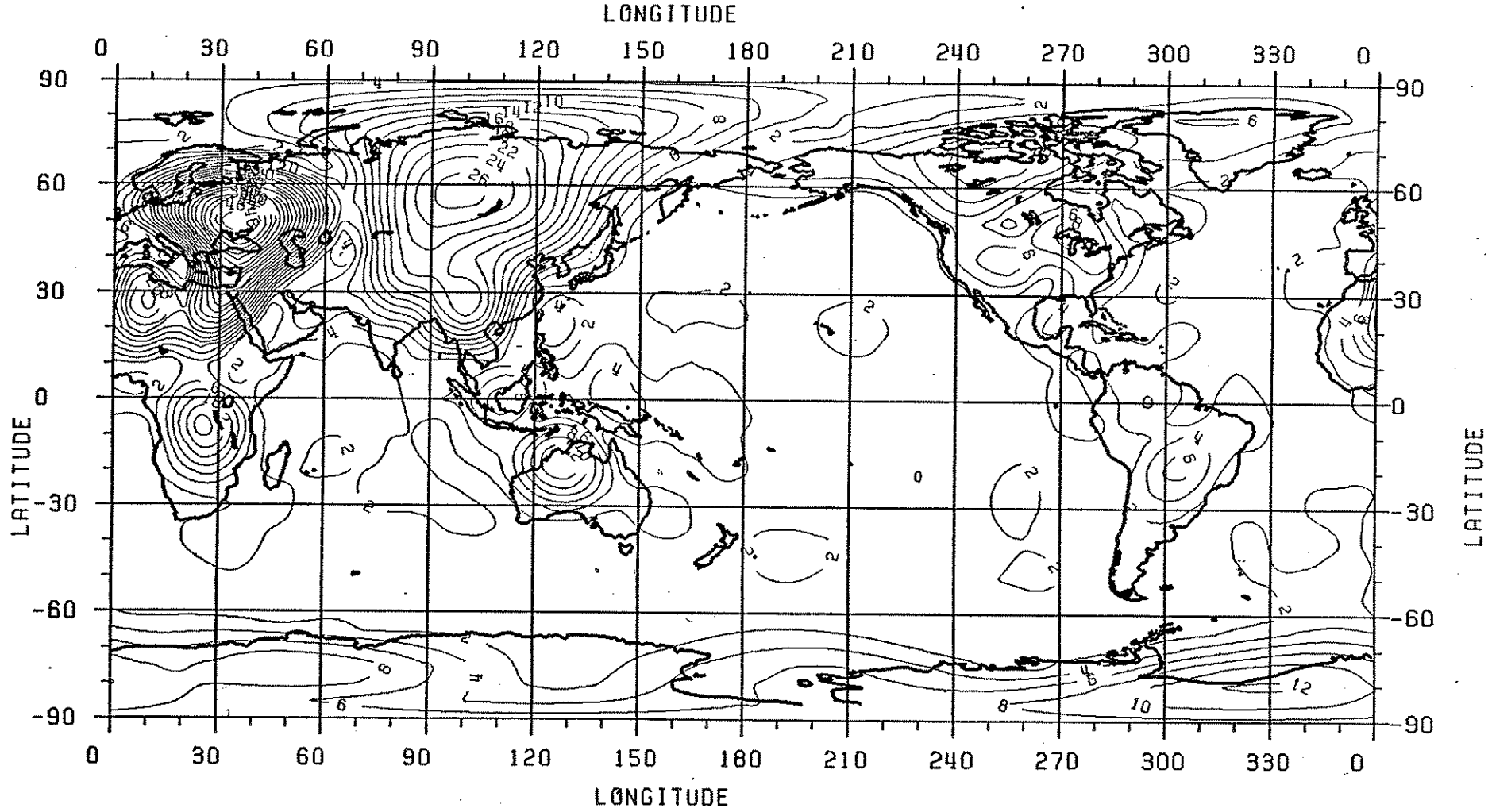

Figure 23. Amplitude of the Seasonal Variation (k = 4) of SST Derived from One Year of Geosat Data Based on a Spherical Harmonic Expansion To Degree 15. Contour interval = 2 cm.

6.0 The Estimation of the Potential Coefficients Above Degree 50.

The previous discussion has described how a potential coefficient model to degree 50 has been selected on the basis of a combination of the GEM-T2 potential coefficients, surface gravity normal equations, and one year of Geosat altimeter data. We now incorporate these coefficients in a development leading to a complete set of potential coefficients to degree 360. The general procedure followed is based on the analysis described by Rapp and Pavlis (1990).

The first step in this process was the updating of the global 30' x 30' mean anomaly file used in the OSU89 model development. The first updating was to incorporate the new data in the 30' data file. The first step was to split the new 1° x 1° mean anomalies into 4 identical 30' x 30' values. A total of 3776 30' values were estimated from the original 944 values of anomaly Source 97. The following corrections were then applied to the 30' values: ellipsoidal corrections; g_1 corrections; transformation to the GEM-T2 implied gravity formula; atmospheric corrections, and second order gravity formula corrections. The details of these corrections are given in Section 2.2 of Rapp and Pavlis (ibid, p. 21,887).

The corrected 30' file was then merged with the 30' input file used for the development of the OSU89B degree 360 model. The merging criteria were that a new value would replace a previous (OSU89B) value only if the previous value was a "fill-in" value, or it was the result of the split up of a previously available 1° x 1° value. More specifically the previous value had to belong to either the SET 3 or SET 5 case of Table 2 in Rapp and Pavlis (ibid, p. 21,896). The standard deviations assigned to the new 30' defined anomalies was equal to that of the value being replaced. The code assigned to these anomalies was 4097. The newly created file contained 3669 out of the 3776 (by split up) 30' anomalies. Of the 3669 values, 3144 replaced fill-ins while 525 values replaced previous 30' values from 1° values (see section 2).

The next step in the updating process was done to reflect a change in philosophy in the calculation of fill-in gravity anomalies from GEM-T2 and topographic/isostatic information. In the OSU89B development the fill-in anomalies (i.e. anomalies in areas where no data was available) were computed from the GEM-T2 model to degree 36 with contributions from degree 37 to 360 from the topographic/isostatic model (see Rapp and Pavlis, ibid, Section 3.4). In the new case we decided to reduce the maximum degree of the T2 model to 9 and then use the topographic/isostatic model from degree 10 to 360. This procedure makes our adjustment procedure somewhat more correct since we do neglect the correlation between the fill-in anomalies and the GEM-T2 coefficients in our adjustment process.

The second modification, then, took place by first generating a set of 30' anomalies, using program F431 using the GEM-T2 potential coefficients to degree 9 and the potential coefficients implied by the topographic/isostatic model from degree 10 to 360. These anomalies replaced the "fill-in" values after the China data had been merged. The code assigned to these fill-ins was 3003. The standard deviations used were identical in the new case and the older case. This data was merged with the anomalies derived from satellite altimeter data using the same process described in Rapp and Pavlis (ibid, Section 3.5). The location of the 30' anomalies, with an indication of their origin is given in Figure 24. This figure can be compared to Figure 4 of Rapp and Pavlis where the only change will be seen in China. Statistics on the number of anomalies that are in the 30' data file (TS0040.DG30X30.MRGD.GEMT209.TI10360.CHINA) are given in Table 19.

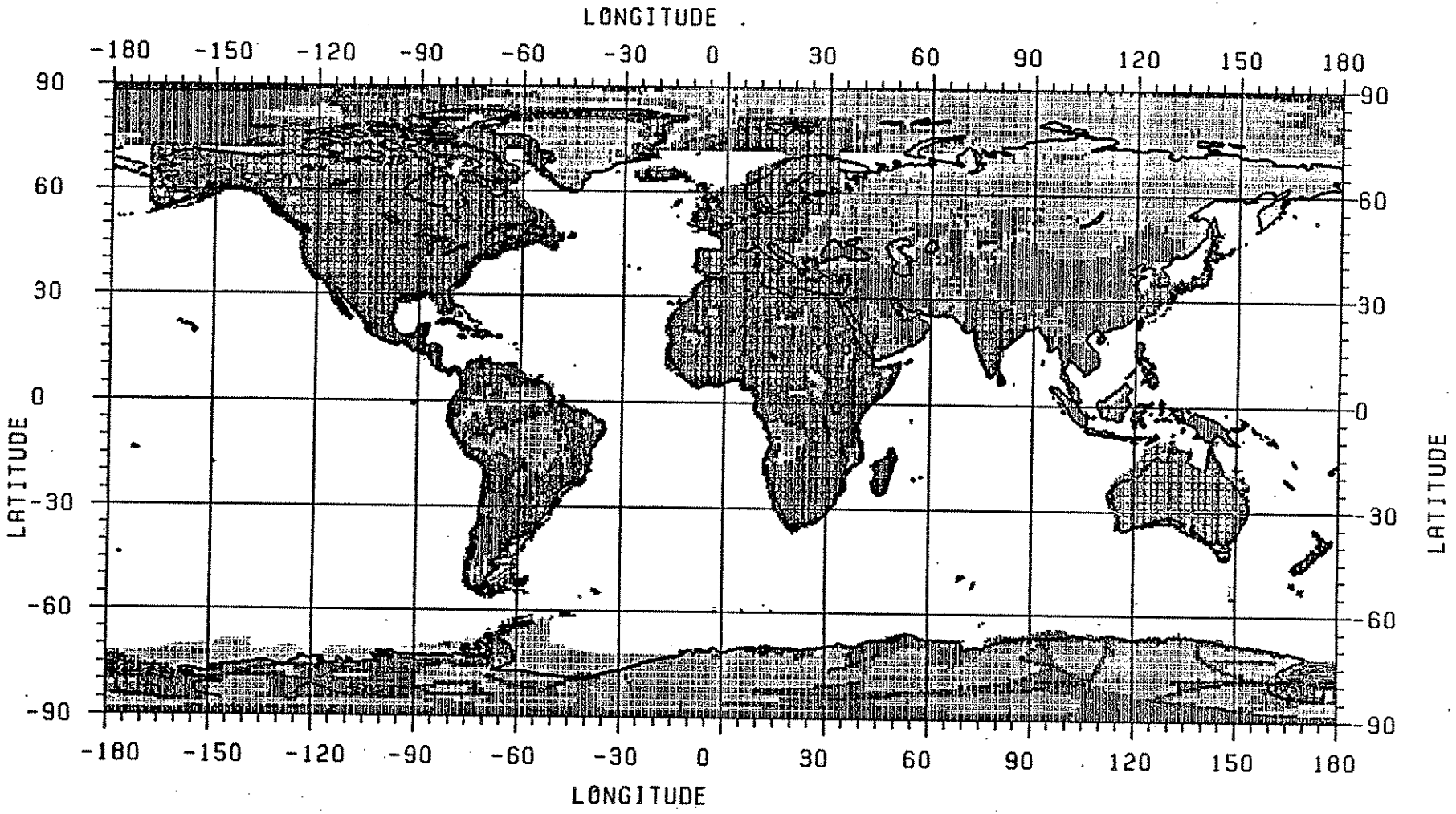

Figure 24. Identification of 30' x 30' anomalies in the merged data file. (The darkest striping represents the original 30' terrestrial anomalies. The darker vertical striping represents 30' terrestrial anomalies obtained from the split up of 1° terrestrial anomalies. The lightest striping represents 30' values determined by "fill-in" techniques. The blank areas designate the location of the altimeter derived 30' anomalies.

Table 19. Statistical Information on the Various 30' Anomalies in the Merged Data File. Anomaly Units are mgal.

	30' Terrestrial	Altimeter Derived	1° Split Up	Fill-Ins
Number of values	45,166	136,270	30,187	47,577
Percentage by area	17.51	64.81	7.95	9.74
Minimum value	-196	-284	-175	-243
Maximum value	391	309	214	310
Mean value	3.8	-1.7	6.2	-0.3
RMS value	33.8	25.0	40.1	27.3
RMS standard dev.	8.5	3.5	33.4	36.0

Using the GEM-T2 model, its error covariance matrix, and the revised 30' data file the combination solution was carried out using the same procedures as described in Rapp and Pavlis (ibid). The solution could be called a OSU89B type with a revised 30' anomaly data set that was consistent with the 1° normal equation, development described in Section 2. The 30' anomaly weighting procedure used in this analysis was identical to that used for OSU89B; that is the original standard deviation was multiplied by 2 and the resultant value restricted to fall in the range 14-27 mgals. In Table 20 statistical information for this combination solution is given.

Table 20. Statistical Information on the OSU89B Type Combination Solution with the OSU91 30' Data File.

Quantity	Value
Standard Deviation Range	14-27 mgal
$\tilde{\sigma}_o^2$	4.51
Number of $v_{\Delta g} > 7$ mgal	14,492
$\bar{k}$	1.096
RMS v, mgal	3.21
Maximum |v|	25

The location of 14492 30' anomaly residuals exceeding 7 mgal in absolute value is shown in Figure 25. This number is substantially higher than the 4130 values shown in Fig. 5 of Rapp and Pavlis (ibid). The primary reason for this is the use, in our current solution of the fill-in anomalies from GEM-T2 to 9 while the OSU89B solution used GEM-T2 to degree 36. The patterns in Figure 25 are primarily those in regions where the fill in anomalies are used.

After the least squares adjustment was completed a set of adjusted 30' mean anomalies was calculated. These anomalies were then converted to potential coefficients using the orthogonalization process described in Rapp and Pavlis (1990, Section 2.1). This led to a set of potential coefficients complete to degree 360. The coefficients from degree 51 to 360 will be used to augment the 2 to 50 coefficients found from the adjustment described in Section 4.0. However it still is of interest to compare the coefficients of the two solutions, up to degree 50, just to obtain a feeling for the differences to be seen from the two adjustment methods using two very different ways in which the altimeter data are treated. These comparisons are shown in Table 21. From the table we see that the undulation difference of the two models is 48 cm. It will turn out that the accuracy of the OSU91A model is 25 cm to degree 50 (see Table 22) and the accuracy of the OSU89B type adjustment, to degree 50, is approximately 34 cm, so that the difference noted in Table 20 are consistent with the accuracy estimates of the two models.

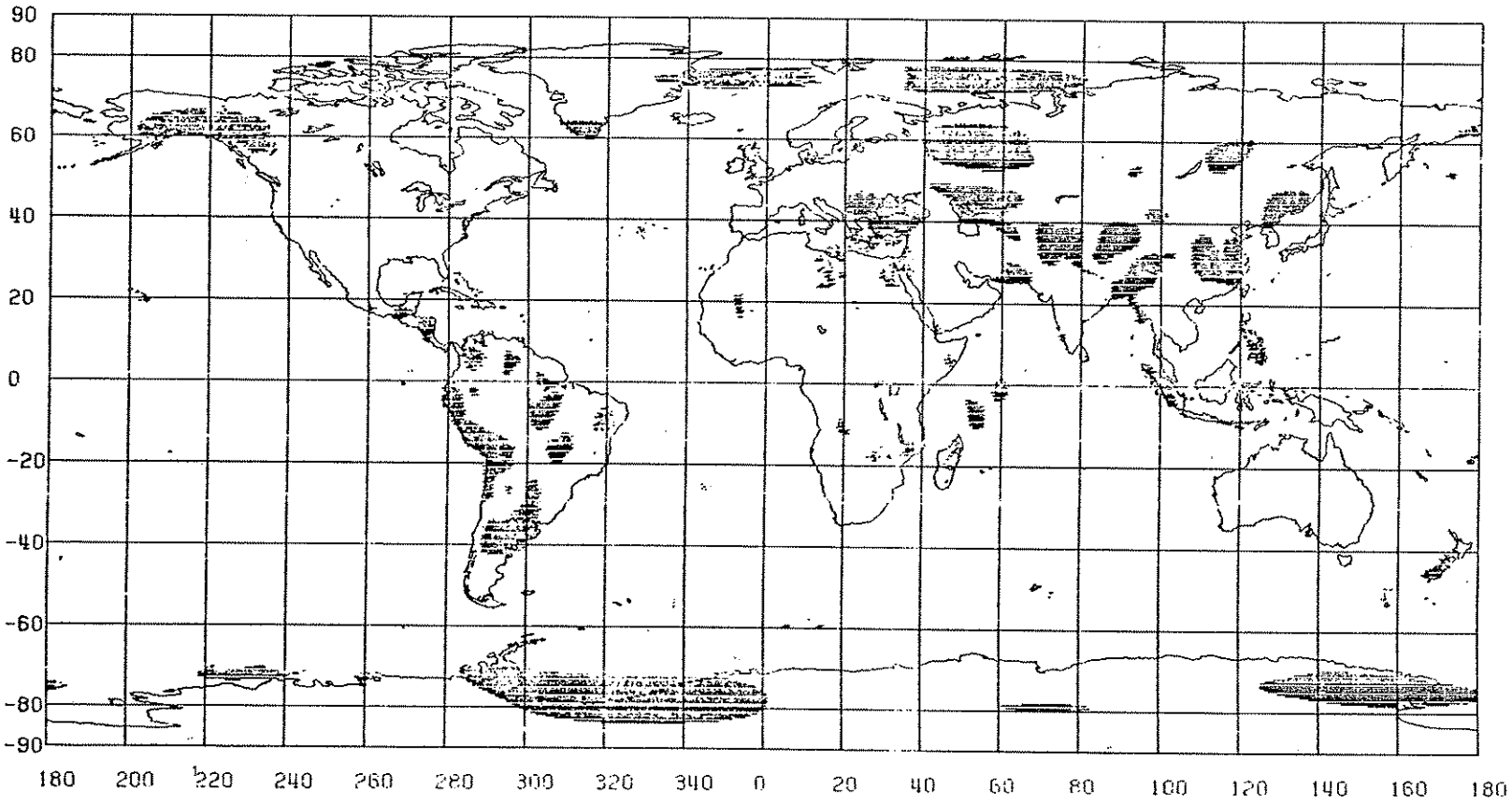

Figure 25. Location of 14,492 30' x 30' cells where the anomaly residuals exceeded 7 mgal in absolute value.

Table 21. Comparison of Two Potential Coefficient Models, To Degree 50, That Differ in Adjustment Procedure and Treatment of Altimeter Data

Degree	% Difference	Undulation Differences (cm)	Anomaly Difference (mgal)
2	.02	0.3	0.00
5	.37	2.8	0.02
10	3.3	7.5	0.10
15	9.8	8.8	0.19
20	16.4	9.6	0.28
30	22.7	8.2	0.36
40	16.2	4.0	0.24
50	17.2	3.9	0.30
Cummulative		48	1.79

At this point we have the set of potential coefficients to degree 50 from the adjustment described in Section 4.0 and a set of coefficients from degree 2 to 360 using the procedure described in the previous sections. In the next section we turn to the merger of the two models.

7.0 The Merger of the Two Potential Coefficients Sets Leading to the OSU91A Potential Coefficient Model

We now simply take the potential coefficients to degree 50 from the combination solution of Section 4.0 and add the coefficients from degree 51 to 360 of the solution described in Section 6. This merger leads to the OSU91A potential coefficient model.

The standard deviations of the coefficients are also established in two steps. For the coefficients to degree 50 the standard deviations are based on the square root of the diagonal elements of the FYS10.W96GW solution. The standard deviation of the coefficients from degree 51 to 360 are exactly the same as the OSU89B coefficients because the anomaly accuracy estimates remain unchanged. The accuracy estimates for these higher degree coefficients are based on a propagated error and a sampling error as described in Section 2.3 of Rapp and Pavlis (ibid). Table 22 shows the geoid accuracy, on a sphere of radius a, for the OSU89B solution and from the OSU91A solution.

Table 22. Geoid Undulation Commission Error, by Spherical Harmonic Degree, for OSU89B and OSU91A. Units are cm.

	OSU89B		OSU91A	
	By Degree	Cumulatively	By Degree	Cumulatively
2	0.2	0.2	0.2	0.2
6	1.8	2.8	1.3	2.2
10	3.9	7.6	2.4	5.0
20	5.4	17.6	3.6	10.6
30	5.5	24.8	4.3	16.8
50	4.6	33.5	3.0	24.8
75	3.7	39.3	3.7	32.3
100	3.2	42.9	3.2	36.5
180	2.2	48.7	2.2	43.2
360	1.3	53.6	1.3	48.7

Up to degree 50 the OSU91A has slightly smaller standard deviations than OSU89B. Beyond degree 50 the two solutions have identical accuracies at each degree. Overall, OSU91A, to degree 360 has a commission error, only, of 48.7 cm vs 53.6 cm for OSU89B.

The standard deviation of the anomaly degree variances, on a sphere of radius a, are plotted in Figure 26. Also shown on the plot are the anomaly degree variances (c_n) and the c_n values implied by the Kaula rule for the decay of the fully normalized potential coefficients (Rapp and Pavlis (ibid, eq. 74). The anomaly power spectrum of OSU89B and OSU91A are very similar as can be seen by comparing Figure 26 with Figure 12 of Rapp and Pavlis (ibid). From Figure 26 we see that the signal to noise ratio becomes 1 near degree 260. Rapp and Pavlis (1990) have argued that coefficients above the degree at which the ratio becomes one should be retained in the solution. This also speaks to setting the error degree variances above degree 260 to be equal to the signal degree variances since the latter are smaller. In this case the commission error, now on a sphere whose mean radius is 6371 km, is 51.9 cm, which, combined with the omission error (based on the Tscherning/Rapp model with the Jekeli parameters) of 24.1 cm, yields a total point geoid undulation error of 57.2 cm. Recall this is a global average and can be poorer or better depending on the data availability in the area. One also should note in Figure 26 the break in the errors at degree 50. This break is caused by the inconsistency in the error estimates from the two combination models. We considered several techniques for artificially avoiding the break and finally decided to leave the errors as they were from the solutions.

In the next section we evaluate the OSU91A model, and several preliminary versions, by comparisons with a variety of data types.

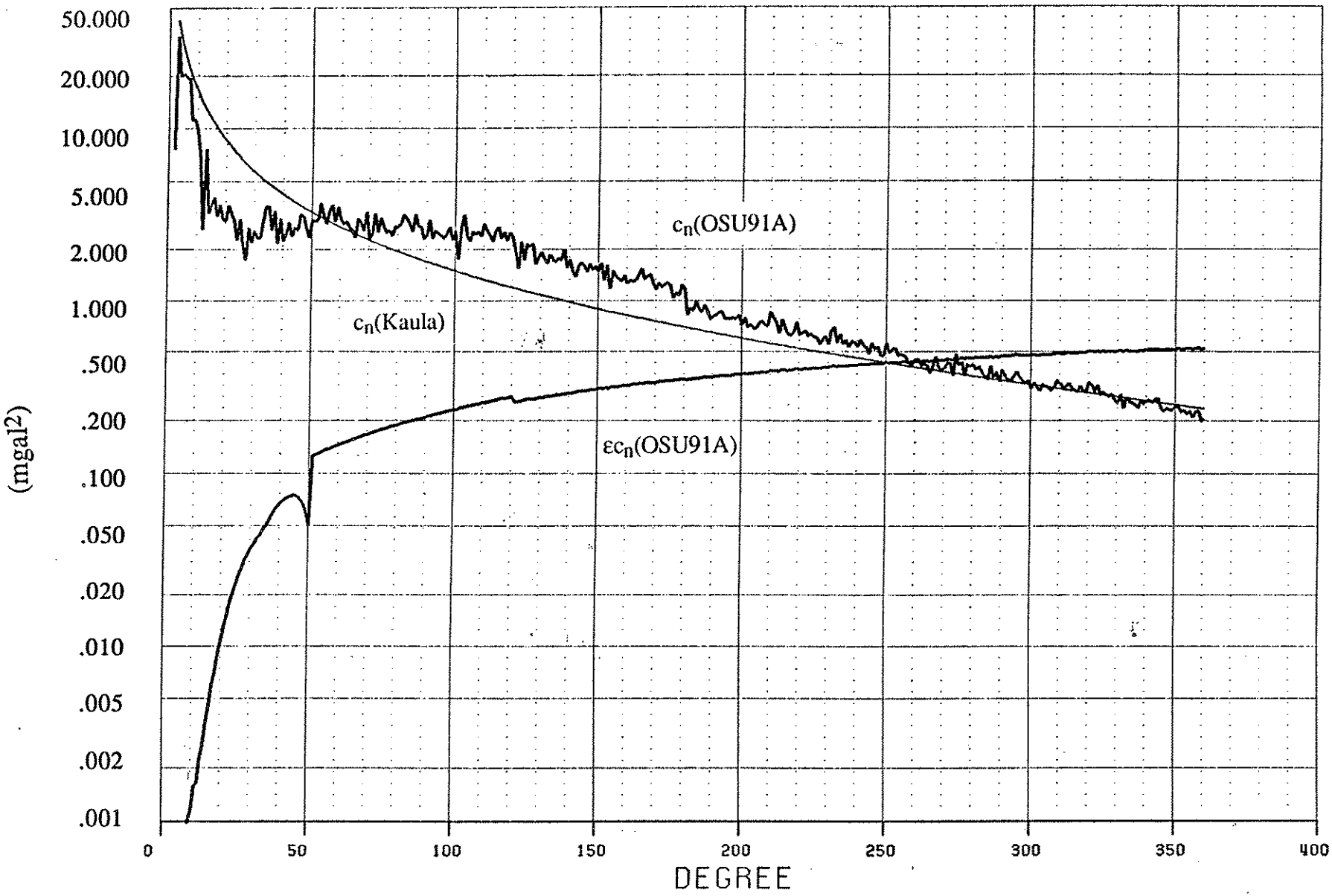

Figure 26. Anomaly signal and error degree variances implied by OSU91A and Kaula's rule. Values refer to the sphere of radius 6378137 m.

8.0 Model Comparisons and Evaluations

In this section we will evaluate some of the preliminary models, as well as the final geopotential model, OSU91A, developed for this report. In addition, for some evaluations, we will incorporate other recently published or developed geopotential models.

8.1 Orbit Accuracy Assessment

In this section we discuss orbit fits or orbit residuals when a geopotential model is used in an orbit determination process. In principle the smaller the residual fit the better the model. However the situation is not as simple as this because a potential coefficient model is only one part of a package used in the orbit estimation process. For example, one needs a set of station coordinates that should be consistently estimated with the geopotential model. In the tests to be described here the station coordinates, tidal models, etc., are held fixed at previously determined values. In some cases drag, radiation, etc. parameters may be estimated. Rapp and Pavlis (1990, Table 10) report, orbit accuracy assessments for a variety of models being evaluated at that time.

The first group of tests were carried out by Fell (1991, private communication) using Doppler data acquired from 45 tracking station for Geosat and NOVA 3 satellites. The results of the tests are given through "station navigation statistics which are the weighted RMS in the radial and tangential directions computed from adjusting the geodetic position of each station on a single pass basis to best fit the estimated ephemeris for the satellite which is held fixed in the adjustment" (Sloop, 1991, private communication).

These statistics are given for several models in Table 23.

Table 23. Navigation Statistics for Various Geopotential Models Based on Doppler Tracking of Geosat. Units are meters.

	RMS Residuals	
Model	Radial	Tangential
GEM-T1	2.2	2.3
GEM-T2	2.3	2.2
OSU89A	2.4	2.2
OSU89B	2.4	2.2
S10.W24GW	2.4	2.2
S10.W96GW(91A)	2.4	2.2

This table does not indicate much sensitivity to the geopotential models tested. In Table 24 statistics for the NOVA 3 satellite are given.

Table 24. Navigation Statistics for Various Geopotential Models Based on Doppler Tracking of NOVA 3. Units are meters.

	RMS Residuals	
Model	Radial	Tangential
GEM-T1	1.8	2.5
GEM-T2	1.4	1.6
OSU89A	1.3	1.6
OSU89B	1.3	1.6
S10.W24GW	1.3	1.3
S10.W96GW(91A)	1.3	1.4

Again the results, except for GEM-T1, are all about the same indicating that the preference between the models can not be determined from the table. On the other hand the combination solution that are represented here do not show a deterioration in fit over a satellite alone model. This, in itself is encouraging.

Additional orbit fits were carried out at the Goddard Space Flight Center by Klosko (1991, private communication) with the 1/24 and 1/96 weighting procedures. Results using "frozen" data sets are given in Table 25.

Table 25. RMS of Fit for Selected Geopotential Models On Selected Satellite Using Laser Tracking and Frozen Data Sets. Units are cm.

	Model		
Satellite	GEM-T2	W24GW	W96GW
Lageos	5.2	5.4	5.3
BEC	28.5	26.5	25.5
Geos-1	20.9	22.1	21.7
Geos-2	50.9	48.3	46.9
Geos-3	17.9	19.6	19.2
Ajisai	10.9	11.7	11.6
Starlette	14.7	17.0	17.0

These tables seem to give a consistent picture that indicates the W96GW (OSU91A) model gives slightly better fits than the W24GW solution. The results are mixed when compared against GEM-T2. In some cases the T2 models gives better results while in others the OSU models are slightly better.

Putney et al. (1991) have reported data fits in orbit tests with independent data with several geopotential models. The TEG-2 model was developed at the University of Texas at Austin (Tapley, private communication, 1991). Results for laser observation on three satellites are given in Table 26.

Table 26. RMS of Fit for Selected Geopotential Models On Three Laser Tracked Satellites (Putney et al., 1991). Units are cm.

Model	Lageos	Ajisai	Starlette
GEM-T2	3.05	10.15	13.28
GEM-T3	2.91	9.99	11.77
TEG-2	2.93	9.77	12.04
OSU91A	2.97	10.18	13.17

These results show that OSU91A gives fits similar to the other models tested but it is always slightly poorer (2% to 12%) than the GEM-T3 model.

Putney et al. (ibid) also described orbit fit tests with SPOT-2 Doris data. Selected results from Putney et al. are shown in Table 27.

Table 27. RMS Fits To Spot-2 Doris Data. Units are mm/sec.

	Arc	
Model	503	702
GEM-T2	6.1	6.6
GEM-T3	3.5	3.4
TEG-2	4.0	4.2
OSU91A	4.7	3.7

This table shows that the OSU91A has made a significant improvement over the GEM-T2 model for both arcs. The fit for arc 503, is significantly better and marginally better for arc 702 with the GEM-T3 model as opposed to OSU91A. The results indicate that the OSU combination model has yielded better results than the initial model but other models are better in these comparisons.

From the tests reported in this section we conclude that OSU91A performs well in the orbit fit tests but it is not the best model for the satellite orbit fits. Based on the results of Putney et al. (ibid) GEM-T3 gives better fits by 2 to 25%. Whether this is important or not must be judged in the context of the other tests to be reported in the next sections.

8.2 Model Undulation Comparisons at Doppler Positioned Stations

The principle in this comparison is to calculate the geoid undulation from the geopotential model and compare the value to that implied by an ellipsoid height from Doppler positioning, and an orthometric height of the station. Before the comparison can be done the Doppler heights must be put into a geocentric reference system that is properly scaled. The procedures followed for this report are identical to those described by Rapp and Pavlis (1990, Section 4.2). The results are given in Table 28 where the mean difference (Doppler minus model), the standard deviation of the difference, and the number of accepted stations are given. Two models, GEM-T3 and TEG-2, were augmented in these comparisons, with the coefficients from degree 51 to 360 from the OSU91A model.

Table 28. Comparison of Geoid Undulations from Doppler Positioning with Geoid Undulations from Potential Coefficient Models

	Mean	Standard	Number of
Model	Difference, m	Deviation, m	Stations
OSU89B	.14	±1.60	1782
OSU91A	.15	1.58	1802
GEM-T3	.12	1.57	1788
TEG-2	.10	1.77	1767

These results indicate a slight improvement of OSU91A over OSU89B. The T3 comparisons shows 14 less stations (than 91A) used in the comparisons while the TEG-2 model has a significantly larger standard deviation.

One can also test to see if the undulation discrepancies in these comparisons have a correlation with elevation. This is done by making a linear fit to the residuals and examining the height dependent term. Table 29 shows results of these comparisons including the RMS residual (after adjustment).

Table 29. Bias and Slope Fits to Undulation Residuals as a Function of Elevation for the Global Station Set

Model	Bias, m	Slope, m/km	RMS Residual, m
OSU89B	.059 ± .104	-.008 ± .086	.226
OSU91A	.034 ± .099	.037 ± .082	.216
GEM-T3	.006 ± .105	.038 ± .087	.230
TEG-2	-.131 ± .140	.159 ± .116	.305

This table shows that the 91A gives smaller residuals than the 89B model. The slope is negligible for 89B, 91A, and T3 and at the edge of being significant for TEG-2. The RMS residual is 41% higher than that found for 91A.

We conclude by noting the 91A model and the augmented T3 model appear to have comparable accuracy although 91A would have the edge because more stations are accepted for use, and the RMS residual, from Table 29, is smaller.

Recently Shibuya (1991, private communication) made available the ellipsoidal height of a station (the S point) at Breid Bay, East Antarctica whose position was determined in the WGS84 terrestrial reference frame using the precise DMA ephemeris. Also available (Shibuya, Fukuda, Michida, 1991) was a mean sea level height for the station. Taking into account the significant (-2.0 m) sea surface topography in this area, and referencing the undulation to the equatorial radius of 6378136.3 m, the geoid undulation was estimated as 22.8 m. Using OSU91A the geoid undulation was 22.2 m, an excellent agreement. A nearby Geosat track, again after correction for sea surface topography, implied a geoid undulation of 21.6 m. These two values are in excellent agreement.

8.3 Comparison with Undulations and Undulation Differences at GPS/Orthometric Height Stations

In the past several years GPS measurements have been made to accurately position stations, primarily in a relative sense. The positions are generally determined by fixing one station through coordinates defined in a terrestrial reference frame. This frame might be in a geodetic datum (e.g. NAD83) or in a space related frame defined by satellite laser ranging or VLBI measurements. Rapp and Pavlis (1990, Section 4) describe four GPS/leveling traverses that will also be analyzed here. In addition Rapp and Kadir (1988) describe an area network of GPS stations in the State of Tennessee that will also be examined here. The Tennessee network consisted of 49 stations distributed uniformly across the State of Tennessee. The positions were not placed in a geocentric system so that systematic undulation differences are to be expected between the geoid undulations implied by the potential coefficient model and the GPS ellipsoidal height/leveling orthometric height. A complete description of other traverses may be found in Rapp and Pavlis (1990, Section 4.3).

Table 30 shows the mean differences (model minus GPS/leveling) between the two undulation estimates.

Table 30. Mean Undulation Difference at GPS Stations. Units are cm.

	Traverse or Networks				
	Europe	Canada	Australia	Scandinavia	Tennessee
Num of Stations	60	63	38	46	49
Model					
OSU89B	26	-38	-3	29	149
OSU91A	40	4	-49	33	157
GEM-T3	35	-16	-18	28	183
TEG-2	78	43	61	64	262

This table shows variations between the models and the traverse/network being tested. The largest mean difference occurs for Tennessee which has not been placed in a geocentric system.

Table 31 shows the standard deviation (mean removed) of the undulation difference for the same traverse/network shown in the previous table.

Table 31. Standard Deviation of the Undulation Difference at GPS Stations in Five Areas. Units are cm.

	Traverse or Networks				
Model	Europe	Canada	Australia	Scandinavia	Tennessee
OSU89B	32	39	34	32	30
OSU91A	33	36	35	32	21
GEM-T3	42	36	35	48	23
TEG-2	70	57	68	75	73

Table 31 shows that 91A is slightly better than 89B although a significant improvement takes place for the Tennessee area. GEM-T3 is comparable to the other OSU solutions in Canada, Australia, and Tennessee and poorer for the European and Scandinavia traverse. The TEG-2 model performs poorer than the other models in these tests.

The next comparison is a relative comparison where undulation differences are compared. Such a comparison removes or reduces long wavelength error in the data. In these computations the differences are computed between adjacent stations in the traverse. In the Tennessee networks comparisons are made provided the station spacing is less than or equal to 55 km. This distance limits the comparisons to adjacent stations in the network. The results are given in terms of RMS differences and in ppm (parts per million) by dividing the RMS difference by the length of the line. The values are given in Table 32.

Table 32. Relative Geoid Undulation Comparisons for GPS/leveling and Model Results

	Traverse or Networks									
Model	Europe		Canada		Australia		Scandinavia		Tennessee	
	RMS	ppm	RMS	ppm	RMS	ppm	RMS	ppm	RMS	ppm
OSU89B	25	3.5	9	6.6	22	5.1	24	4.3	28	4.9
OSU91A	23	3.6	9	6.6	22	5.3	25	4.4	26	3.9
GEM-T3	24	3.7	9	6.6	22	5.3	26	4.6	26	3.9
TEG-2	30	5.2	10	6.8	26	5.6	33	5.8	57	6.0

The results in Table 32 indicate the first three models listed are of comparable accuracy while the TEG-2 model performs somewhat poorer.

In judging these differences it is of interest to compare the results with what is expected from the errors given for the coefficients of the OSU91A model. To do this we write the commission error for a undulation difference computed from potential coefficients to degree N and perfect gravity data in a spherical cap of radius to ψ_o as follows (Christodoulidis, 1976, eq. (135)):

$$C_{PQ}^2 = \frac{R^2}{2\gamma^2} \sum_{n=2}^{N} Q_n^2(\psi_o) \varepsilon_n^2 s^{n+2} [1 - P_n(\cos\psi_{PQ})] \tag{8.1}$$

where: R is a mean Earth radius:
γ is an average value of gravity
ϕ_n is the Molodensky truncation coefficient at degree n;
ε_n^2 is the error anomaly degree variances;
s is a factor to refer results to the mean sphere.

The omission or truncation error would be written as:

$$T_{PQ}^2 = \frac{R^2}{2\gamma^2} \sum_{N+1}^{\infty} Q_n^2(\psi_o) c_n s^{n+2} [1 - P_n(\cos\psi_{PQ})] \tag{8.2}$$

where c_n are the anomaly degree variances implied by a model.

If only potential coefficient information is to be used, $\psi_o = 0$ and

$$Q_n(\psi_o = 0) = \frac{2}{n - 1} \tag{8.3}$$

Equations (8.1) and (8.2) now become:

$$C_{PQ}^2 = \frac{2R^2}{\gamma^2} \sum_{n=2}^{\infty} \frac{1}{(n-1)^2} \varepsilon_n^2 s^{n+2} [1 - P_n(\cos\psi_{PQ})] \tag{8.4}$$

$$T_{PQ}^2 = \frac{2R^2}{\gamma^2} \sum_{n+1}^{\infty} \frac{1}{(n-1)^2} c_n s^{n+2} [1 - P_n(\cos\psi_{PQ})] \tag{8.5}$$

Letting R = 6371000 m, $\gamma = GM/R^2 = 9.820$ ms^{-2}, and using the Jekeli parameters in the Tscherning/Rapp degree variance model equation (8.4) and (8.5) have been evaluated. The ε_n^2 values have been based on the actual error degree variances of OSU91A to degree 260, and the actual anomaly degree variances of 91A from degree 261 to 360. The individual results and total results are given in Table 33 for the OSU91 model. In addition the total error has been expressed in parts per million of the distance.

Table 33. Commission and Omission Error in the Computation of Geoid Undulation Differences from the OSU91A Potential Coefficient Model

Linear Separation	Angular Separation	Commission Error	Truncation Error	Total Error	Error in ppm
0 km	0.00	0 cm	0 cm	0 cm	0 cm
10	.09	9.2	10.3	13.8	13.8
20	.18	18.1	17.9	25.5	12.7
30	.27	26.6	22.7	35.0	11.7
40	.36	34.4	25.3	42.7	10.7
50	.45	41.3	26.2	48.9	9.8
70	.63	52.4	24.8	57.9	8.3
90	.81	59.6	22.6	63.7	7.1
100	.90	62.0	22.1	65.8	6.6
200	1.80	71.8	23.1	75.4	3.8
400	3.60	77.1	23.6	80.6	2.0
600	5.40	77.7	23.6	81.2	1.4
800	7.19	77.7	23.5	81.2	1.0
1000	8.99	77.8	23.5	81.2	0.8
1600	14.39	77.4	23.5	80.9	0.5
2000	17.99	77.4	23.5	80.9	0.4
10000	89.93	77.4	23.5	80.9	.08

The results from Table 33 can be compared to results from actual comparisons as represented in Table 32. Note that the errors given in Table 32 are errors in all data used in the comparison: geopotential model; GPS; leveling. Even then the actual results are much better than is expected from the projected OSU91 model errors shown in Table 33 noting the average line length in Table 32 is 30 km.

8.4 Comparison with Undulation and Undulation Differences at Two VLBI Sites.

Forsberg and Madsen (1990) have pointed out that precise ellipsoidal and orthometric heights exist at the VLBI sites which have been tied into the geocentric terrestrial reference system FSC-2. Knowing the ellipsoidal height in the geocentric system and the orthometric height a "standard" geoid undulation can be defined. The coordinates of the two stations are as follows:

Tromso	69°40'N, 18°56'E
Onsala	57°24'N, 11°56'E

The standard undulation, undulation from a variety of models, and undulation differences relative to the standard are given in Table 34 for Tromso and Table 35 for Onsala.

Table 34. Undulation and Undulation Discrepancies at the Tromso VLBI Station

Solution	Undulation	Difference w.r.t.VLBI
VLBI	31.11 m	—
NKG89*	31.45	34 cm
OSU89B	31.67	56
OSU91A	31.22	11
GEM-T3	31.48	37
TEG-2	31.36	25

* detailed geoid solution; see Forsberg and Madsen.

Table 35. Undulation and Undulation Discrepancies at the Onsala VLBI Site

Solution	Undulation	Difference w.r.t.VLBI
VLBI	36.54 m	—
NKG89*	36.28	-26 cm
OSU89B	36.65	11
OSU91A	36.71	17
GEM-T3	36.54	0
TEG-2	36.32	-22

These two tables show different levels of agreement, all of which are fairly good. It is interesting to note that the OUS91A and TEG-2 model both show better agreement with the "standard" than the detailed geoid, NKG89.

A final comparison can be made by calculating the undulation difference, Tromso - Onsala, from VLBI and from the models. These results are given in Table 36.

Table 36. Geoid Undulation Difference Comparisons Between the Tromso and Onsala VLBI Sites

	Value	Difference w.r.t.VLBI
VLBI	-543 cm	—
NKG89	-483	60 cm
OSU89B	-498	45
OSU91A	-549	6
GEM-T3	-506	37
TEG-2	-496	47

The results from this table show a great variety of differences, with OSU91A clearly giving the best agreement with the standard.

8.5 Comparison with Geoid Undulations Derived from Geosat Altimeter Data

In this section we discuss the geoid undulations derived from Geosat altimeter data with the geoid undulations derived from the various geopotential models. Such comparisons were described in Rapp and Pavlis (1990, Section 4.4). The basic principle in finding the geoid undulation from satellite altimeter data is to assume that sea surface topography (ζ) is known, and to remove it from a sea surface height that has been determined from an accurate satellite ephemeris. Specifically we have:

$$N = SSH - \zeta \tag{8.6}$$

For the calculations to be described here the sea surface heights have been calculated from the orbits developed as part of the adjustment process described in Section 2 and Section 4. The sea surface topography was the (10, 10) model, based on the 1/96 altimeter weighting, as described in Section 5. In the comparisons the Geosat data consisted of 768286 points in the following time period: 870220 (11 hr 8 min), 870307 (23 hr 55 min). This 17 day time frame corresponds, approximately, to the Exact Repeat Mission 7. This time period has been used because it corresponds to the summer time in the Antarctic region so that data, in normally ice covered areas, is available.

In carrying out these comparisons it is important to recognize the role of the permanent Earth tides (Rapp, 1989, Rapp et al., 1991). In our case, the Geosat surface is in a "mean" system. The geoid undulations (N_n) that are computed from the potential coefficient models are

placed in the non-tidal system which is consistent with the system used for the development of GEM-T2. We then define the undulation discrepancy as follows:

$$d = N_n - 0.257\left(\frac{3}{2}\sin^2\phi - \frac{1}{2}\right) - (SSH - \zeta) \qquad (8.7)$$

where the second term on the right hand side of (8.7) follows from eq. (18) of Rapp (1989) with $k_2 = 0.3$. Table 37 gives statistical information on "d" for several geopotential models. This table is analogous to Table 8 of Rapp and Pavlis (1990). For consistency reasons the sea surface topography was kept at the OSU91 degree 10 model. However one test was carried out with a degree 10 (TEG-2) model supplied by Shum (1991, private communication). The geopotential model is defined by the model identified augmented by the OSU91A model from degree 51 to 360 except in the case of OSU89B which is itself complete to 360.

Table 37. Results from the Comparison of Model and Geosat (ERM 7) Implied Geoid Undulations. Units are m.

Differences	OSU89B	OSU91A	GEM-T3	TEG-2	TEG-2*
Minimum	-8.34	-6.92	-6.52	-8.67	-7.71
Maximum	5.53	4.54	4.49	10.03	10.86
Mean	0.005	0.008	0.019	0.033	0.057
Std. Dev.	0.529	0.342	0.485	0.739	0.785
No ≥ 1.5 m	14291	4505	16204	43181	48298
No ≥ 2.0 m	4008	1456	5176	22280	25929
No ≥ 4.0 m	82	39	128	1774	3196

* with TEG-2 SST model.

From this table we see that the 89B model gives better results (53 cm vs 61 cm) than presented in Table 8 of Rapp and Pavlis (ibid). This is presumably due to the improved Geosat orbits described in this paper. The OSU91A model shows a significant improvement over 89B (± 34 cm vs 53 cm) with a considerable reduction (14291 to 4505) in the number of discrepancies ≥ 1.5 m. The augmented GEM-T3 model performs better than the TEG-2 model in these tests but still does not give as good a fit as the OSU91A model. The last two columns of Table 37 differ in the sense that the last column uses the TEG-2 SST model while the second from the last uses the OSU91 SST model. The comparisons are better when the OSU91 model is used. This may be due to the error in the TEG-2 SST model in geographic areas for which data was not included in the solution. In assessing these comparisons one must recognize that the orbits being used are those consistent with the OSU91A gravity field up to degree 50. Since the orbit is dependent on the gravity field, it would be appropriate to carry out these comparisons with Geosat orbits that are consistent with the GEM-T3 or TEG-2 model. No such tests were carried out because such orbits were not available.

It is appropriate to point out that the standard deviation of 34 cm associated with the OSU91 model is smaller than would be expected from the discussion near Table 22 where it was argued that the total undulation error, at a mean radius of 6371 km, is 57 cm, considerably more than the 34 cm found from the Geosat comparisons. However the 57 cm is a global estimate and the results for the ocean area would be slightly smaller but not enough to account for the apparent pessimistic accuracy estimate obtained through formal error propagation.

We next examine the location of the residuals that exceeded 1.5 m for the 91A (Figure 27), GEM-T3 (Figure 28), and TEG-2 (Figure 29) models. A similar figure for the OUS89B model is Figure 8 in Rapp and Pavlis (ibid).

Figure 27, for the OSU91A model shows that the discrepancies occur primarily in areas of high frequency where contributions from the harmonics above degree 360 may be significant. Figure 28, for the augmented GEM-T3 model shows the high frequency discrepancies noted for the OSU91A model, but also discrepancies in the Mediterranean and Caspian Seas as well as large patches of discrepancies below -60°. Figure 29 for the augmented TEG-2 model (with the OSU91 SST model) shows the high frequency effect as well as substantial discrepancies in the Mediterranean and Caspian Seas and large patches of discrepancies below -60° latitude. In addition track related discrepancies are obvious north of Australia and west of South America.

The large patterns of residuals for the GEM-T3 and the TEG-2 model is apparently traceable to editing criteria that deleted data from these areas in the analysis leading to GEM-T3 and TEG-2. This criteria specifically deleted data below -60° latitude, in shallow water areas, and in areas where the tide model was not defined on the GDR. These editing criteria would seem to be too

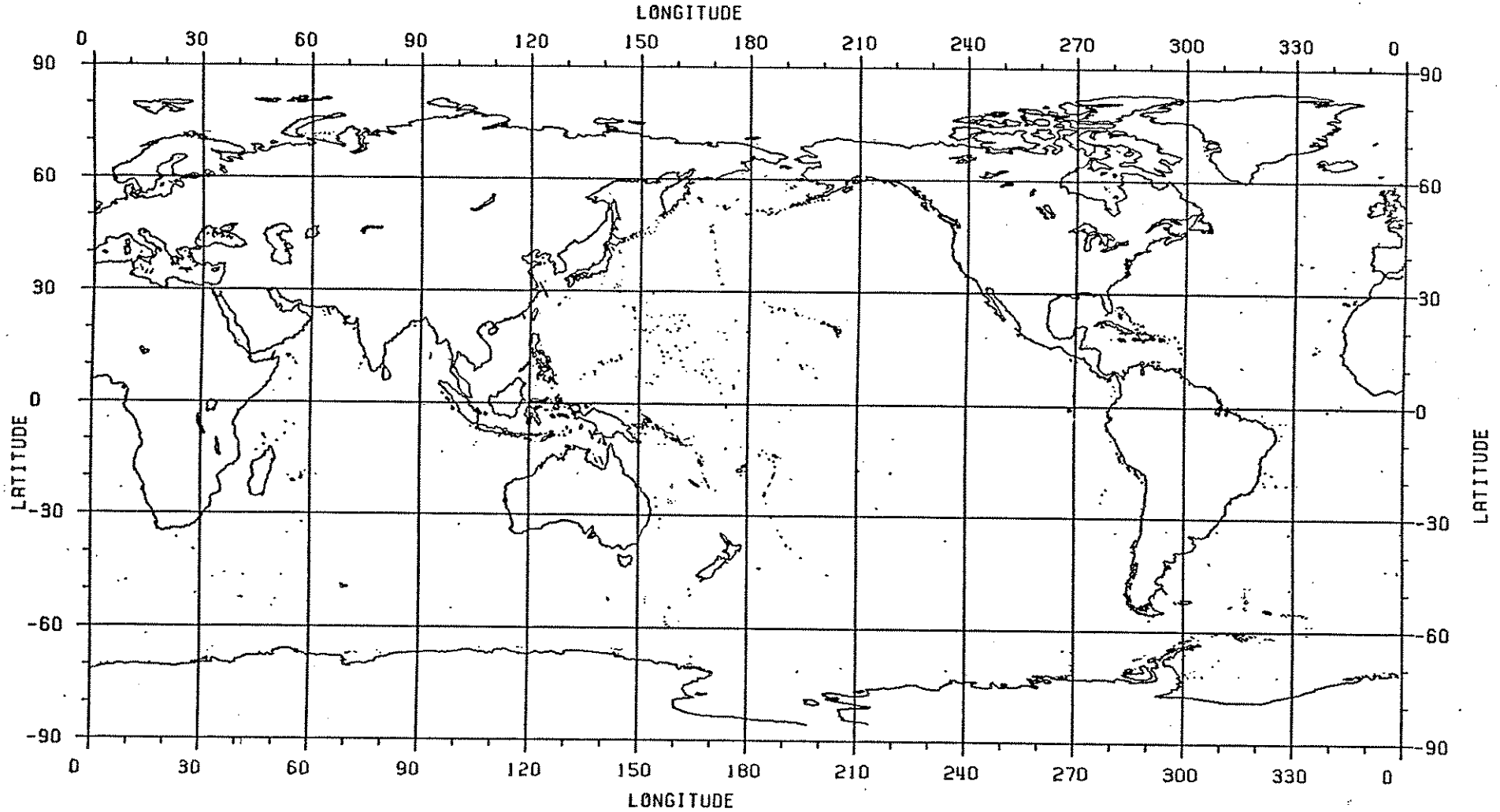

Figure 27. Location of 4505 Points on Geosat ERM7 Where the Corrected Geoid Model (OSU91A) Minus the Corrected Sea Surface Height Is ≥ 1.5 m.

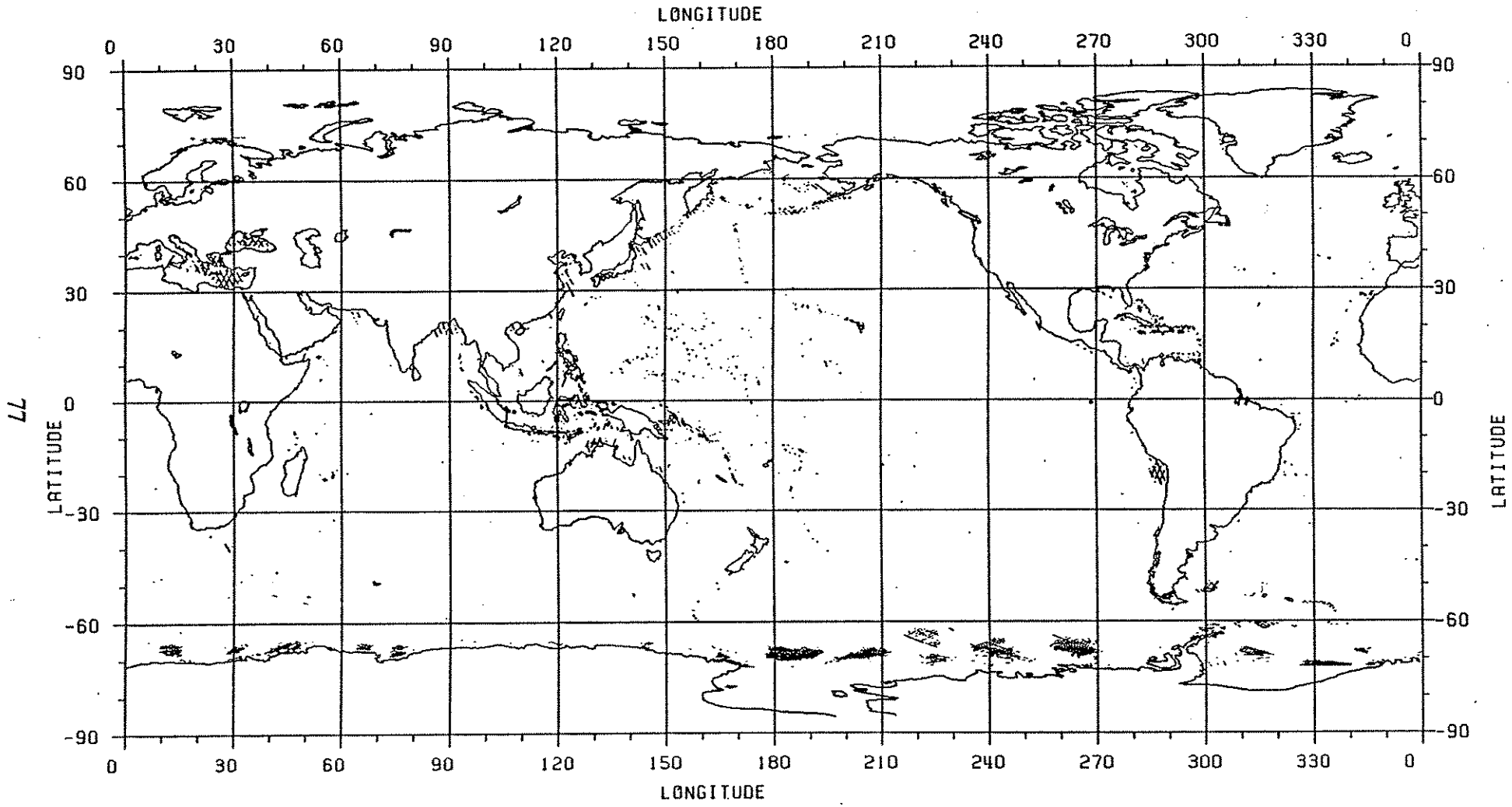

Figure 28. Location of 16204 Points on Geosat ERM7 Where the Corrected and Augmented Geoid Model (GEM-T3) Minus the Corrected Sea Surface Height Is ≥ 1.5 m.

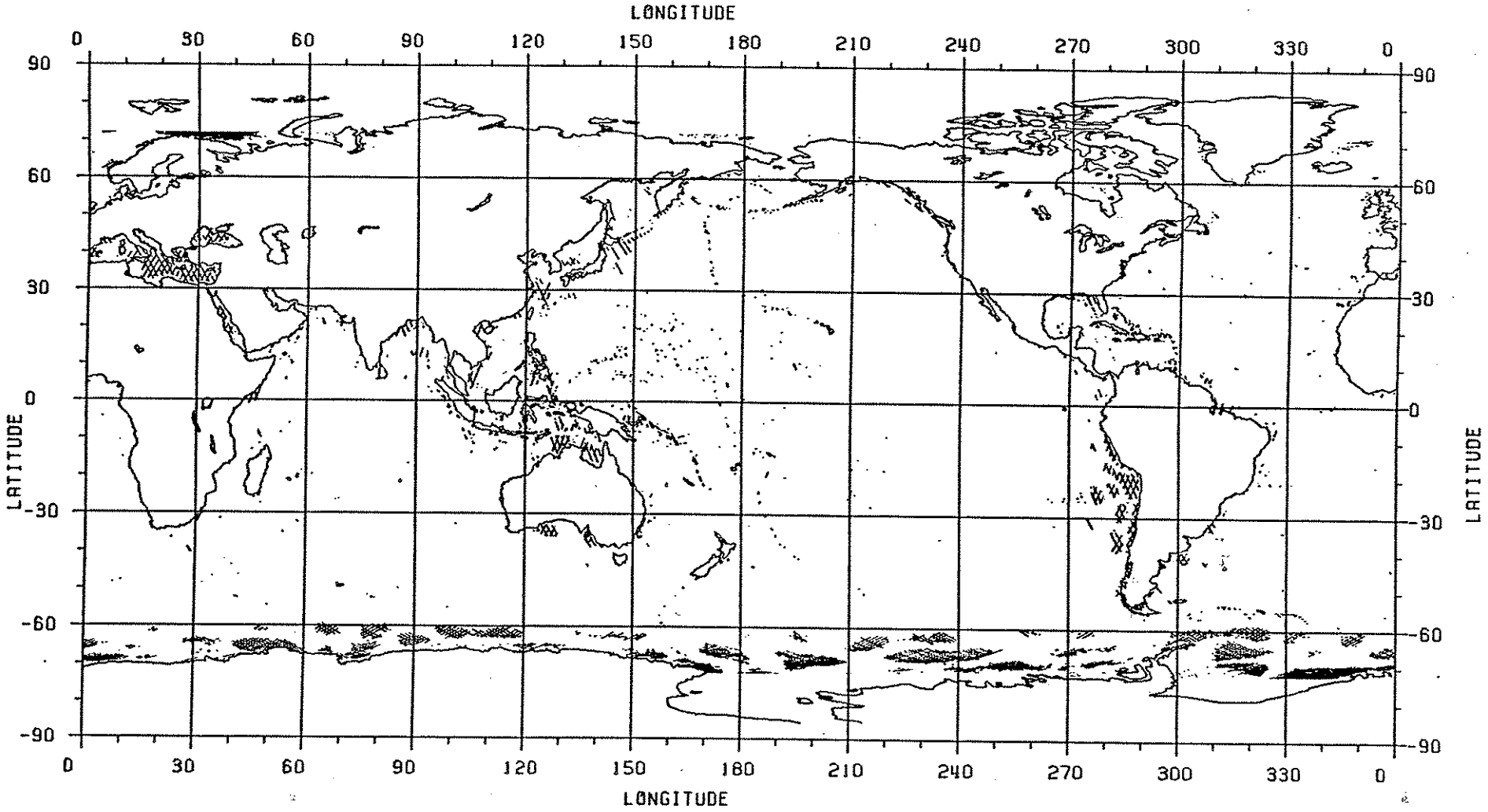

Figure 29. Location of 43181 Points on Geosat ERM7 Where the Corrected and Augmented Geoid Model (TEG-2) Minus the Corrected Sea Surface Height Is ≥ 1.5 m.

restrictive and have led to a gravity model that does not fit the data in areas where the data was not used in the solution. No surprise.

Another set of comparisons were made when data below -60° latitude, and in the Mediterranean area ($30° < \phi < 46°$, $0° < \lambda < 38°$) were excluded from the comparisons. These results are shown in Table 38 where 668534 points were compared.

Table 38. Altimeter/Model Geoid Undulation Comparisons Deleting Data Below -60° and in the Mediterranean Area. Units are m.

	Model			
	OSU91A	GEM-T3	TEG-2	TEG-2*
Std. Dev.	0.34	0.40	0.53	0.53
No ≥ 1.5 m	3656	6054	15672	14589

* with TEG-2 SST model.

From this table we see no change in the standard deviation for the OSU91A model as compared to the complete case given in Table 37. The results for GEM-T3 are improved significantly although the TEG-2 model shows residuals 2.5 times greater in number than GEM-T3. Additional tests are described by Rapp, Wang, and Pavlis (1991a) in which sea surface heights along Geosat tracks on the Mediterranean Sea were compared with the corresponding undulation from selected models. With the TEG-2 model the discrepancies reached 6.2 m while other models showed better agreement. Statistics on the agreement along two Geosat arcs are given on Table 39.

Table 39. Standard Deviation of Geoid Undulation Differences for Two Geosat Tracks (ERM 7) in the Mediterranean Sea

Model	Track 90874	Track 90888
PGS4233	45 cm	242 cm
TEG-2	139	625
OSU91A	20	54

Track 90874 starts south of Italy and goes to the African coast. Track 90888 crosses the Agean Sea and the Mediterranean. It is in an area of extreme variations of the geoid accounting for the poorer fit for the track as compared with track 90874.

8.6 Conclusion

This lengthy section has been developed to report comparisons of a number of geopotential models with selected data for evaluation purposes. The evaluations range from orbit fit tests to the comparison of undulation differences from VLBI/leveling data. The orbit fits with OSU91A showed reasonable results but for some tests (e.g. with DORIS data) not quite as good as GEM-T3. Many other orbit tests could be run and the results would depend on how the satellite data was weighted in the solution. The tests with the Doppler undulation data showed the 91A and T3 solutions are comparable and TEG-2 is poorer. The undulation comparisons at GPS/leveling stations showed 91A gives somewhat better results than GEM-T3 while TEG-2 is significantly poorer than 91A or T3. Undulation and undulation difference comparisons at two VLBI sites in Europe indicate good agreement with 91A.

One of the most revealing tests was with the altimeter implied geoid undulations. Using a complete Geosat ERM statistics on the undulation differences for several models were computed. The OSU91A model gave the best agreement which is to be expected to some extent since there

was Geosat data used in the solution to degree 50. Poorer comparisons were obtained with GEM-T3 and TEG-2 although GEM-T3 was significantly better than the TEG-2 model. Examination of the location of larger residuals indicated areas for which data was edited out in the T3 and TEG-2 data analysis. These results indicate careful consideration must be given to data editing since models will not fit well in areas where no data has been included in a solution.

9.0 Undulation Differences Between Models

Rapp, Wang, and Pavlis (1991b, 1991c) have compared several geopotential models primarily in terms of global undulation differences. Selected results from these papers are described in this section.

We first compute the geoid undulation on a 1° x 1° grid from the potential coefficient model to degree 50. Table 40 gives the standard deviation of the global differences, Table 41 gives the differences for land (positive elevation) and Table 42 gives the differences for ocean (negative elevations) areas.

Table 40. Standard Deviation of Geoid Undulation Differences on a Global Scale. Units are cm.

Model	91A	T3	TEG-2
OSU91A	—	47	106
GEM-T3	47	—	83

Table 41. Standard Deviation of Geoid Undulation Differences in Land Areas. Units are cm.

Model	91A	T3	TEG-2
OSU91A	—	73	176
GEM-T3	73	—	131

Table 42. Standard Deviation of Geoid Undulation Differences in Ocean Areas. Units are cm.

Model	91A	T3	TEG-2
OSU91A	—	24	65
GEM-T3	24	—	47

The best agreement between the models takes place in the ocean areas. The ±73 cm difference (SD) between 91A and GEM-T3 in land areas can be attributed to different weighting procedures. The differences between TEG-2 and the OSU91A and GEM-T3 are due to different surface normal equations used, TEG-2 used a set of normal equations based on 1986 surface data while OSU91A and GEM-T3 used a set of normal equations based on 1990 data. Table 43 gives the magnitude of the largest discrepancies:

Table 43. Maximum Absolute Geoid Undulation Difference Between Selected Geopotential Models to Degree 50. Units are cm.

Model	91A	T3	TEG-2
OSU91A	—	446	910
GEM-T3	446	—	623

The 9.1 m difference between 91A and TEG-2 occurs in western South America near latitude -19°. An additional large difference of 9.0 m occurs in the eastern Mediterranean Sea near longitude 30°. The largest difference between the 91A and GEM-T3 model occurs in the Himalaya Mountains. Figure 30 shows the undulation differences GEM-T3 minus OSU91A. The good agreement (± 24 cm) in the ocean areas is clearly contrasted with the poorer agreement (±73 cm) in the land areas. Also clear from this figure is the poorer agreement below -69° and in the Mediterranean Sea.

In Figure 31 we show the geoid undulation differences by degree for GEM-T3 and TEG-2 with respect to the OSU91A model. TEG-2 shows significant differences after degree 10. At degree 10 there is a 5.8 cm difference between OSU91A and TEG-2 while the difference is 3.8 cm

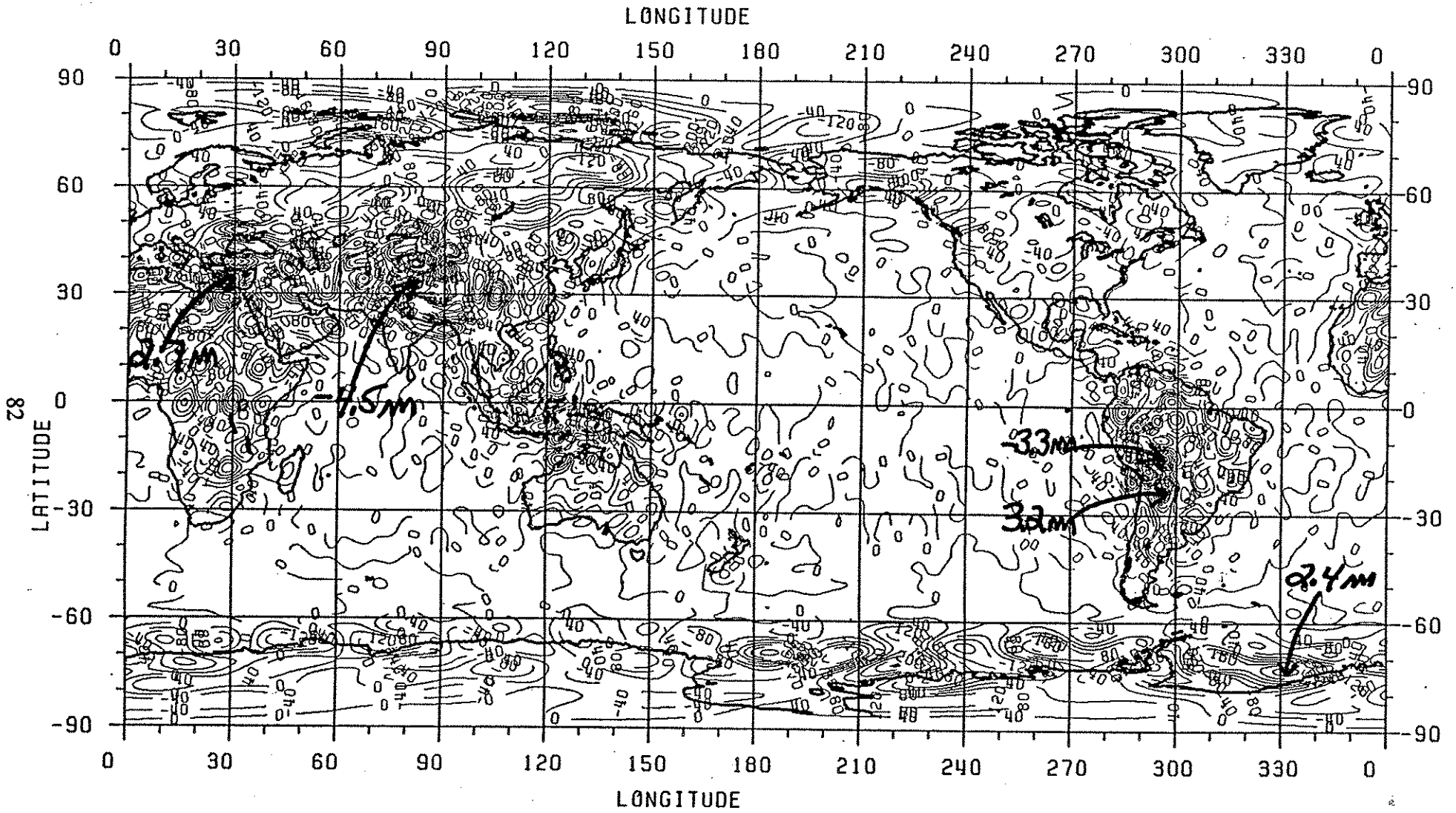

Figure 30. Geoid Undulation Differences, GEM-T3 Minus OSU91A, Band on a 3° x 3° Grid with Coefficients to Degree 50. Contour Interval is 40 cm.

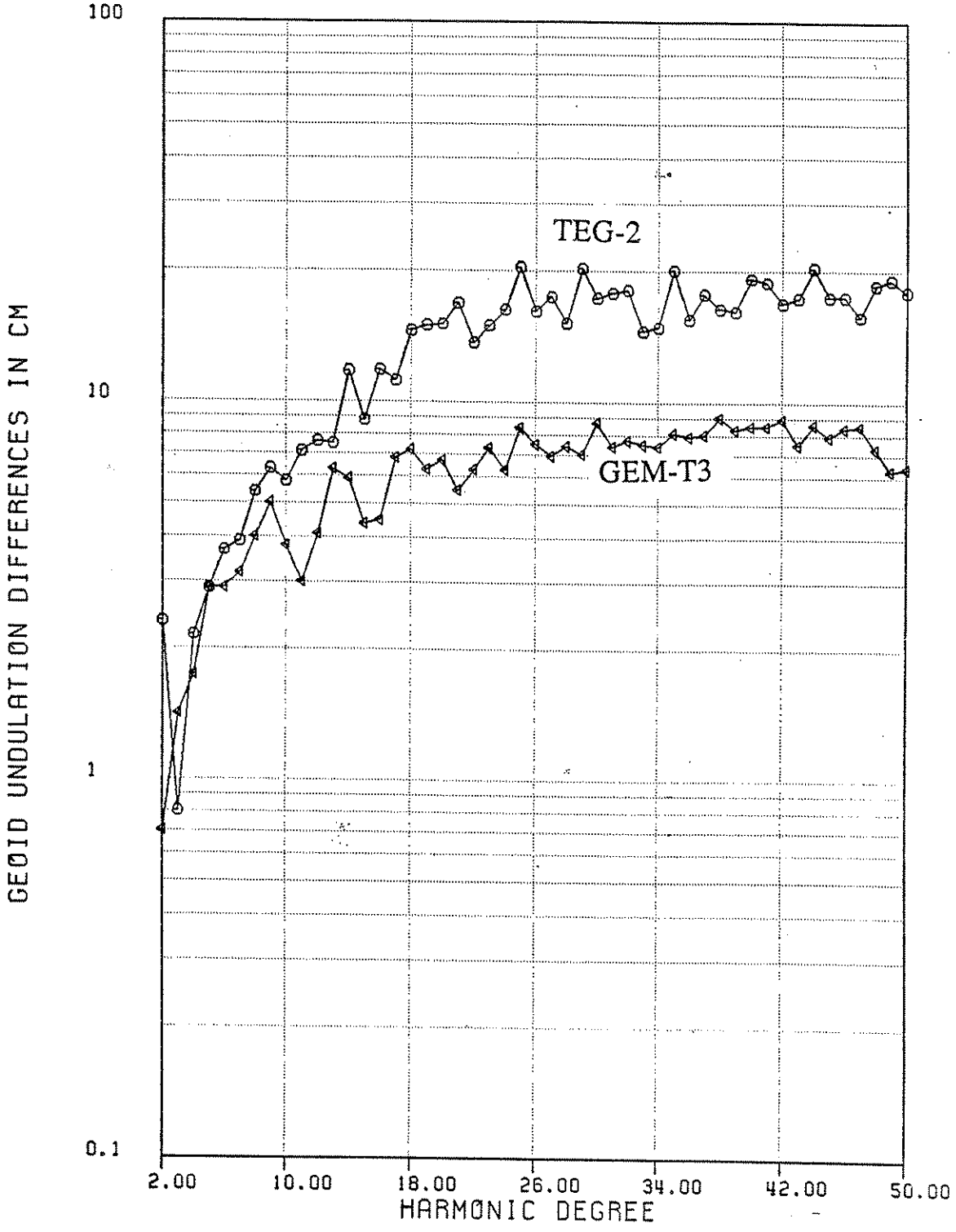

Figure 31. Geoid Undulation Difference by Degree With Respect to OSU91A.

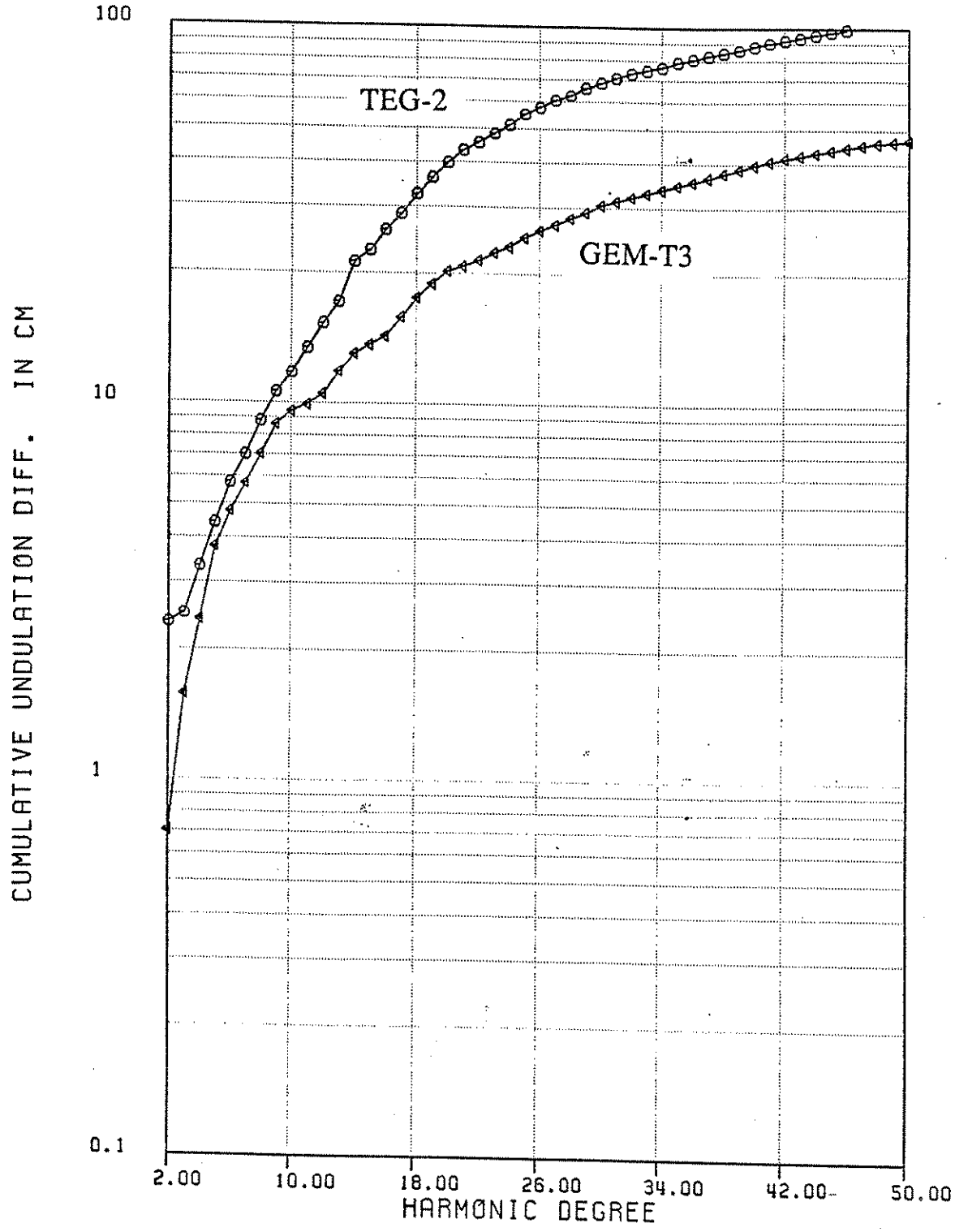

Figure 32. Cumulative Undulation Difference by Degree With Respect to OSU91A.

with GEM-T3. Table 44 gives the undulation differences by degree. Figure 32 shows the cumulative undulation difference up to the specified degree.

Table 44. Geoid Undulation Differences By Degree With Respect to OSU91A. Units are cm.

Degree	GEM-T3	TEG-2
2	0.7	2.4
5	2.9	2.9
10	3.8	5.8
20	6.7	15.9
30	8.7	17.9
40	8.5	19.4
50	6.4	18.4
Cumulative	47	106

The better agreement with GEM-T3 may be attributed, in part, to the OSU91A model development starting from the GEM-T2 model.

This section has examined the geoid undulation differences between three geopotential models: OSU91A, GEM-T3, and TEG-2. All comparisons have been made to degree 50. We find that OSU91A agrees better with the GEM-T3 model than with TEG-2. The models agree best in the ocean areas with significant (9 m) differences in some areas.

Similar comparisons could be made for gravity anomalies and for comparisons with the OSU89B potential coefficient model which is complete to degree 360 as is the OSU91A model. Table 45 gives such comparisons.

Table 45. Cumulative Undulation and Anomaly Differences Between OSU91A and OSU89B. Up to Degree 50 and 360.

	Maximum Degree	
	50	360
Geoid Undulation	57 cm	59 cm
Gravity Anomaly	2.2 mgal	3.5 mgal

The small change in going from degree 50 to 360, in the geoid undulation, reflects the small change in gravity material used in the 91A solution from the 89B model.

10. Conclusions

This report describes the computation of a geopotential model to degree 360, a sea surface topography model to degree 10/15, and adjusted Geosat orbits for the first year of the exact repeat mission(ERM). This study started from the GEM-T2 potential coefficient model and it's error covariance matrix and Geosat orbits (for 22 ERMs) computed by Haines et al. (1990) using the GEM-T2 model.

The first step in the study followed the general procedures described by Denker and Rapp(1990). This procedure used a radial orbit error theory originally developed by Engelis(1987a). The Geosat data was processed to find corrections to the a priori geopotential model, corrections to a radial orbit error model for 76 Geosat arcs, and coefficients of a harmonic representation of the sea surface topography. The processing of Denker and Rapp(ibid.) was extended by the addition of surface gravity normal equations from a recent 1° x 1° gravity anomaly data set. Using this data strengthened the separation between the potential coefficients and the sea surface topography harmonic coefficients. The results of this analysis led to sea surface estimates that were more realistic than found in the Denker/Rapp study where the sea surface slope across the Pacific Ocean was unrealistic when judged against oceanographic data. The results presented in this report appear realistic and attest to the improvement made in the Geosat orbits based on the GEM-T2 model and consistent tracking station coordinates. The RMS residual and crossover discrepancies were about the same as before (20 cm and 18 cm respectively). In this analysis we included altimeter data in areas not used previously (e.g the Mediterranean Sea and areas of high frequency gravity signal). This led to improved gravity fields in these areas as well as a sea surface topography estimate in the Mediterranean area that seems realistic. Our final solution in this first stage of processing was selected after testing several different weighting options and testing (through the help of the Goddard Space Flight Center) the different solutions in orbit fit tests. The primary weighting considerations related to the altimeter data weights trying to take into account the duplicative gravity signature sensed by the 22 repeat orbits analyzed. The weights used for the surface gravity data were not studied in detail but were selected considering the original standard deviations of the original data and calibration factors computed in several test solutions. Error covariance matrices were computed for the potential coefficients as well as the sea surface harmonic coefficients. The potential coefficient errors were used to compute geoid undulation accuracies at specific degree as well as cumulatively. For example up to degree 10 the cumulative geoid undulation error was 5.0 cm which is 25% smaller than reported by Rapp and Pavlis for the OSU89B potential coefficient model.

Time variations of the sea surface topography were also studied through spherical harmonic expansions carried out at one month intervals. These variations were used to compute sea level changes on an ocean wide basis. In addition, specific areas in the Pacific Ocean were studied to see if the sea level changes reported by Cheney and Miller(1990) could be detected. Although the agreement was not perfect it was clear that the techniques developed for this study gave reasonable agreement with the Cheney and Miller results. Based on the monthly sea surface topography solutions, the spectral analysis of the time variations of the sea surface height were also studied. The analysis of sea surface topography in this report should be regarded as a first step with additional study needed.

The second stage of geopotential analysis took place by carrying out a combination of the GEM-T2 coefficients with 30' gravity data derived from surface gravity data and anomalies obtained from altimeter data, primarily, GEOS-3 and SEASAT. This data was identical to that used by Rapp and Pavlis (ibid.). For areas lacking gravity information the gravity anomalies were derived from a potential coefficient model defined by the GEM-T2 model to degree 9 plus the coefficients from a topographic-isostatic model to degree 360. This was different from the approach used in the OSU89B model development where the GEM-T2 model was taken to degree 36 plus the topographic information. The combination solution gave a set of coefficients complete

to degree 50 plus a set of adjusted 30' mean gravity anomalies. These anomalies were used to compute the potential coefficients to degree 360. The coefficients of this model to degree 50 were replaced by the coefficients to degree 50 found in the first stage of the analysis. By doing this we take advantage of the improved analysis of the Geosat data that was carried out starting from the GEM-T2 Geosat orbits. The merged set of potential coefficients were designated the OSU91A potential coefficient model. The standard deviations for the coefficients were computed from the error covariance matrix and the error propagation/sampling error considerations for the coefficients above degree 50.

The 91A potential coefficient model was evaluated by comparison with several external data types. Orbit fit tests were carried out at the Goddard Space Flight Center and the Naval Surface Weapons Center. These tests indicated that the 91A model was comparable to other current potential coefficient models but other models could be better for some satellite applications. Tests were made comparing geoid undulations derived from space and levelling data and the corresponding quantities derived form the geopotential models. These tests indicated that the 91A model was about comparable with the 89B model although in some cases (e.g. in the State of Tennessee and at two VLBI sites) better. The undulations computed from the 91A model were also compared to the undulations implied by a complete ERM of Geosat data computed from the new Ohio State orbits. The standard deviation of the difference between the two undulation estimates was 34cm a considerable improvement over the OSU89B 53 cm standard deviation. The 34 cm fit was considerably better than fits obtained with the GEM-T3 or TEG-2 geopotential coefficient models (augmented by the OSU91A coefficients above degree and order 50). The most serious problem encountered with these other models is the large number of residuals in areas where altimeter data was edited out on the solutions. The specific areas include the Mediterranean Sea and the region below -60 latitude. Such data was included in the OSU91A model development.

The analysis in this report has shown how we can determine a high degree spherical harmonic model combining the best aspects of two different analysis techniques. The selection of weights for the data combination were made to give an overall fit to different data types. In this sense it is a compromise solution. Tests however indicate the compromise has not significantly degraded the solution for any of the data type being tested. Additional study is need to learn about optimum weighting procedures in the sense that data fits tests are needed with a variety of data.

There are a number of things that could be done to improve the solutions described in this report. For example, we have used the wet tropospheric correction that was given on the original Geosat GDRs. Literature has shown that these estimates may be in error by an amount that is significant with respect to the accuracy we are trying to achieve. Study is therefore warranted on the influence of the wet tropospheric correction errors on the parameters estimated in this study. We are also concerned about the appropriate representation of sea surface topography. As pointed out in Denker and Rapp(ibid.) the harmonic coefficient representation may not be the most appropriate when dealing with a non-global data set. Hwang(1991) has recently explored an alternative approach to this representation which may be much more satisfactory than the current modeling procedure. This modeling needs to be tested.

The proper reduction of the surface gravity material to the geoid seems to be an important factor in the analysis where cm accuracy in geoid computations is being attempted. Our studies have used an assumption about gravity and elevation correlations to compute certain corrections based on elevation data. We need to investigate this assumption. In addition we need to improve the elevation data models so that more reliable correction terms can be computed. Specifically this calls for the improvement of the ETOP5U 5'x5' elevation model that is distributed by the National Geophysical Data Center.

This report has described the error analysis that has led to the accuracy estimates for all the coefficients to degree 360. However this analysis from degree 51 to 360 is subject to a number of

assumptions that need to be evaluated. We are concerned that the accuracy estimate projected for the geoid undulation is significantly higher than that found by comparison with altimeter data in sea and undulation differences on land. The development of the higher degree coefficients throughout the orthogonality relationships also rests on assumptions related to the development of optimum desmoothing factors. The solutions being used in this report date back to studies made in the early 1980's. Newer studies are needed in this area. The most recent attempt at doing this is described by Sacerdote and Sanso(1991).

Although the analyses reported in this paper have shown improved ways to estimate the Earth's gravitational potential significant work is need to improve the modelling effort. We need additional surface gravity data for many regions now lacking data. We need to strive to get a global land coverage of 30' mean gravity anomalies. We need an improved analysis of satellite altimeter data to determine mean anomalies in the ocean areas. This new solution would take into account the improved Geosat orbits we now have as well as the new reference geopotential developed as part of this study. And we need the analysis in several areas as noted in the paragraphs above. Combining all this information together can help us reach an improved determination of the Earth's gravity field and the ocean surface through the altimeter data.

REFERENCES

Brigham, E.O., The Fast Fourier Transform and Its Applications, Prentice Hall, Englewood Cliffs, N.J., 1988.

Cheney, R. and L. Miller, Recovery of the Sea Level Signal in the Western Tropical Pacific from Geosat Altimetry, J. Geophys. Res. 95, C3, 2977-2984, 1990.

Christodoulidis, D., On the Realization of a 10 cm Relative Oceanic Geoid, Report No. 247, Dept. of Geodetic Science and Surveying, The Ohio State University, Columbus, 1976.

Cízek, V., Discrete Fourier Transforms and Their Applications, ADAM Hilger Ltd., Bristol and Boston, 1986.

Denker, H. and R. Rapp, Geodetic and Oceanographic Results from the Analysis of 1 Year of Geosat Data, J. Geophys. Res., 95, C8, 13,151-13,168, 1990.

Denker, H., Radial Orbit Error Reduction and Sea Surface Topography Determination Using One Year of Geosat Altimeter Data, Report No. 404, Dept. of Geodetic Science and Surveying, The Ohio State University, Columbus, 69A, 1990.

Despotakis, V., The Development of the June 1986 1° x 1° and the August 1986 30' x 30' Terrestrial Mean Free-Air Anomaly Data Bases, Internal Report, Dept. of Geodetic Science and Surveying, The Ohio State University, 1986.

Elliott, D.F., and K.R. Rao, Fast Transforms, Algorithms, Analyses, Applications, Academic Press, N.Y., London, Paris, 1982.

Engelis, T., Radial Orbit Error Reduction and Sea Surface Topography Determination Using Satellite Altimetry, Report No. 377, Dept. of Geodetic Science and Surveying, The Ohio State University, Columbus, 1987a.

Engelis, T., Spherical Harmonic Expansion of the Levitus Sea Surface Topography, Report No. 385, Dept. of Geodetic Science and Surveying, The Ohio State University, Columbus, 1987b.

Forsberg, R. and F. Madsen, High-Precision Geoid Heights for GPS Levelling, presentation at GPS-90 Symposium, Ottawa, September 1990.

Haines, B.J., G. Born, G. Rosborough, J. Marsh, and R. Williamson, Precise Orbit Computation for the Geosat Exact Repeat Mission, J. Geophys. Res., 95, C3, 2871-2885, 1990.

Haines, B.J., G. Born, J. Marsh, R. Williamson, A Summary of Precise Orbit Computation for the Geosat Exact Repeat Mission, John Hopkins APL, Technical Project, Vol. 10, No. 4, 393-404, 1989.

Hwang, C., Modeling Sea Surface Topography in Satellite Orbit Determination (abstract), EOS supplement, p. 89, April 23, 1991.

Hwang, C., Modeling Sea Surface Topography in Satellite Orbit Determination (abstract), EOS, 72, 17, 89.

Kim., J. and R.H. Rapp, The Development of the July 1989 1° x 1° and 30' x 30' Terrestrial Mean Free-Air Anomaly Data Bases, Report No. 403, Dept. of Geodetic Science and Surveying, The Ohio State University, Columbus, January 1990.

Koblinsky, C., J. Marsh, B. Beckley, A. Brenner, R. Williamson, Geosat Orbit Replacement Software for Altimeter Geophysical Data Records, GEM-T2 Ephemerides for November 1986 to November 1988, Geodynamics Branch, Goddard Space Flight Center, Greenbelt, MD, 20771.

Lerch, F., An Improvement Error Assessment for the GEM-T1 Gravitational Model, NASA Tech. Memo., TM 100713, 1988.

Levitus, S., Climatological Atlas of the World Ocean, NOAA Professional Paper 13, U.S. Govt. Printing Office, Washington, D.C., 1982.

Lisitzin, E., Sea Level Changes, Elsevier Scientific Publishing Co., New York, 1974.

Marsh et al., Dynamic Sea Surface Topography, Gravity and Improved Orbit Accuracies From the Direct Evaluation of Seasat Altimeter Data, J. Geophys. Res., 95, C8, 13,129-13,150, August 15, 1990.

Marsh J. et al., The GEM-T2 Gravitational Model, J. Geophys. Res., 95,313, 22,043-22,072, 1990.

Mather, R.S., Determination of Some Dominant Parameters of the Global Dynamic Sea Surface Topography from GEOS-3 Altimetry, NASA Technical Memorandum 19558, Goddard Space Flight Center, Greenbelt, MD, 1978.

Miller, L. and R. Cheney, Large Scale Meridionial Transport in the Tropical Pacific Ocean During the 1986-1987 El Niño from Geosat, J. Geophys. Res. 95, C10, 17905-17,919, Oct. 15, 1990.

Nerem, S., B. Tapley, C.K. Shum, Determination of the Ocean Circulation Using Geosat Altimetry, J. Geophys Res., 95, C3, 3163-3179, 1990a.

Nerem, R.S. et al., Determination of the Time-Variations of the Long Wavelength Dynamic Topography Using Geosat Altimetry, (abstract), EOS, 71, No. 43, p. 1266, Oct. 23, 1990b.

Pavlis, N.K., Modeling and Estimation of a Low Degree Geopotential Model from Terrestrial Gravity Data, Report No. 386, Dept. of Geodetic Science and Surveying, The Ohio State University, Columbus, p. 178, 1988.

Pavlis, N.K. and R.H. Rapp, The Development of an Isostatic Gravitational Model to Degree 360 and its Use in Global Gravity Modeling, Geophys. J. Int., 100, 369-378, 1990.

Press, W.H., B.P. Flannery, S.A. Teukolsky, W.T. Vetterling, Numerical Recipes, The Art of Scientific Computing. Cambridge University Press, 1986.

Putney, B. et al., Earth Gravity Model Development at NASA/GSFC: Preliminary Results from GEM-T3S, EOS, p. 89, April 23, 1991.

Rapp, R.H. and M. Kadir, A Preliminary Geoid for the State of Tennessee, Surveying and Mapping, 48, #4, 251-260, December 1988.

Rapp, R.H. and N.K. Pavlis, The Development and Analysis of Geopotential Coefficient Models to Spherical Harmonic Degree 360, J. Geophys. Res., 95, B13, 21,885-21,911, 1990.

Rapp, R.H. et al., Consideration of Permanent Tidal Deformation in the Orbit Determination and Data Analysis for the Topex/Poseidon Mission, NASA Technical Memorandum 100775, January 1991.

Rapp, R.H., The Treatment of Permanent Tidal Effects in the Analysis of Satellite Altimeter Data for Sea Surface Topography, manuscripta geodaetica, 14, 368-372, 1989.

Rapp, R.H., Y.M. Wang, N.K. Pavlis, Geoid Undulation Differences Between Geopotential Models, presentation at the meeting of the European Geophysical Society, Wiesbaden, Germany, April 1991a.

Rapp, R.H., Y.M. Wang, N.K. Pavlis, Spatial and Spectral Differences Between Geopotential Models, EOS, (abstract), p. 89, April 1991b.

Sacerdote, F. and F. Sanso, Spectral Calculus and Moving Average Operators on the Sphere,in Contributions to Geodetic Theory and Methodology, prepared by Section IV of the International Association of Geodesy, for the XX General Assembly of the IUGG, Vienna, 1991.

Shibuya, K., Y. Fukuda, Y. Michida, Determination of Geoid Height at Breid Bay, East Antarctica, to appear in Journal of Geophysical Research, 1991.

Torge, W., et al., Long Range Geoid Control Through the European Traverse, Dtsch. Geod. Komm. Ser. B, 290, 1989.

Wang, Y.M., Downward continuation of the free-air gravity anomaly to the ellipsoid using the grading solution Poisson's integral and terrain connections, Rep. 393, Dept. of Geodetic Science and Surveying, The Ohio State University, Columbus, 1988.

Wieser, M., The Global Digital Terrain Model TUG87, Internal Report on Set-up, Origin and Characteristics, Institute of Mathematical Geodesy, Technical University of Graz, Austria, 1987.

Yi, Y. and R.H. Rapp, The October 1990 1° x 1° Mean Anomaly File Including an Analysis of Gravity Information from China, Internal Report, Dept. of Geodetic Science and Surveying, The Ohio State University, Columbus, February 1991.

Appendix

Appendix A

Start and Stop Times of the 76 Geosat Arcs Analyzed in This Study

Arc #	Start Time (UTC)	Stop Time (UTC)	No. of rr obs.	rms (cm/sec)	No. of xovers	rms* (cm)	overlap rms(cm)
1	861108	861114	7057	.5054	1999	51.87	
2	861113	861119	6214	.5127	2053	68.48	22.40
3	861118	861124	6334	.5150	2167	49.40	38.38
4	861123	861124	7236	.5918	2233	57.98	14.46
5	861128	861204	8216	.5175	2283	48.15	26.58
6	861202	861207 2018	7732	.5318	2146	58.98	13.49
7	861207 2100	861214	8037	.4822	2419	53.65	Burn
8	861213	861219	8203	.4955	2409	50.37	15.78
9	861218	861224	7798	.5400	2419	51.13	13.06
10	861223	861229	8570	.5574	2460	50.30	6.84
11	861228	870103	8138	.4788	3446	48.57	7.99
12	870102	870107 2240	9334	.4955	2594	47.97	8.43
13	870107 2323	870114	8663	.5095	2842	47.27	Burn
14	870113	870119	9642	.4970	2505	47.34	9.04
15	870118	870124	9182	.5277	2672	44.28	6.64
16	870123	870129	8677	.4930	2915	49.45	16.77
17	870128	870203	7496	.5161	2919	56.65	22.97
18	870202	870208	7400	.5012	2567	52.16	31.66
19	870206	870212	8654	.4975	2744	47.00	8.13
20	870210	870216	8466	.5087	2729	57.31	17.30
21	870214	870220 1021	11329	.5051	2987	55.49	36.44
22	870220 1103	8702226	8516	.5160	2345	43.72	Burn
23	870225	870303	9302	.4895	2712	50.28	18.48
24	870302	870308	9163	.5140	2953	55.99	51.65
							68.40

25	870307	870313	8674	.5021	2697	44.71	12.67
26	870312	870318	8494	.4963	2784	45.92	19.00
27	870317	870323	8817	.5569	2813	51.26	30.95
28	870322	870328	7677	.5679	2898	41.80	23.28
29	870327	870402	8920	.5261	2560	43.21	20.74
30	870401	870407	9371	.5336	2348	44.34	24.20
31	870406	870412	8675	.5521	2704	43.77	34.10
32	870411	870417	9916	.5169	2687	47.53	32.38
33	870416	870422	9393	.5268	2309	44.51	13.71
34	870420	870426	10202	.5378	2106	45.54	9.39
35	870424	870430	11321	.5371	2224	47.47	35.57
36	870428	870503 1713	9874	.5502	2165	48.82	Burn
37	870503 1755	870510	12071	.5036	2732	44.23	3.64
38	870509	870515	12247	.5233	2411	47.59	48.88
39	870514	870520	12082	.5133	2314	54.91	61.58
40	870519	870525	9322	.5165	2169	46.04	3.34
41	870523	870529	9003	.5005	2041	53.32	52.31
42	870527	870602	7394	.4860	2130	55.02	62.07
43	870531	870605 1829	8359	.5310	2198	56.52	Burn
44	870605 1912	870612	10995	.5574	2929	47.67	15.02
45	870611	870617	10406	.5367	2112	58.22	77.35
46	870616	870622 1910	11446	.5626	2840	60.52	Burn
47	870622 1951	870629	9741	.5172	2386	49.34	18.52
48	870628	870704	9663	.5338	2234	51.30	27.94
49	870703	870709	10502	.5268	2045	47.38	13.07
50	870708	870714	9588	.4877	1825	51.12	50.07
51	870713	870719	9166	.5357	1896	52.17	10.16

52	870717	870723	10436	.5115	2009	43.90	11.20
53	870721	870726 1230	10547	.5230	1746	43.76	Burn
54	870726 1312	870802	11395	.5245	2697	56.78	59.59
55	870801	870807	10802	.4795	2478	49.66	33.98
56	870806	870812	10045	.4920	2491	48.59	64.94
57	870811	870817	11484	.5146	2525	60.00	77.38
58	870816	870822	9643	.4886	2383	57.49	49.40
59	870820	870825 1517	8930	.5356	2057	50.25	Burn
60	870825 1558	870901	10300	.5258	2274	55.67	81.86
61	870831	870906	9673	.5661	2259	56.82	74.11
62	870905	870911	9611	.4992	2220	56.16	81.92
63	870910	870916	10600	.5189	2203	51.04	60.55
64	870915	870921	9805	.5456	1877	54.23	82.27
65	870919	870924 1614	8752	.5443	1880	64.12	Burn
66	870924 1655	871001	10921	.5257	2479	58.95	59.84
67	870930	871006	10156	.5407	2142	52.49	48.60
68	871005	871011	9684	.5402	1890	52.08	44.78
69	871010	871016	11660	.5076	1677	62.86	15.45
70	871015	871021	11870	.5252	1940	60.49	9.61
71	871019	871024 1908	10911	.5340	1810	57.68	Burn
72	871024 1951	871031	11628	.5876	2092	57.25	8.56
73	871030	871105	10153	.5655	2193	65.18	8.70
74	871104	871110	10137	.5591	2252	58.24	26.17
75	871108	871114	10855	.5386	1955	58.64	5.69
76	871112	871118 0017	11131	.5458	1324	63.90	
	1st year average					52.16	31.69

Table from Koblinsky et. al (1990)